TOPFARM wind farm optimization tool

Réthoré, Pierre-Elouan; Fuglsang, Peter; Larsen, Torben J.; Buhl, Thomas; Larsen, Gunner Chr.

Publication date:
2011

Document Version
Publisher's PDF, also known as Version of record

TOPFARM wind farm optimization tool

Risø-R-Report

Pierre-Elouan Rethore, Peter Fuglsang, Torben J. Larsen,
Thomas Buhl, Gunner C. Larsen
Risø-R-1768(EN)
February 2011

Risø DTU
National Laboratory for Sustainable Energy

Author: Pierre-Elouan Rethore, Peter Fuglsang, Torben J. Larsen, Thomas Buhl, Gunner C. Larsen
Title: TOPFARM wind farm optimization tool
Division: Wind Energy Division

Abstract :
A wind farm optimization framework is presented in detail and demonstrated on two test cases: 1) Middelgrunden and 2) Stags Holt/Coldham. A detailed flow model describing the instationary flow within a wind farm is used together with an aeroelastic model to determine production and fatigue loading of wind farm wind turbines. Based on generic load cases, the wind farm production and fatigue evaluations are subsequently condensed in a large pre-calculated database for rapid calculation of lifetime equivalent loads and energy production in the optimization loop.. The objective function defining the optimization problem includes elements as energy production, turbine degradation, operation and maintenance costs, electrical grid costs and foundation costs. The objective function is optimized using a dedicated multi fidelity approach with the locations of individual turbines in the wind farm spanning the design space. . The results are over all satisfying and are giving some interesting insights on the pros and cons of the design choices. They show in particular that the inclusion of the fatigue loads costs give rise to some additional details in comparison with pure power based optimization. The Middelgrunden test case resulted in an improvement of the financial balance of 2.1 M€ originating from a very large increase in the energy production value of 9.3 M€ mainly counterbalanced by increased electrical grid costs. The Stags Holt/Coldham test case resulted in an improvement of the financial balance of 3.1 M€.

Risø-R-1768(EN)
February 2011

ISSN 0106-2840
ISBN 978-87-550-3884-4

Contract no.:
TREN07/FP6EN/S07.73680/038641

Group's own reg. no.:
1110062-01

Sponsorship:
European Commission in the framework of the NonNuclear Energy Programme Sixth Framework

Cover :

Pages: ??
Tables: ??
References: ??

Information Service Department
Risø National Laboratory for
Sustainable Energy
Technical University of Denmark
P.O.Box 49
DK-4000 Roskilde
Denmark
Telephone +45 46774005
bibl@risoe.dtu.dk
Fax +45 46774013
www.risoe.dtu.dk

Contents

Preface

This work was funded by the European Commission in the Framework of the Non-nuclear Energy Programme 6th Framework, contract TREN07/ FP6EN/ S07.73680/038641 (TOPFARM—Next Generation Design Tool For Optimization of Wind Farm Topology and Operation).

1 Introduction

This report describes the wind farm optimization tool that was developed in the TOPFARM project [1]. The ultimate goal of the TOPFARM project has been to develop tools for optimization of wind farm topology layout and control taking into account not only energy production but also installation, wind turbine fatigue driven degradation, and operation and maintenance (O&M) costs.

1.1 Background

During recent years, wind energy has moved from an emerging technology to become a nearly competitive technology. An increasing part of the turbines to be installed in the future are foreseen to be sited in large wind farms. Establishment of large wind farms requires enormous investments, putting steadily greater emphasis on optimal topology layout and control of these. Today, the design of a wind farm is typically based on an optimization of the power output only, whereas the load aspect is treated only in a rudimentary manner, in the sense that the wind turbines are required only to comply with the design codes.

This trend is also visible on the research carried out on this topic. Wind farm layout optimization is a relatively new topic, with the first article on the subject written by Mosetti and colleagues in 1994. The following article on the topic came nearly a decade later, with Costa et al. (2004) [2]. Since then the topic has became gradually more popular to reach around ten journal and conference articles produced every year (see Samorani, 2010 [3] and Réthoré, 2010 [4] for a more exhaustive review). The vast majority of the research work on this topic has been focused on the types of optimization algorithm used to solve the problem, keeping the various cost functions as simple as possible. A notable exception to this observation is the work of Elkinton (2007) [5], which presents a rather sophisticated modeling of different costs function, in particular the electrical grid and foundation costs. While most consider the power losses due to wake effect, none consider the costs associated the wake induced fatigue loads on the wind turbine components. However, a complete optimization of layout and control of these farms requires, in addition to the power production, a detailed knowledge of the loading of the individual turbines. This is not a trivial problem. The power production and loading, related to turbines placed in a wind farm, deviate significantly from the production and loading pattern of a similar stand-alone wind turbine subjected to the same (external) wind climate. Crucial factors in this connection are the relative position of the individual wind turbines and the wind turbine control/operation strategy for wind turbines interacting through wakes.

To achieve the optimal economic output from a wind farm, an optimal balance between capital costs, O&M costs, fatigue lifetime consumption and power production output is to be determined on a rational background. The overall objective of the TOPFARM project is to establish this background in terms of advanced flow models that include dynamic wake effects, advanced (and fast) aeroelastic models for load and production prediction, dedicated cost and control strategy models, and subsequently to synthesize these models in an optimization algorithm subjected to various kinds of constraints, as e.g. area constraints and turbine interspacing constraints. The design variables for the optimization algorithm are the relative position of the wind turbines (including the possibility for positioning a given number of turbines in one or more wind farms) and wind turbine control strategies on wind farm level as well as for the individual wind turbine.

When involving a computational demanding iterative process, it is of crucial importance that the resulting models of the complex wind field within a wind farm can be "condensed" into fast, though accurate, flow simulation tools. The basic strategy for achieving this goal goes through a chain of flow models of various complexities, where the advanced and computational very demanding CFD based models, together with available experimental evidence, are used to formulate, calibrate and verify simpler models ranging from simplified CFD models to more engineering stochastic type of models.

Aeroelastic modeling is needed to calculate the loads for each of the turbines in the wind farm. It is a challenge on one hand to keep computational costs limited while on the other hand to have accurate values for the loads of each turbine. Complete aeroelastic calculations for each turbine are clearly not feasible due to the very large number of cases that need to be considered when taking into account wind direction and wind speed variations. In this work, the solution has been to base the fatigue load calculations on a database of pre-calculated generic load cases for turbines in wake operation. Based on an interpolation scheme, total lifetime equivalent loads can then be found by summing up contributions from individual load cases.

When aiming at economic optimization of wind farm topology, a cost model is essential, encompassing both financial costs and operating costs. Only costs that depend on wind farm topology (including wind farm infra structure, wind turbine foundations, production and loading) are relevant. In the context of this work these costs are variable costs, contrary to fixed costs which are, e.g. cost of planning and projecting of the wind farm, cost of the land available for the intended wind farm project, price of turbines, civil engineering costs. The cost needs to be evaluated only on a relative basis, whereas the knowledge of the absolute cost is not necessary for the optimization to reach convergence.

A proper optimization approach is essential for successfully carrying out of the optimization. One aspect is the choice of optimization algorithm among global methods and gradient based methods, where the likelihood of arriving in a local minimum needs to be traded off against rate of convergence and total computational costs. Other aspects are the clever mapping of the wind farm layout design variables using as few variables as possible and how to include constraints on the wind farm performance characteristics (e.g. power fluctuations, space used etc.). In order to limit the computational requirements a multi-fidelity optimization approach is proposed. The basic idea is to use a global optimization algorithm on simplified cost functions over a coarse discretization of the domain as well as the wind direction and wind speed distributions considered; and then to refine the resulting layout by increasing gradually the complexity of the cost functions and the resolution of the discretization using a gradient based optimization algorithm.

1.2 Report outline

The present report contains the following chapters:

- Chapter 2 contains a general description of the approach including an overall flow chart of the optimization tool and a brief explanation of the involved sub models;
- Chapter 3 contains details on the wind farm flow field modelling approach;
- Chapter 4 contains information about the aeroelastic load calculations and the establishment of a load database for fast assembly of lifetime equivalent fatigue loads on an individual basis for all turbines in a wind farm;

- Chapter 5 describes the optimization objective function;
- Chapter 6 contains information about the optimization tool and the mapping of the wind farm layout into design variables;
- Chapters 7 to 9 contain results from various test cases and for the Middelgrunden and Stags Holt/Coldham wind farms;
- Chapter 10 contains the conclusions.

2 Program workflow

2.1 Global approach

The goal of the program is to find an optimum layout for a wind farm. The global approach is to maximize the financial balance of the wind farm costs and the wind farm income. The program is divided in two separate entities. One part has the task to propose wind farm layouts based on an optimization algorithm. The second part has the task to calculate the financial balance, and all the costs functions associated, of a given wind farm layout. The program workflow is essentially a loop, in which the optimization algorithm sends a layout to the financial balance calculator, which then returns the financial balance and several other results that are used by the optimization algorithm for the next iteration.

In the current implementation, the optimization part is carried out using HAWTOPT [17], which is a general purpose optimization toolbox. The financial balance calculator part is a set of functions developed in Matlab. The global approach is illustrated bellow.

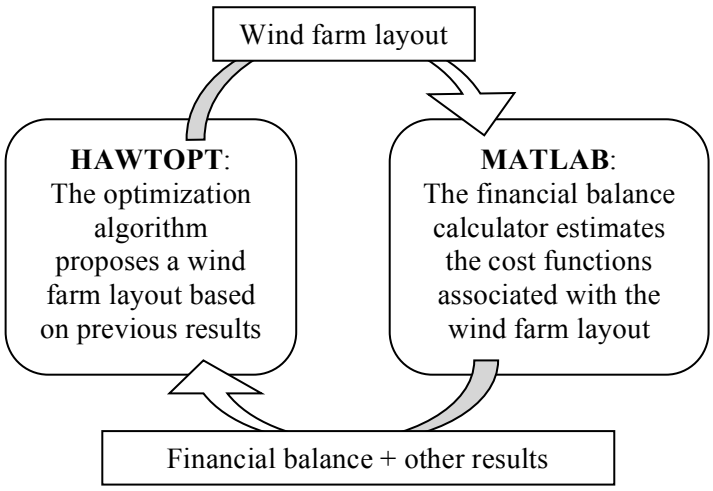

The main loop of the optimization and financial balance calculation is developed in Matlab. The Matlab code is therefore responsible for managing HAWTOPT. It communicates with HAWTOPT through two files - one containing the wind farm layout description and one containing the results of the cost functions. The Matlab code is moreover responsible for loading the various requested inputs describing the wind farm site and type of turbine and finally for controlling the cost functions as well as the optimization process. These inputs are briefly introduced in the following section.

2.2 Inputs types

The input is classified into wind turbine related input, site related input, input related to the optimization procedure, and input related to various cost functions.

Wind turbine input:

- The turbine radius (to scale distances and wake effects);
- The turbine height (to calculate the wind speed and wake effects);
- The rated power(to scale the turbine(?) prices and the power curves);

- The power and C_t curve (to estimate the annual energy production and the wake effects);
- The components maximum fatigue resistance (to estimate the component write off percentage and the probability of replacing the components).

Site specific input:

- The surface roughness (to determine the wind shear);
- The cut-in wind speed and cut-out wind speed (to define the number of cases);
- The minimum distance between turbines (to constraint the optimization);
- The number of turbines in the wind farm;
- The boundaries of the domain, defined as min/max values and polygon vertices;
- The probability distribution of site mean wind speed, turbulence intensity and wind direction;
- The site type (onshore or offshore).

Optimization input:

- The number of allowable iterations;
- The type of optimization algorithm;
- The constraints to be considered (for example the domain boundaries, the minimum distance between the turbines, grid costs and water depth);
- The objective function to be minimised (e.g. the financial ballance);
- The convergence criteria;
- The optimization specific inputs (to be described in more details in the optimization section).

Cost functions inputs

Each cost function has its own type of inputs. These are mostly related to calibration of the models, or constants to estimate the price of different elements. ?? What is meant: Those prices might be subject to changes in the future and in different locations??.

2.3 Structure of the program

The program execution can be decomposed in three phases.

First comes a *loading phase*, where the inputs specific to the wind turbines and site the options specific to the optimisation, and the constants of the cost functions are loaded.

Then follows an *initialisation phase*, in which the various structures, arrays and variables that are needed for the different cost functions are created. The configuration file and the "first guess" design variables used by HAWTOPT are also created during this phase.

The *optimization phase* is then started (see Figure 1). The program launches HAWTOPT, which then produces a design variable file. This file is used by the TOPFARM platform as an input to the global financial balance function. The financial balance function is first testing, if the design variables are violating the constraints specific to the particular wind farm layout. The norm of the minimum distance between the turbine and the norm of the distance to the layout limits are calculated.

Secondly, the financial balance function calculates the hypothetical undisturbed wind field seen by all the wind turbines associated with each of the mean wind speed and mean wind direction cases to be considered. This database is used as input to the function that estimates the 20-year fatigue degradation of the different wind turbine

components and the annual energy production of each wind turbine. Based on this information, the total value of the wind farm electricity production as well as the total cost of component degradation and O&M is estimated.

Thirdly, the financial balance function is calling the foundation cost function and the electrical grid cost function. The financial balance is finally calculated based on all those cost functions results and written to an output file together with the results of the different cost functions and the constraint norms?..

During the optimization phase, HAWTOPT awaits for the creation of this output file. When available, this output file is read by HAWTOPT and subsequently used to produce new design variables based on the optimisation algorithm output. The loop continues until the algorithm reaches convergence, or the maximum number of iterations is reached.

The outputs of the program allow to re-enact the evolution of the design variables produced by the optimisation method and the corresponding results. It is also possible to restart the program using the outputs from a previous computation as "first guess" for obtaining more refined results. A typical process would be for example to run the *genetic algorithm* to find a global optimum on a coarse grid, and subsequently to refine this solution using a *gradient based method* using a finer resolution.

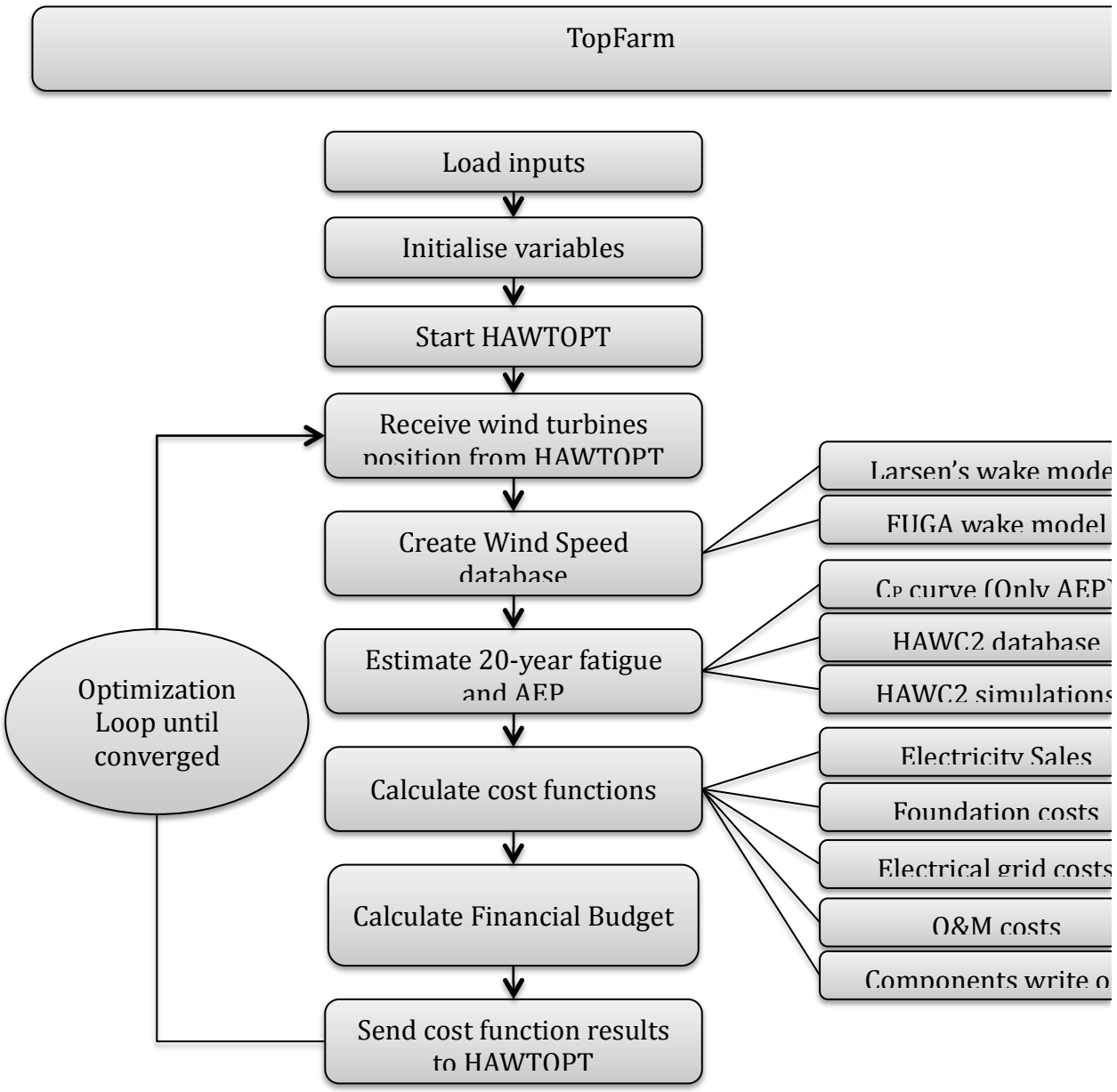

Figure 1 Block diagram of TOPFARM main loop

3 Wind farm mean flow

This chapter describes the goal and the two methods used to estimate the mean wind speed acting on the wind turbines.

The wind speed and turbulence intensity estimation can serves two purposes in the TOPFARM framework.

- It can be used as an input to a power curve to estimate the power output of a wind turbine for a given wind speed and wind direction. This information is used to estimate the annual energy production;
- It can be used to estimate the power output and wake induced fatigue loads based on a HAWC2 simulation. In this case the wind speed estimation is used as an input to the upstream wake generating wind turbine. The information is thus used to estimate the annual energy production and the fatigue associated costs.

Note that in both cases it is the hypothetical inflow wind speed – without induction – that is needed. For that reason the wind turbine located at the position of interest, and the downstream wind turbines are not considered.

3.1 Semi-empirical wake model

A stationary wake model for wind farms has been developed for the TOPFARM project [6]. It uses the thrust coefficient and the atmospheric turbulence intensity upstream the wind farm to estimate the deficit of an axis-symmetric single wake. The estimation of the individual wake contributions are based on a closed form asymptotic solution to the thin shear layer approximation of the NS equations, assuming rotational symmetry flow conditions.

The expansion of stationary wake fields is believed to be significantly affected by meandering of wake deficits as e.g. described by the Dynamic Wake Meandering (DWM) model [10]. In the present model, this effect is approximately accounted for by imposing suitable empirical downstream boundary conditions on the closed form formulation of the wake expansion, which depends on the rotor thrust and the ambient turbulence conditions, respectively. For downstream distances beyond approximately 10 rotor diameters (at which distance the calibrated wake expansion boundary conditions are imposed), the present formulation of wake expansion is although believed to underestimate wake expansion. This is because the analytical wake formulation dictates the wake expansion to behave as $x^{1/3}$ with the downstream distance x, whereas wake expansion as primary controlled by wake meandering develops approximately linearly with the downstream distance.

In order to account for multiple wakes, all the upstream single wake deficits are combined using a linear perturbation approach. In order to estimate a hypothetical uniform inflow wind speed at a wind turbine location, the model performs a Gauss integration over the rotor area of the undisturbed inflow wind profile combined with the upstream generated wake deficits.

3.2 Linearized CFD wake model

Ott et al. [7] have designed a wind farm wake model based on linearized Navier-Stokes equations. A database is created for each wind turbine type (size and thrust coefficient) and location type (surface roughness). In its current implementation only the hub height is stored in the database.

In a similar fashion as in the Larsen's semi-empirical wake model the contribution of each wind turbine wake deficit are added up linearly. The hypothetical inflow wind

speed to a wind turbine is taken at the center of the rotor, at hub height. This wind speed is then used with a thrust coefficient curve to estimate the thrust coefficient of the wind turbine considered.

4 Fatigue load database

This chapter describes the method for calculation of life time equivalent fatigue loads for the turbines in a wind farm using limited computational costs. It has been the ambition to obtain a time efficient approach, which can be integrated with the numerical optimization approach to ultimately optimize the wind farm layout using the loads as input for either cost modeling or as constraints during the optimization.

The objective is to include the impact of the actual wind farm layout on the individual turbines and to include dynamic wake meandering (DWM) effects from upstream turbines on the loads of the actual turbine according to [9]. The final outcome should be a lifetime equivalent fatigue load index for the current wind farm layout, which is normalized by the corresponding fatigue loads for a stand-alone turbine in free wind, seeing the same inflow as the wind farm as a whole.
The fatigue calculation approach was split into the following sub tasks:

- Pre-calculation of a database of short term fatigue loads for different inflow parameters for a turbine in wake and a reference stand-alone turbine;
- Summing of the total lifetime equivalent fatigue loads for each turbine on basis of the pre-calculated database using the wind farm layout and the wind farm overall mean flow;
- Calculation of the total lifetime equivalent load index for each turbine and subsequently for the entire wind farm relative to a stand-alone turbine.

In the summation for the lifetime equivalent loads, the closest upstream turbine will be identified in each of the wind directions, and the wake of this turbine will be deciding the loads for the actual (downstream) turbine using the geometrical distance between the turbines and the wind farm overall mean wind distribution and turbulence distribution. The event that a turbine further away might cause higher loads will not be considered.

4.1 Database of short term loads and electrical power

A set of time series was calculated for a number of different inflow conditions. The aeroelastic code HAWC2 [8] was used for calculation of 600 second response time series of the UPWIND 5 MW turbine using the DWM model implementation described in [9].

HAWC2 is a multi body Finite Element (FE) model based on Timoshenko beam elements. The input to the model is divided into substructures: tower, nacelle and rotor blades. Each substructure is divided into a number of bodies, which again is divided into finite elements. There are six Degrees Of Freedom (DOF) for each element node. Aerodynamic torque, thrust and other loads are dynamically calculated in HAWC2 using an unsteady Blade Element Momentum (BEM) model. The local aerodynamic load is calculated at the blade section using 2D lift, drag and moment profile coefficients, having been corrected for 3D and rotational effects using the Viterna method [11].

A newly developed dynamic wake meandering model, described in [9] and [10], was used to properly model turbine operation in wake. The objective of this model is to model the basic wake flow mechanisms with sufficient accuracy while keeping the model as simple as possible. The underlying hypothesis in the DWM model is that

the wake deficit from the upstream turbine, in combination with meandering of this deficit, is the major contributor to the increased loading.

The basic philosophy of the DWM model is a split of scales in the wake flow field, based on the conjecture that large turbulent eddies are responsible for stochastic wake meandering only, whereas small turbulent eddies are responsible for wake attenuation and expansion in the meandering frame of reference as caused by turbulent mixing. It is consequently assumed that the transport of wakes in the atmospheric boundary layer can be modeled by considering the wakes to act as passive tracers driven by a combination of large-scale turbulence structures and a mean advection velocity, adopting the Taylor hypotheses. The DWM model is essentially composed of three corner stones – 1) a model of the wake deficit as formulated in the meandering frame of reference; 2) a stochastic model of the downstream wake meandering process; and 3) a model of the self induced wake turbulence described in the meandering frame of reference.

The turbine used in this work is the 5MW reference turbine used in the EU-project, Upwind. The aeroelastic model of this turbine was developed at NREL [12]. The blade uses the Delft DU profile series and has a length of 63.0m and a maximum chord length of 4.7m. The tower has a height of 79.6 m, and the shaft and nacelle have a total weight of 240t.

A set of response time series were calculated for a number of different generic wake inflow conditions.. A total of 7436 time series of 600 seconds were obtained from combinations of the parameters illustrated in Figure 2:

- Wind speed, U, varied from 4 m/s to 26 m/s in steps of 2 m/s;
- Inflow turbulence intensity, I, calculated for I = {1%, 5%, 10%, 15%};
- Azimuth angle, Θ, calculated for Θ = {0^o, 0.5^o, 1^o, 2^o, 3^o, 4^o, 5^o, 10^o, 15^o, 20^o, 25^o, 35^o, 45^o};
- Distance from upstream turbine, D, calculated for D = {1, 2, 3, 4, 5, 6, 7, 8, 9, 10, 12, 16, 20}.

In addition, 44 time series were calculated for the reference turbine at free inflow for the relevant combinations of wind speed and turbulence intensity.

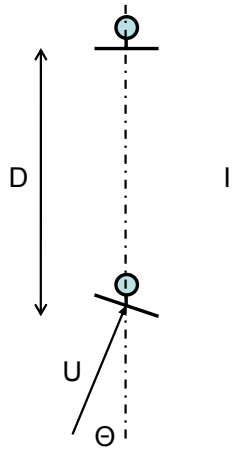

Figure 2 Definition of inflow parameters for the turbine being in wake of an upstream turbine.

The load analysis involved computation of statistical information as well as traditional Rainflow counting using Wöhler curve exponents representative for

relevant component materials. The Rainflow counting was done using a standard Rainflow counting routine from [13].

The sensors described in Figure 3 were defined for the load analysis. In addition to the six load sensors, the electrical power was included in the statistical analysis to enable estimation of annual energy yield (AEP) on basis of the results.

Sensor #	**Sensor**	**Wöhler curve exponent**
17	Tower base over turning bending moment, Mx_{Tower}	4
18	Tower base transverse bending moment, My_{Tower}	4
20	Nacelle (tower top) tilt moment, $Mx_{Nacelle}$	8
22	Nacelle (tower top) yaw moment, $Mz_{Nacelle}$	8
29	Blade root flapwise bending moment, My_{Blade}	12
30	Blade root edgewise bending moment, Mz_{Blade}	12
88	Electrical power, P_{Elec}	-

Figure 3 HAWC2 sensors for load analysis

For each load sensor, an equivalent load cycle range, R_{eq} , was determined based on the Rainflow counting results:

$$R_{eq} = \left(\frac{\sum n_i R_i^m}{n_{eq}} \right)^{1/m} \quad (1)$$

where $\sum n_i R_i^m$ is the accumulated fatigue loading resulting from the Rainflow counting, with n_i being the number of load cycles with range R_i , m denoting the Wöhler exponent, andn_{eq} is the number of equivalent cycles - here set to 600.

Figure 4 to Figure 10 show results for a parameter study defined by combinations of the input parameters Θ and D for U=10m/s and 22 m/s and for I=5%. More detailed results can be found in Appendix 0???.

The tower base Mx and My moments are shown in Figure 4 and Figure 5. For small values of Θ the loads on the downwind turbine increase with D, whereas for larger Θ the magnitude of the load is determined by the actual D, since the downwind turbine will sometimes be outside of the wake depending on the combination of Θ and D. In Appendix 0?? it can be seen that for D=1, the load generally increases with U, whereas for higher values of D, the load peaks around rated power and then reduces towards higher wind speeds. It can also be seen that there is a clear trend with increasing load for increasing I. In general, the load increase from wake operation is significant, except for the cases where the downwind turbine is outside of the upstream turbine wake, where the load then corresponds to the reference turbine.
The tower top Mx and Mz moments are shown in Figure 6 and Figure 7. The trend of increasing load with D for small values of Θ is also seen here, and the highest loads are generally seen for smaller values of Θ, whereas the downstream turbine seems to outside of the wake at higher values of Θ and D. In general, the resulting load values show some scatter with U and I, however, with a clear trend on increasing with U and I.

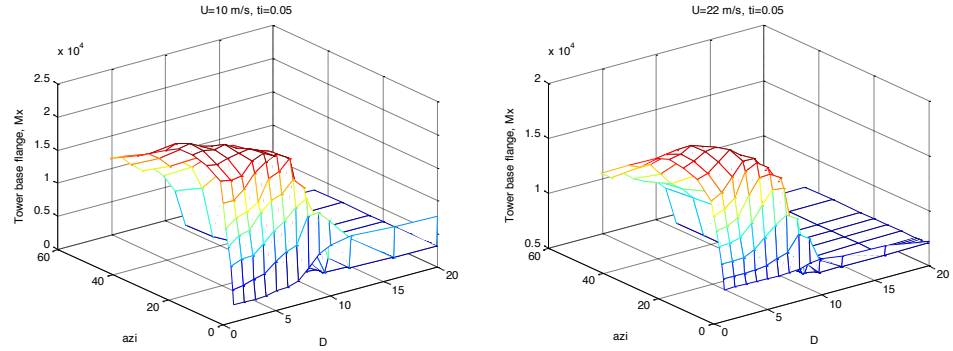

Figure 4 Tower base flange Mx (Sensor 17) equivalent load (m=4) versus wake distance (D) and wake azimuth (azi) ??filnavne?: måske skulle disse fjernes. Dette gælder generelt i det flg.??(S_17_D_A_ti_5U_10.emf, S_17_D_A_ti_5_U_22.emf).

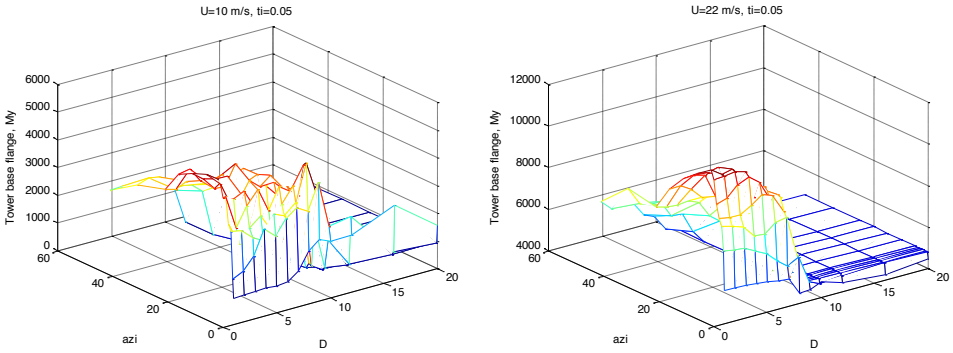

Figure 5 Tower base flange My (Sensor 18) equivalent load (m=4) versus wake distance (D) and wake azimuth (azi) (S_18_D_A_ti_5U_10.emf, S_18_D_A_ti_5_U_22.emf).

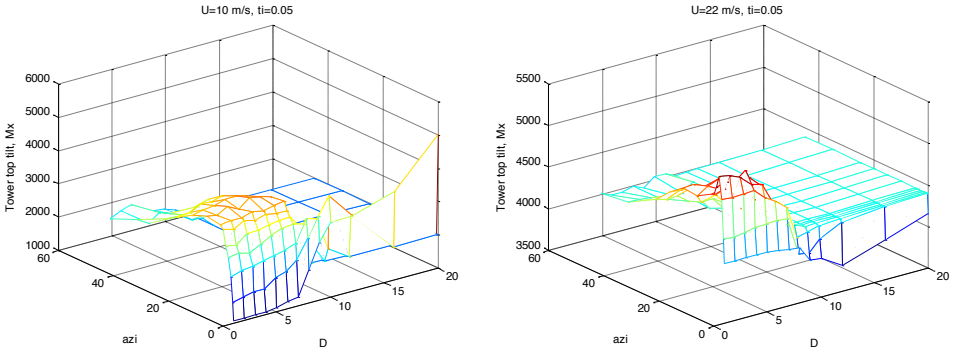

Figure 6 Tower top tilt Mx (Sensor 20) equivalent load (m=8) versus wake distance (D) and wake azimuth (azi) (S_20_D_A_ti_5U_10.emf, S_20_D_A_ti_5_U_22.emf).

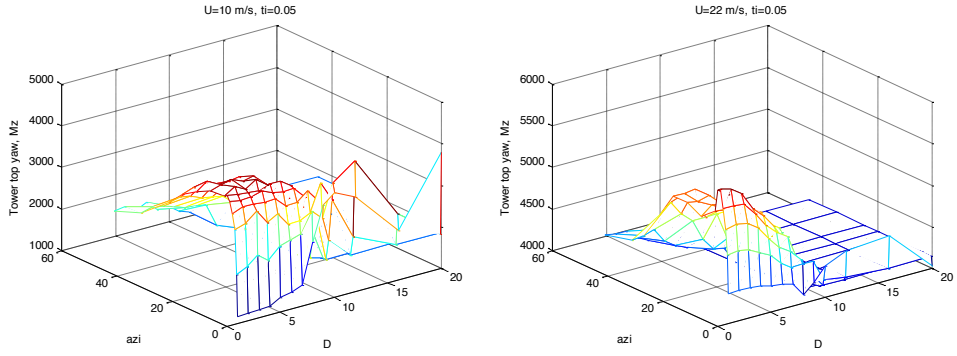

Figure 7 Tower top yaw Mz (Sensor 22) equivalent load (m=8) versus wake distance (D) and wake azimuth (azi) (S_22_D_A_ti_5U_10.emf, S_22_D_A_ti_5_U_22.emf).

The blade flapwise moment, Mx, is seen Figure 8. A clear trend is observed for increased loads with increasing wind speed and increasing turbulence. At small values of D higher values of Θ are needed for increasing the load, whereas for higher D, the load is increasing for smaller values of Θ, which is similar as for the tower base and top moments.

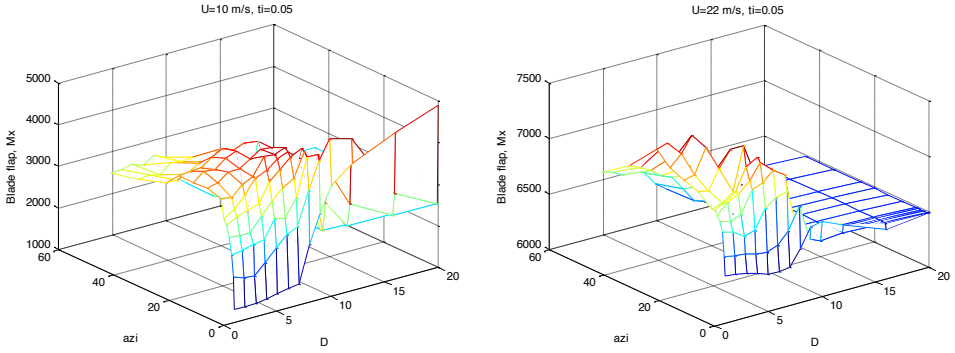

Figure 8 Blade flap Mx (Sensor 29) equivalent load (m=12) versus wake distance (D) and wake azimuth (azi) (S_29_D_A_ti_5U_10.emf, S_29_D_A_ti_5_U_22.emf).

The blade edgewise moment, My, is seen in Figure 9. The load values show a clear increase with turbulence, but are not very sensitive to U and Θ, except for at small values of D, where the load is increasing with Θ.

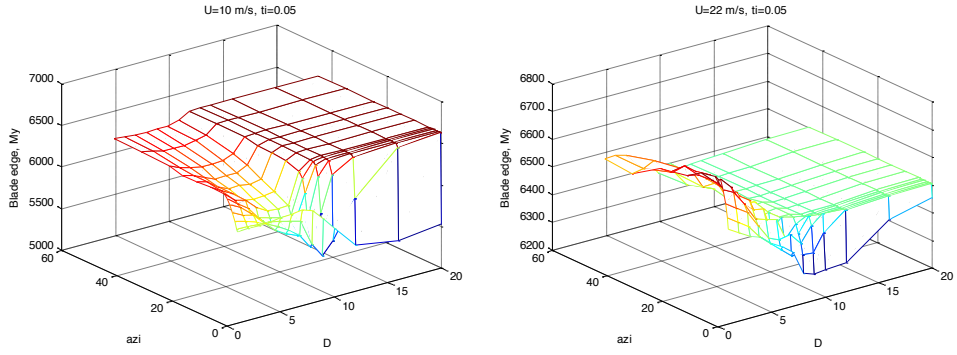

Figure 9 Blade edge My (Sensor 30) equivalent load (m=12) versus wake distance (D) and wake azimuth (azi) (S_30_D_A_ti_5U_10.emf, S_30_D_A_ti_5_U_22.emf).

Figure 10 shows the rotor electrical power. There is a clear trend of increasing power with increasing D and increasing Θ until the rated power plateau is reached, and power is constant at high wind speeds independently of D and Θ.

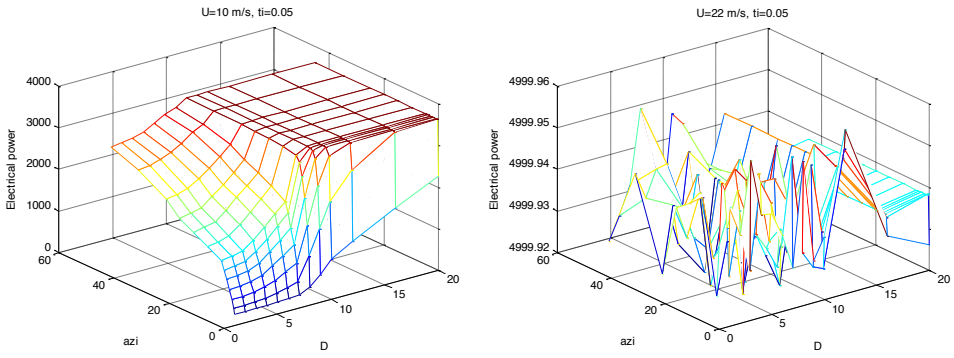

Figure 10 Rotor electrical power (Sensor 88) versus wake distance (D) and wake azimuth (azi) (S_88_D_A_ti_5U_10.emf, S_88_D_A_ti_5_U_22.emf).

4.2 Lifetime equivalent fatigue loads

The lifetime equivalent fatigue load can be calculated by summation of contributions from individual load cases taking into account the probability of each load case and the total number of equivalent cycles:

$$L_{eq} = \left[\frac{\int R_{eq}(U)^m n_{eq} p(U) n_T dU}{n_{eq,L}} \right]^{1/m} \tag{2}$$

where

$R_{eq}(U)$ is the equivalent load cycle range for the load case U;
n_{eq} is the number of cycles corresponding to $R_{eq}(U)$ - here set to 600;
$p(U)$ is the probability for the load case U (equal to the number of operation hours for load case U in the 20 year lifetime divided by number of hours in 20 years);
n_T is the number of 10-minute sequences corresponding to 20 year lifetime ($6 \cdot 24 \cdot 365 \cdot 20$);
$n_{eq,L}$ is the lifetime equivalent number of cycles - here set to 10^7 cycles.

For the fatigue load cases that appear from normal operation at different wind speeds and different wind directions, the probability is determined from the wind rose, which defines the number of hours for each wind sector and the wind sector wind climate. This means that the summation for L_{eq} is done for all wind speeds in each wind sector giving a total number of contributions as the multiplication of the number of wind rose divisions, n_{WR}, and the number of wind speeds, n_{WS}:

$$L_{eq} = \left[\frac{1}{n_{eq,L}} \sum_{j=1}^{n_{WR}} \sum_{i=1}^{n_{WS}} R_{eq}(U_{i,j})^m n_{eq} p(U_{i,j}) n_T \right]^{1/m} \tag{3}$$

By using the wind rose defined in Figure 11, the lifetime equivalent loads were calculated for the reference turbine for the sensors in Figure 3. The results show the lifetime equivalent loads versus wind direction in Figure 12 to Figure 14. All sensors

show the largest load contributions to appear from the dominating wind directions according to the wind rose in Figure 11, which could be expected. The blade edgewise moment shows a more uniform load distribution on wind directions compared to the other sensors, reflecting that edgewise moments are dominated by gravity loading.

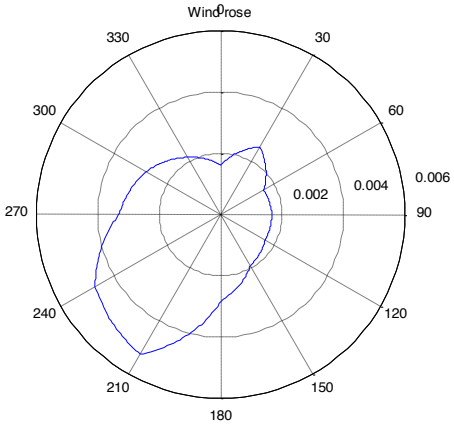

*Figure 11 Wind rose corresponding to the Stags Holt/Coldham wind farm from [**Error! Reference source not found.**]*

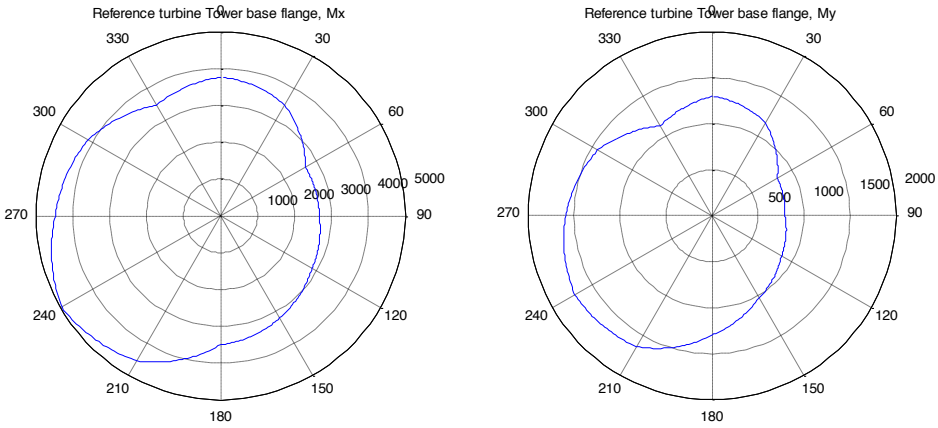

Figure 12 Tower base flange Mx (Sensor 17) and My (Sensor 18) Leq (m=4) versus wind direction (WD) (LEQ_REF_S_17.emf, LEQ_REF_S_18.emf).

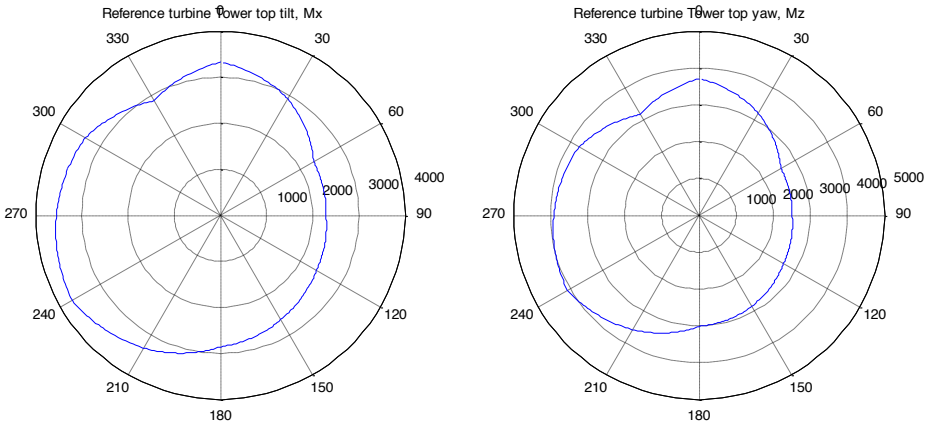

Figure 13 Tower top tilt Mx (Sensor 20) and yaw Mz (Sensor 22) Leq (m=8) versus wind direction (WD) (LEQ_REF_S_20.emf, LEQ_REF_S_22.emf).

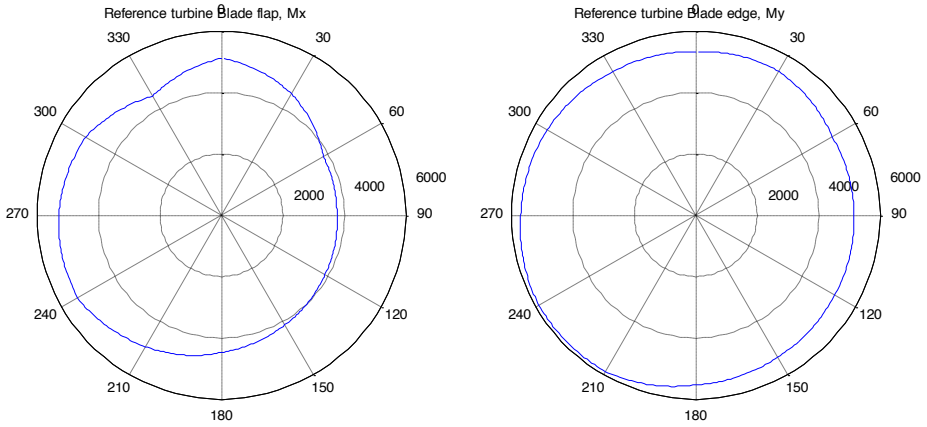

Figure 14 Blade flap Mx (Sensor 29) and edge My (Sensor 30) Leq (m=12) versus wind direction (WD) (LEQ_REF_S_29.emf, LEQ_REF_S_30.emf).

4.3 Wind farm layout test case

To illustrate the calculation of wind farm lifetime equivalent loads, a 3x3 wind farm layout with nine 5 MW turbines was investigated (Figure 15).

Figure 16 and Figure 17 show the wind directional distribution of the equivalent load relative to the reference turbine results (Figure 12 to Figure 14), so that a value of 1 equals the loading of the reference turbine, whereas a value larger than 1 implies that the turbine is in wake and therefore exposed to higher loading.

For Turbine 1, which is in the south-west corner of the wind farm (Figure 16), it can be seen that the turbines, 2, 4, 8, 5 and 6 cause wake operation leading to higher loads. Most dominant contributions come from turbine 2 and 4. The tower base moments and the blade flapwise moment show the biggest influence, whereas the remaining sensors are less affected, with the blade edgewise moment showing negligible influence.

For Turbine 5, which is in the middle of the wind farm (Figure 17), all the other turbines have influence on the loads, which results in a 'star' type of pattern corresponding to the geometrical layout of the wind farm. Again, the blade edgewise moment shows little variation with wind direction.

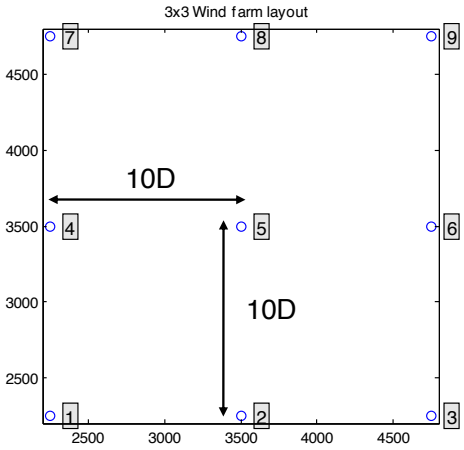

Figure 15 Wind farm test case with turbines positioned in a 3x3 configuration. Turbine numbers start with 1 at the lower left corner and end with 9 at the upper right corner.

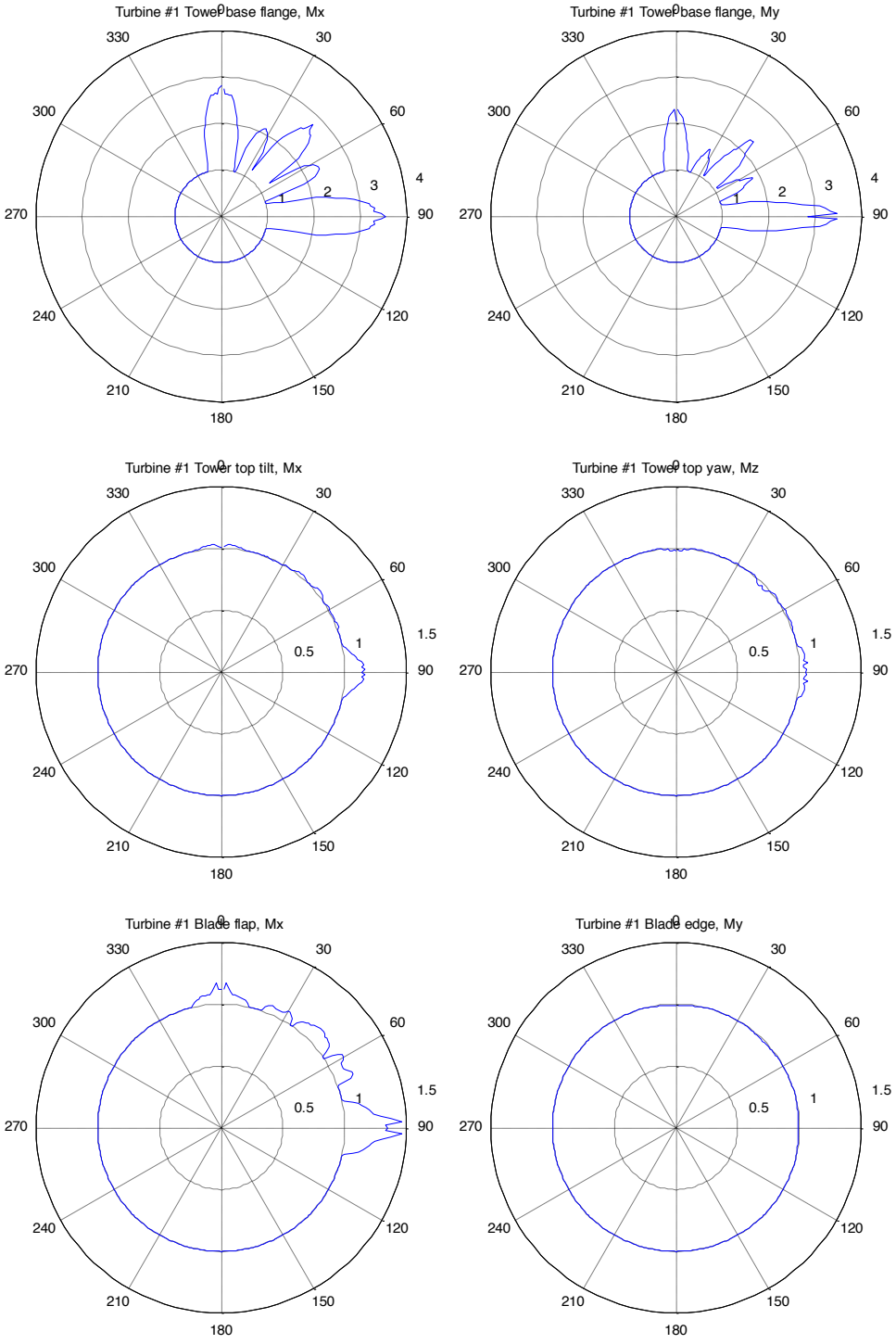

Figure 16 Turbine 1 L_{EQ} loads versus wind direction (WD) (LEQ_T_1_S17.emf, LEQ_T_1_S18.emf, ...)

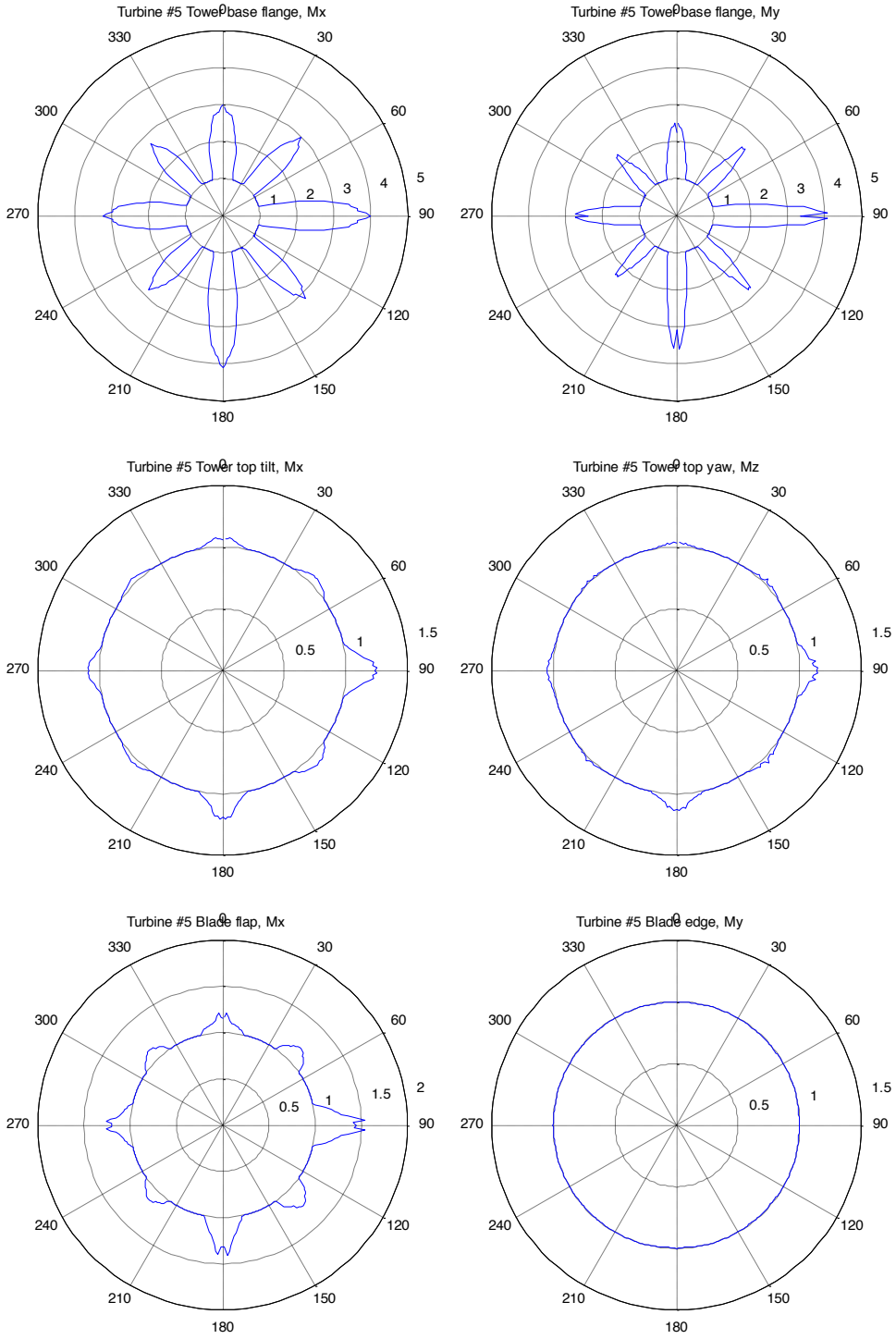

Figure 17 Turbine 5 L_{EQ} loads versus wind direction (WD) (LEQ_T_1_S17.emf, LEQ_T_1_S18.emf, ...)

Figure 18 shows contour plots generated on basis of the lifetime equivalent loads for the individual turbines. This is to visualize how the loads change within the wind farm between the turbines. It can be seen that Turbine 5 in general has the highest loads, whereas Turbine 1 and 7 have the lowest loads. Turbine 5 is in wake for a considerable amount of its lifetime, which explains the higher loading. Even though Turbine 1 and 7 have free inflow resulting in a higher mean wind speed for a larger proportion of their lifetime, this does not counterbalance the wake operation of Turbine 5, except for the blade edgewise moment, which is slightly higher for

Turbine 1 due to the higher mean wind speed. The biggest difference is clearly seen for the tower base moments and the blade flapwise moment, whereas the tower top moments are more similar between the turbines.

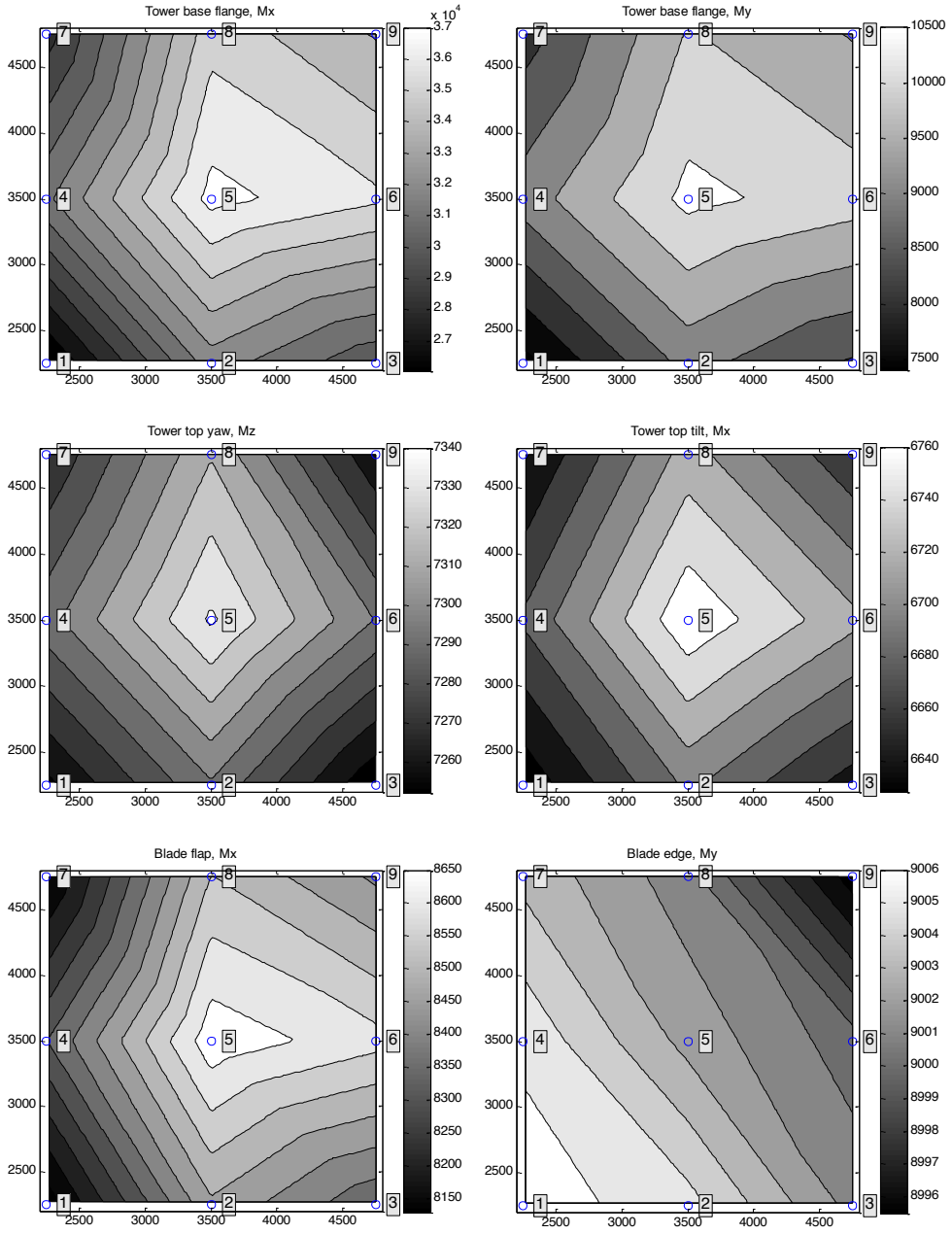

Figure 18 Wind farm overall L_{EQ} loads (WF_S17.emf, WF_S18.emf, ...)

4.4 Annual energy production

The annual energy production (TAEP) for a particular turbine is calculated by summing up the power contributions from the different wind speeds at the different wind directions taking into account the probability of each wind speed at each wind direction:

$$TAEP = \int P_{elec}(U)\, p(U) n_T dU \qquad (4)$$

where

$P_{elec}(U)$ is the electrical power at wind speed/wind direction case U;
n_T is the number of 10-minute sequences corresponding to 20 year lifetime ($6 \cdot 24 \cdot 365 \cdot 20$);
$p(U)$ is the probability for the load case U.

The summation for TAEP is done for all wind speeds in each wind sector giving a total number of contributions as the multiplication of the number of wind rose divisions, n_{WR}, and the number of wind speeds, n_{WS}:

$$TAEP = \sum_{j=1}^{n_{WR}} \sum_{i=1}^{n_{WS}} P_{elec}(U_{i,j}) p(U_{i,j}) n_T \tag{5}$$

Figure 19 shows the distribution of electrical power on wind directions for the reference turbine. It can be seen that this follows closely the wind rose from Figure 11, which is not surprising.

Figure 20 and Figure 21 show the annual energy production versus wind direction for Turbine 1 and Turbine 5 relative to the reference turbine, so that a value less than 1 corresponds to an energy loss due to operation in wake. The presence of upstream turbines can be clearly seen as small dips in power in the directions corresponding to the neighboring turbines. This is more pronounced for the Turbine 5 being in the middle of the wind farm compared to Turbine 1.

Figure 22 shows the contour plot of the overall wind farm TAEP showing a loss for the turbines, 5, 6, 8 and 9 being in wake more of the time compared to the other turbines. The low value for Turbine 9 clearly results from the high probability of being in wake. Also shown is the wind farm overall power distribution on wind directions, which follows the overall trend of the wind rose, but with smaller kinks corresponding to the rows in the wind farm at polar angles 0, 90, 180 and 270 deg and to less extend 45, 135, 225 and 315 deg.

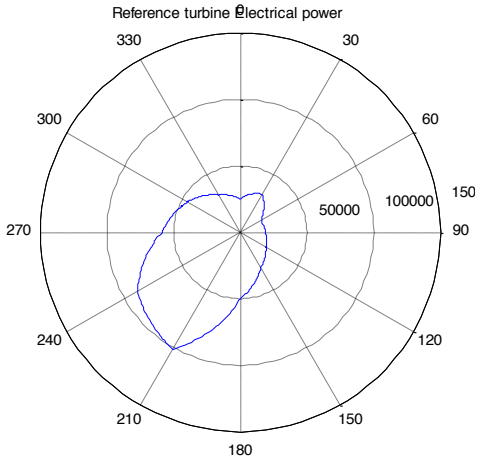

Figure 19 Reference turbine total annual energy production (LEQ_REF_S_88.emf)

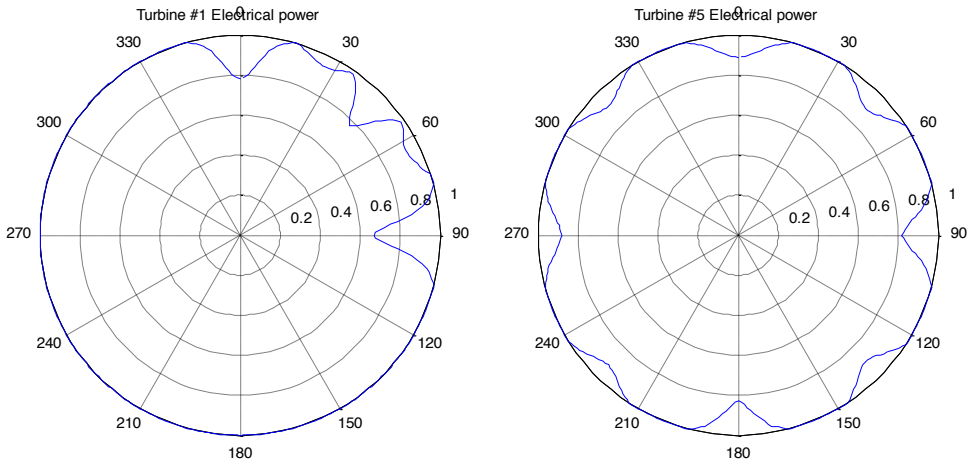

Figure 20 Turbine 1 (left) and turbine 5 (right) total annual energy production versus wind direction (WD) (LEQ_T_1_S88.emf, LEQ_T_1_S88.emf)

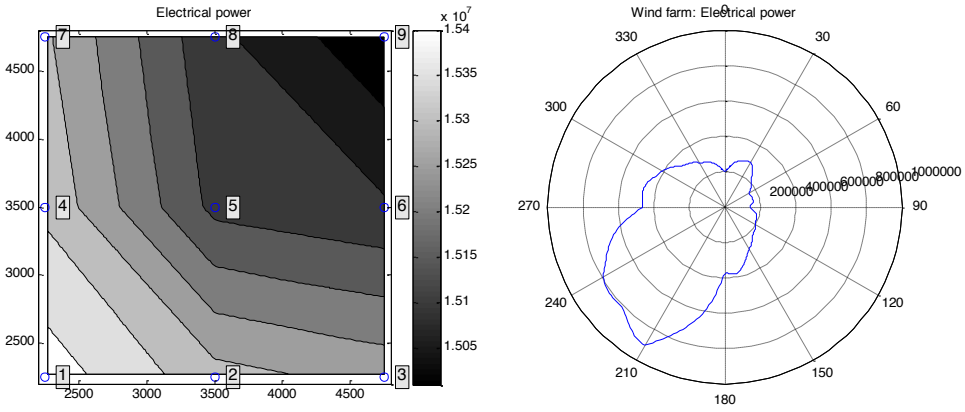

Figure 21 Wind farm overall annual energy production (left) (WF_S88.emf) and power distribution on wind directions (right) (WFDIST_S_88.emf)

4.5 Reducing computational time

The results in sections 4.2 to 4.4 were generated using a resolution of 1 deg for the wind direction and a resolution of 1 m/s for the wind speed. This results in 360×20 contributions for each turbine in a wind farm and thereby a considerable amount of computational time for a large wind farm. During an optimization, where a large number of different wind farm layouts are investigated, the use of a coarser resolution would result in significant savings of computational costs.

The consequence of using a coarser resolution for wind direction and wind speed was therefore investigated by repeating the calculations at various resolution levels; up to 12 deg for the wind distribution and up to 6 m/s for the wind speed. The error from using a coarser resolution was calculated for each turbine and each load sensor in the 3×3 wind farm layout, taking the finest resolution as reference point. Figure 22 shows the percentage error for each of the load sensors for the different turbines. The results are shown for the combinations of wind direction bin sizes 4 deg and 8 deg and wind speed bin sizes 4 m/s and 6 m/s, since these form the most interesting regime. It can be seen that a wind speed bin size of 6 m/s is in general not acceptable due to large errors on the tower base moments. Also, it can be seen that increasing

the wind direction bin size to 8 deg from 4 deg is causing the error on the tower base moments to exceed 5% for some of the turbines. It was therefore decided to stay at a wind direction bin size of 4 deg and a wind speed bin size of 4 m/s resulting in a time saving of factor 16 compared to the initial fine resolution.

It should be noted that for the 3×3 wind farm layout, some of the load sensors are not very sensitive to the resolution, which is due to the distance between the turbines of 10 diameters causing only little difference in some of the loads. At a denser spacing, the difference in loads would be more pronounced thus leading to an increase in the error from using a coarser resolution.

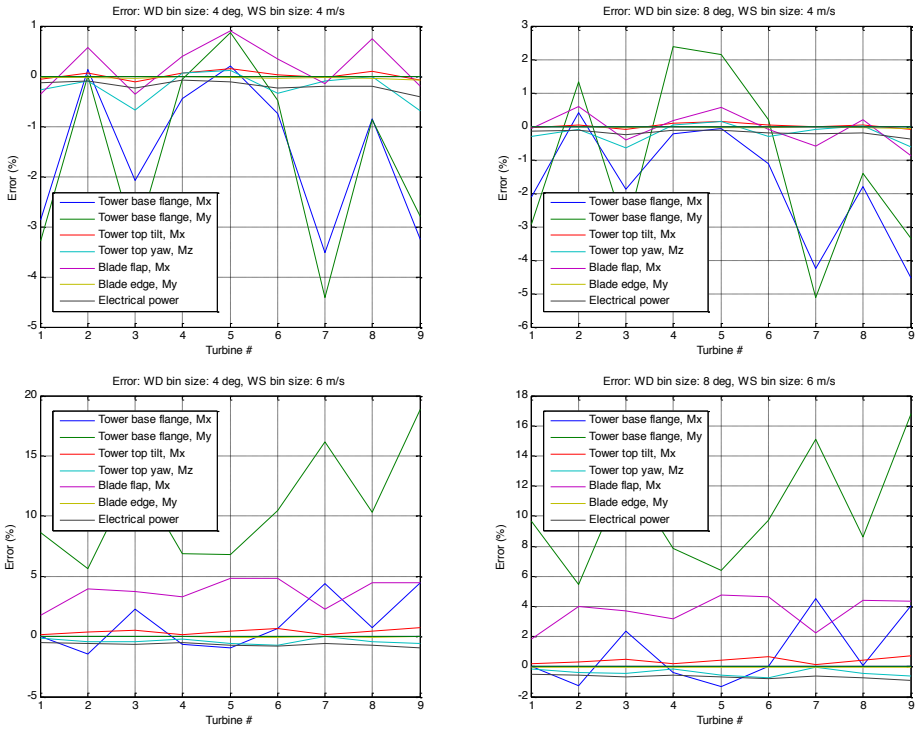

Figure 22 Percentage error for each sensor at each turbine when using coarser resolution for wind direction and wind speed (ERR_WD4_WS4.emf, ERR_WD4_WS6.emf, ERR_WD8_WS4, ERR_WD8_WS6).

4.6 Scaling of loads to different turbine sizes

The database should ideally be updated with load calculations for the specific turbine in question. If this is not possible, this section describes a first order approach to adapt the current load set to a different turbine size [TOPFARM final report].

The scaling of loads will only be valid for turbines having a similar power and load control and for turbines that are geometrically similar and of same concept as for the current load set. The scaling was simplified to depend on the rotor radius, R, and the rated power.

For the tower, we only take into consideration the aerodynamic loads, and we assume that the rotor load scales with R^2, while the moment arm scales with R when assuming that tower height scales with R for geometrically alike turbines. This makes the static tower moment to scale with R^3. We assume that the fatigue lifetime equivalent loads scale likewise.

For the blade, we distinguish between flap and edgewise moments. The edgewise moments are dominated by the blade mass and static moment, while the flapwise loads are dominated by the aerodynamic loading.

For the flapwise moment, the aerodynamic load scales with R^2. The blade chord, and obviously also the blade length, scale with R. In conclusion the static aerodynamic flapwise moment scale with R^3. As for the tower, we assume that the blade flap fatigue lifetime equivalent load scales with R^3.

For the edgewise moment, the blade mass scales with R^3 and the moment arm with R. Thereby the edgewise moment static as well as fatigue lifetime equivalent moments scale with R^4.

For the drive train and main shaft, the static moment scales with the rotor power, P, and we assume that this holds also for the lifetime equivalent loads.

Finally, the rotor power scales with the nominal power of the turbine.

Note that the placing of turbines in a wind farm is a relative exercise, where different configurations of turbines of the same make and size are compared. Therefore, the relative comparison of tower and blade loads will be independent on the actual turbine scaling with R. Consequently, the current load set can be used with confidence for other rotor sizes as long as only relative load differences are looked at, and as long as shaft moments and power are scaled with the nominal rotor power, P.

5 Cost function

The cost function is based on a general generic wind farm cost model developed for the TOPFARM project and described in detail in [14]. This model includes a financial balance between installation costs and operation costs that are held up against the value of the wind farm energy production. The cost model is build upon two governing principles: *relevance* and *relative cost basis*.

Only costs that are *relevant* to the optimizations problem are included in the cost model, in contrast to costs that are irrelevant. Relevant costs are costs that are variable and depending on the actual wind farm topology being optimized. Variable costs are costs of wind turbine foundations, price of cabling between turbines, costs of operation and maintenance, cost of energy production loss due to wake operation, etc.

Irrelevant costs are costs that are fixed because they are not influenced by the actual wind farm topology. This is in the context of the optimization only, since fixed costs obviously matter for the calculation of the total wind farm investment balance equation. Fixed cost are cost of planning and projecting of the wind farm, cost of the land available for the intended wind farm project, civil engineering costs to roads connecting the wind farm with the surrounding community (but not internal road infrastructure), price of cabling from the wind farm to the main grid (but not the internal grid infrastructure), etc. These are all costs that do not vary with the actual wind farm topology, as long as the number of turbines is kept constant.

Costs are evaluated on a *relative cost basis*. The optimization seeks to find the optimum wind farm layout applying mathematical concepts, which compare the actual wind farm topology with alternatives and thereby only needs the relative difference in cost for these different alternatives. It is therefore not necessary to model the total costs.

5.1 Financial balance

We have adapted the philosophy of only *relative expenses* being of interest in a wind farm optimization context, and we will expand this concept to include also considerations on the interrelationship between rate of inflation and relevant interest rates as done in [14]. The financial balance, *FB*, defined in [14] operates with a split of the total (variable) investment on consortium loans and consortium financial assets, respectively. For the present analysis we will consider the investment to be financed by loans only. Introducing two financial parameters – both referring to a one year period – the rate of inflation, r_i, and the interest rate that the wind farm consortium has to pay for loans (i.e. price of money in banks or by other investors), r_c.

Assuming interest of loans to be paid N_L times a year, the financial balance may thus be expressed as

$$FB = WP_n - C\left(1 + \left(\frac{r_c - r_i}{N_L}\right)\right)^{XN_L}, \tag{6}$$

with X is denoting the wind farm life time in years, and net value of the power production, WP_n, defined as

$$WP_n = WP - CD - CM \ , \tag{7}$$

where WP is the value of the wind farm power production over the wind farm lifetime, CD is the cost of fatigue driven turbine degradation, and CM is the costs of maintenance. For convenience, we have interpreted all operating costs (i.e. CD and CM) as referring to year Zero, with the implicit assumption that the development of these expenses over time follows the inflation rate, and that the inflation rate is the natural choice for the discounting factor transforming these running costs to *net present value*. We have also, through equation (6), implicitly referred the value of the wind farm power production over the wind farm lifetime, WP, to year Zero.

The power production and the loading of the individual wind farm turbines are obtained from detailed aeroelastic calculations. In the present optimization study we will base these on the load database described in section 4.1. We have set the inflation rate to r_i =2.5% p.a. and the interest rate to r_c =6.5% p.a. We have assumed a X=20 year payback time. We have not distinguish between UK and Danish electricity prices, and the price of 1kW was set to 0.05€.

5.2 Fatigue degradation and maintenance costs

The cost of (fatigue) degradation of the turbines is accounted for by linear writing off [14]. For a particular structural member, identified by S, the *mean* cost of fatigue load degradation is presumed proportional to the *mean* accumulated equivalent fatigue load, associated with a suitable component "hot spot", caused by turbine operation during the lifetime of the wind farm. We introduce the mean *relative degradation* as

$$D_S = \frac{L_{Sa}}{L_{Sd}} \ , \tag{8}$$

where subscript S referring to structural member S, and where L_{Sa} and L_{Sd} are the (mean) accumulated and the design equivalent fatigue load, respectively. Using equation (8), the *cost of degradation*, CD_S, is defined as

$$CD_S = P_S D_S \ , \tag{9}$$

where P_S denotes the price of the particular structural component.

In the formulation of maintenance costs we apply a probabilistic failure criterion. Assuming the component equivalent moment resistance to be described by a log-Gaussian distribution [14] the *cost of maintenance*, CM_S, related to the structural member S, is approximated as

$$CM_S = W_{R+1} \times P_{S_r} F\left(D_S; \mu_{S,(R+1)}, \sigma_{S,(R+1)}\right) + P_{S_r} \sum_{j=1}^{R} F\left(D_S; \mu_{S,j}, \sigma_{S,j}\right), \tag{10}$$

where P_{Sr} denotes the replacement cost (i.e. cost of the physical replacement and additional expenses originating from the derived production loss), R is the maximum number of allowable replacements defined by the designer, and W_{R+1} is a weight factor large enough to assure that more than R replacements is unfavorable for the optimal wind farm topology. $F(D_S; \mu_{S,j}, \sigma_{S,j})$ is the log-Gaussian cumulative distribution function (CDF) with distribution parameters μ_j and σ_j. The j'th distribution parameter set is related to the mean component resistance, $E[M_{Sr}]$, and

variance of the component resistance, $VAR[M_{Sr}]$, through the respective mean and variance of the relative degradation measure as

$$\sigma_{S,j} = \sqrt{Ln\left(\frac{VAR[M_{Sr}]}{j^2 M_{Sd}{}^2} + 1\right)}, \tag{11}$$

and

$$\mu_{S,j} = Ln(j) - \sigma_{S,j}^2 . \tag{12}$$

The costs of degradation, described in equation (9), and the costs of maintenance, described in equation (10), are straight forwardly generalized to all main components.

In this work, the design equivalent fatigue load, L_{Sd}, is defined in percent to the accumulated equivalent fatigue load, L_{Sa}, of a hypothetical solitary wind turbine (i.e. without wind farm wake effect). For this reason some components, like the gearbox and generator, which normally scale with the power output and would therefore have – under the current assumptions – a lower fatigue than for a solitary turbine, are here assumed to be part of the nacelle components.

For the purpose of demonstrating the optimization method, turbine component costs were estimated to be able to calculate *CD*. Figure 23 shows the used split of cost on the different main components. These costs were estimated on basis of [15] and [16]. In addition the cost driver dictating the degradation of each component was assumed. Using the numbers in Figure 23 implies that 70% of the turbine cost is variable and driven by changes in fatigue load. This is obviously a debatable assumption and for a specific wind farm design case, detailed knowledge of the turbines should be used to accurately estimate the cost figures.

Together with the identified cost driver, the replacement costs defined in Figure 23 are needed to estimate *CM*. Clearly the replacement costs should be different for onshore and offshore conditions due to the significantly higher logistic costs offshore.

Turbine component	Component cost relative to turbine (%)	Replacement cost relative to turbine (%)		L_{Sd} relative to the L_{Sa} of a solitary turbine (%)	Cost driver
		Onshore	Offshore		
Rotor	20	5	25	250	Blade root flapwise moment
Nacelle components	10	7.5	30	250	Nacelle (tower top) tilt moment, $Mx_{Nacelle}$
Gearbox & generator	20	7.5	30	250	Electrical power, P_{Elec}
Tower	20	10	50	250	Tower base over turning bending moment, Mx_{Tower}
Fixed part	30				

Figure 23 Costs distribution for wind turbine main component and cost drivers

The total turbine cost was set to 1 M€ per MW of installed power not including installation, foundation, project cost, etc.

5.3 Total investment costs

The variable part of the total wind farm investment costs, C, may according to [14] be expressed as:

$$C = CF + CI + CT + CE \ , \tag{13}$$

where CF is the cost of foundations, CI the cost of installation, CT the costs of civil engineering infrastructure, and CE denotes electrical infrastructure costs.

For onshore sites CI is in general variable in the sense that it depends on the accessibility of the individual wind turbine location, which in turn depends on the wind farm topology. For off-shore sites, the installation costs may depend on the water depth. In the present context we will assume that CI is constant. For the onshore case this is motivated by the fact that the onshore site is characterized by flat and homogeneous terrain. For the off-shore case we consider CI constant, because the water depths in question varies only moderately, and consequently the same installation equipment and effort in human resources is needed for all possible locations.

Civil engineering infrastructure denotes in the present context transportation infrastructure within an onshore wind farm (i.e. establishment of the necessary roads to access the turbines and enable installation of these). The cost of civil engineering infrastructure is in general a variable cost that depends on the topography of the terrain, the soil conditions, etc. However, as already mentioned, the onshore site in question is characterized by homogeneous conditions, and consequently CT can be considered as constant in the present context.

Based on the considerations above, for the optimization study of the Middelgrunden and Coldham/Stags Holt wind farms, the variable part of the total wind farm investment costs may be simplified as

$$C = CF + CE \tag{14}$$

5.4 Foundation costs

Cost of foundation is in general a variable cost in the sense that it depends on the soil conditions and/or the water depth at the location of each individual turbine. For the present study we will, however, consider CF as constant for the onshore case, as homogeneous terrain conditions prevail. For the *onshore case*, the wind farm investment costs may therefore be further simplified by discharging cost of foundation. For the *off-shore case* we will assume that the investment costs depends on water depth only, and that CF can be expressed as

$$CF = \sum_{i=1}^{N_T} CT_i\left(x_i, y_i\right), \tag{15}$$

where CT_i is the cost of foundation for the i'th wind turbine, (x_i,y_i) is the position of the i'th turbine in a Cartesian grid, and N_T is the total number of turbines in the wind farm considered. For the water depths relevant for the present off-shore case we will more specifically assume that CT_i depends linearly with the water depth as

$$CT_i\left(x_i, y_i\right) = CT_r + \Delta h\left(x_i, y_i\right) CT_g \ , \tag{16}$$

where the reference foundation cost CT_r equals 20% of the total turbine cost and refer to a reference water depth of 8 m, the gradient foundation cost pr. meter

deviation from the reference water depth, CT_g, equals 2% of the total turbine cost and $\Delta h(x_i,y_i)$ is the water depth at location (x_i,y_i) minus the reference water depth measured in meters.

5.5 Electrical infrastructure costs

??smal introduction to sub-sections ??

Cable considerations

The electrical cables used to connect wind turbines to the grid can carry different voltages. According to the voltage of the cable, a specific maximal number of wind turbines can be connected per cable.

These types of design limits are not considered in the present work. The idealized cables used in this analysis are assumed to be able to carry all the electricity produced by the wind turbines connected through them. However, this type of considerations could have a significant impact on the optimization process and the final optimal solution and should therefore be considered in future work.

Travelling salesman problem

The first approach proposed for grid layout is to consider the wind farm grid as a continuous line connecting all the wind turbines. In this approach, each wind turbine is connected to minimum one turbine and maximum to two. Finding the minimum length of this cable is a similar problem as the so-called travelling salesman problem, where a salesman has to go through different cities in various locations and try to reduce his travelling mileage. This is a well known mathematical problem, which becomes relatively complex to solve, when the number of locations becomes big. The brute force approach, where all the possible solutions are calculated, is a *O(n!)* problem (see [25]). There are various ways to solve this problem - some exact and some iterative solutions. In general the iterative solutions give a faster solution, but might not yield the best solution possible.

Several methods were investigated. The one that was selected for its computational speed performance is based on random permutations. The algorithm starts from a first guess, which could be the previously found solution. It then tests how the total length of the cable is affected by switching two random elements in the order of the turbines. If the switching has resulted in a positive change (i.e. a reduction in total cable length), then the new order is kept for the following iteration.

This is a heuristic, non-deterministic method. With enough iterations it should in theory converge to the best possible solution. However, as it is based on random numbers, there is no guaranty that the number of iterations needed to converge will be smaller than *O(n!)*. Moreover, each run of this algorithm, with a limited number of iterations, might produce different results, which will result indifferent cable costs for the same layout. This can in turn compromise the convergence of the optimization, as the algorithm may make wrong choices based on this cost function.

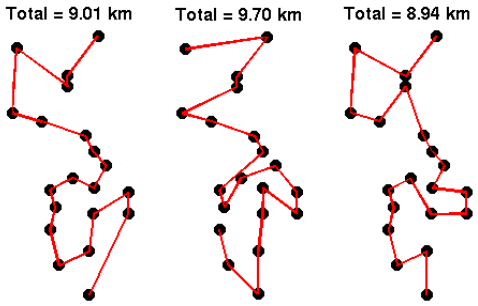

Figure 24 Different solutions of the travelling salesman method

Wind turbine clustering

Another approach, proposed to design wind farm grid connections, is to try to reduce the total cable length without the restrictions imposed on the traveling salesman approach. Thus in this approach, there is no limits on how many connections a turbine can have. It could also be argued that this approach is more close to real wind farm layouts. Beside this, the advantage of this method compared to the previous one is that there is an inexpensive deterministic solution to the problem.

The algorithm to find the optimum grid connection is decomposed in two phases (see Figure 25). In the first phase, each wind turbine is connected to its closest neighboring wind turbine. This creates some groups of turbines not necessarily connected to each others. The second phase is recursively reducing the number of groups of turbines by connecting them together until there is only one left that regroups all the turbines of the wind farm. For each group, the minimum distance between each turbine of the group and the turbines not belonging to the group is looked for. The minimum couple is then connected, and their respective groups of turbines are merged into one group.

Proving that this solution is the best possible is outside of the scope of this report. We can nonetheless say, that we have systematically observed that the total length of the electrical cable found with this solution is smaller or equal than the solution found with the travelling salesman algorithm.

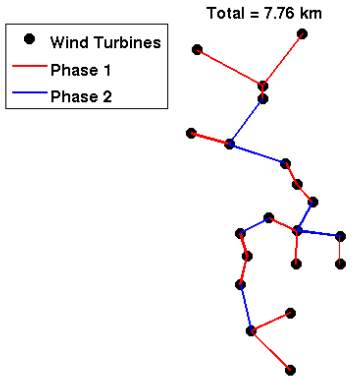

Figure 25 Grid clustering algorithm

Electrical Grid Costs

The electrical infrastructure costs associated with the wind farm includes cables connecting the individual turbines to the wind farm transformer, as well as expenses

related to the cable laying. These expenses will depend on the distance between turbines and the site conditions. The cost of the electrical infrastructure is modeled as

$$CE = \int_C c(x,y)ds \ , \tag{17}$$

where $c(x,y)$ is the cabling cost pr. running meter, C is the cabling trace connecting all turbines as described previously, and ds is an infinitesimal curve element on the trace. Note, that for a more detailed modeling, the best strategy is not necessary to base the cabling on the shortest possible cabling, but rather on the cheapest possible cabling. This in principle involves an embedded cabling optimization problem within the overall topology optimization problem and will be left for future studies. As indicated we decompose $c(x,y)$ as

$$c(x,y) = c_c(x,y) + c_l(x,y) \ , \tag{18}$$

with $c_c(x,y)$ being the cable cost pr. running meter, and $c_l(x,y)$ being the cable laying cost pr. running meter. Figure 26 shows the assumed prices for cable costs [26]:

In DDK / m	**Offshore??**	**Onshore??**
Cable	2000	1000
Installation	3000	1000
Total	50000	2000

Figure 26 Assumed prices for cable costs [26].

6 Optimization tool

It is the purpose of the optimization tool to alter the wind farm layout, so that the financial balance is maximized. In the current work, the Risø in-house code, HAWTOPT, was used as the optimization engine. The HAWTOPT program has been developed at Risø National Laboratory from 1994 and onwards, and it is predominantly used for optimization of wind turbines, and in particular aerodynamic design of wind turbine rotors [17], [18] and [19]. HAWTOPT is a general purpose optimization tool with several different optimization algorithms as options.

In the present optimization context, the financial balance that results from the cost functions becomes the objective function, with the wind farm layout being described as design variables. Technically, the financial balance multiplied by -1 is the objective function, which is by convention minimized. The constraints are then defined to limit the domain spanned by the design variables into a feasible region. Constraints are both explicit limits on the individual wind turbine coordinates as well as integral values resulting from calculations in addition to the cost function. These could be maximum allowable turbine loads, minimum distance between turbines, distance norm to wind farm allowable boundary, power quality, etc.

Figure 1 from Chapter 2 showed the overall concept for the interfacing between Matlab and HAWTOPT. The optimization problem is defined within Matlab, and during the optimization Matlab is acting as the working horse of the optimization. This means that a new design vector (i.e. a new wind farm layout) is generated by HAWTOPT and subsequently passed on to Matlab. Matlab then calculates the cost function, which is returned to HAWTOPT. As the optimization process is iterative, a significant number of cost function evaluations are needed before the optimization is completed, thus resulting in an optimized wind farm layout.

6.1 Optimization algorithms

The HAWTOPT code includes four different optimization algorithms:

1. The Method of Feasible Directions (MFD) is a search direction method using Steepest Descent and Conjugate Gradient. If constraints are active, the MFD principle is applied to move the design point along the constraint. The Golden Section method is used to find the step length, and quadratic refinement is applied to find the new design vector [20], [21];
2. The Sequential Linear Programming (SLP) method is linear program within a linear sub-space of the design space. Move-limits are applied in all dimensions to ensure smooth convergence. The move-limits are adaptive and automatically adjusted according to the convergence toward an optimum [21];
3. The Simple Genetic Algorithm (SGA) is a genetic algorithm based on the original work of Goldberg, in which the design variables are converted into chromosomes (binary strings). Using an analogy to the theory of evolution, parents create children by use of the genetic operators, crossover and mutation. Automatic Fitness scaling is used, and constraints are included using a penalty formulation [22];
4. The Simulated Annealing (SA) method is a global optimisation method that distinguishes between different local optima. Starting from an initial point, the algorithm takes a step and the function is evaluated. When minimising a function, any downhill step is accepted and the process repeats from this new point. An uphill step may be accepted. Thus, it can escape from local optima. This uphill decision is made by the Metropolis criteria. As the optimisation

process proceeds the length of the steps decline, and the algorithm closes in on the global optimum. Since the algorithm makes very few assumptions regarding the function to be optimised, it is quite robust with respect to non-quadratic surfaces. The user can adjust the degree of robustness [23].

For the current work, all 4 algorithms are available. However, the most suited ones are the simple genetic algorithm (SGA) and the sequential linear programming (SLP).

In the present study, we will take advantage of the global nature of the SGA algorithm. The global nature of the SGA algorithm allows a clever mapping by transformation of the wind farm *x*-*y* domain into a single parameter. This will be utilized to reduce the number of design variables and to better match the philosophy of the SGA algorithm forming chromosomes on basis of the design variables.

The SLP algorithm is gradient based and therefore sensitive to finding a local optimum. However, it is very robust and capable of handling constrained optimization effectively. It is therefore well suited to refine an optimum arrived at by the SGA algorithm. In this way it is possible to take advantage of using a coarse discretization of the SGA design variables, and then subsequently to rely on the SLP algorithm to refine the solution.

The present approach will therefore be to start an optimization with the SGA algorithm and when this has converged, to refine the solution by using the SLP algorithm.

6.2 Wind farm layout concepts

Keeping the number of design variables as low as possible is key to keep the computational costs at a minimum, since more design variables slows down convergence and requires more objective function evaluations.

There are three general different approaches to map the wind farm layout into design variables:

1. Defining a structured and regular pattern for the turbines. This can be done by using a structured grid, for example as rows and columns with fixed spacing but also other types of structured patterns as it is shown in [24]. In this way, the number of necessary design variables can be reduced substantially.

2. Using the unstructured turbine *x* and *y* coordinates directly as design variables, thus resulting in two design variables for every turbine.

3. Using a transformation of the wind farm *x*-*y* domain into a single parameter, as it is explained in more detail below. This has the advantage that turbines cannot end up outside of the domain, and therefore it is not necessary to define constraints, to make sure that turbines stay in the feasible region. Especially the SGA method and other native unconstrained methods will benefit from this by avoiding the use of a penalty function. This will increase the convergence rate.

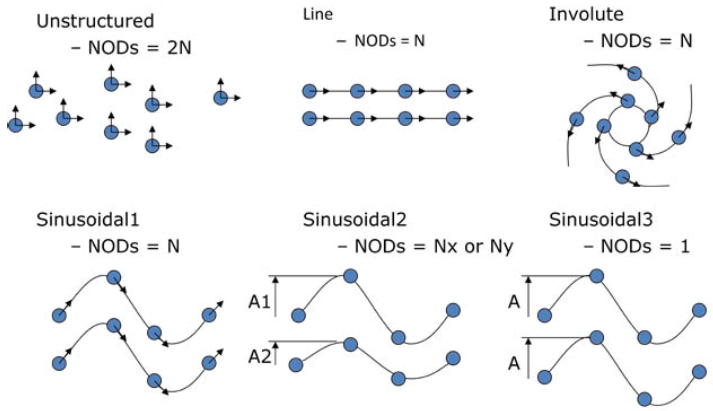

Figure 27 Wind farm layout concepts with minimum use of design variables from [24]

It was not the purpose of the present work to go deeper into structured and regular patterns, since this was investigated in [24]. An example of a regular turbine pattern, taken from [24], is shown in Figure 27, where the unstructured approach (top/left) is compared with various regular patterns. It is evident that the imposing of a structured pattern has the advantage of reducing the number of design variables significantly and thereby reducing the computational costs. But, it also evident, that a structured approach constrains the degrees of freedom in arriving at an optimum depending on the actual site in question. An off-shore site with an irregular sea bed will likely not fit well to a structured layout, whereas a regular flat sea bed will likely fit a structured approach.

In the present work a combination of unstructured *x*-*y* design variables for each turbine will be used together with the SLP algorithm, whereas for the SGA algorithm, a transformation will be used. A grid will be defined inside of the feasible domain, and a single parameter will be used to identify the location of each turbine on this grid.

6.3 Position constraints

HAWTOPT handles multiple objectives by making a compound objective function as the weighted sum of individual objectives. By convention, the optimisation objective is always minimised. Constraints are always defined as either $g <= g_0$ or $g >= g_0$, not $g = g_0$. Hence, either a minimum and/or a maximum right hand side value has to be specified to each constraints. Constraints are internally handled as either $g - g_0 <= 0$ or $-g_0 - g <= 0$.

For the SLP algorithm, the mathematical formulation directly includes the constraints as they are defined. This is not the case for the SGA algorithm, which is only capable of handling constraints directly on the design variables through the mapping approach. Indirect or integral constraints need to be added to the objective function as a separate penalty function.

Two types of position constraints are enforced in this work: the wind turbine absolute position inside the boundaries of a region; and the relative position of two turbines in the farm, which should not be located closer than one rotor diameter. They are enforced differently in the SGA and in the SLP methods, respectively.

Domain boundaries

Some external factors can limit the possible locations of the wind turbine (e.g. ship routes, bird migration path, protected areas) in the wind farm optimization process.

For this reason it is necessary to be able to constrain the possible positions of the wind turbines. In this work the boundaries of the domain are defined by a polygon. Depending on how the design variables are defined, the boundaries of the domain are enforced differently. The SLP algorithm uses unstructured design variables for each of the possible iterative displacements of the turbines. To restrain the displacement of the turbines, a norm is created that calculates the distance between each turbine and the domain boundaries. If all the wind turbines are within the domain, then the norm returns the distance between the boundary and the closest wind turbine. If one or more wind turbines are outside the boundaries, the norm sums the negative distances between the boundary and the outlier wind turbines. The constraint is therefore defined in terms of this norm, enforcing the optimization algorithm to keep it positive.

As the SLP algorithm is a gradient based method, it is sensitive to discontinuous variables and would therefore react inappropriately to a binary norm (inside/outside). The advantage of the introduced norm is, that it is "gradient friendly" The SLP algorithm knows in which direction, it needs to change the design variables to increase the norm.

The SGA algorithm is, however, not very efficient with constraints due to the penalty formulation that is necessary. A more effective method is therefore to limit the possible layout candidates directly, by defining the design variables as an index on a list of points located inside the boundaries of the domain (see Figure 28).

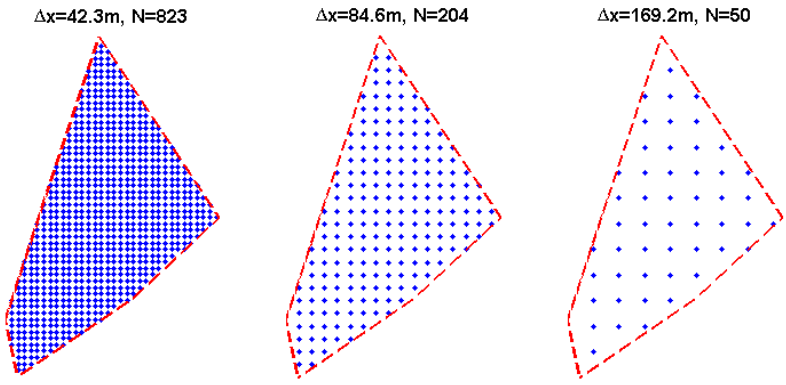

Figure 28 Discretization of the domain with different spacing

The advantage of this approach is that the wind turbine positions are automatically bounded inside the polygon domain. There is therefore no need to use a constraint on the wind turbine position. Furthermore it is possible to control the spacing between the possible locations, and consequently limiting the number of possible wind farm layout N_F to

$$N_F = \prod_{i=1}^{M} (N_L - i), \tag{19}$$

where M is the number of turbines, and N_L denotes the number of possible turbine locations. The spacing of the imposed grid is therefore directly linked with the speed of convergence of the genetic algorithm. Moreover, this approach results in a number of design variables equal to the number of turbines, which is reducing by a factor of two the number of combinations and consequently speeding up further the convergence.

This type of design variable definition would perform poorly with a gradient based method, as it would only allow discrete 1D displacement of the wind turbines in the

direction of the indexing. However, a global approach such as the genetic algorithm in SGA is not affected by the indexation of the positions.

Minimum Distance between Wind Turbines

There is a practical minimum distance, under which two wind turbines are too close to each other to operate under normal conditions. For instance, two wind turbines next to each other cannot operate, if they are positioned at a distance smaller than one rotor diameter from each other. Therefore there is a need to impose this constraint to avoid unrealistic solutions (e.g. when two turbines are located at the same position). As for the domain boundaries, this type of constrain is enforced differently for the two involved types of optimizations algorithms.

For the gradient based algorithm, the approach is to define a norm quantifying the distance between each turbine and its closest neighboring turbine. Similarly to the domain boundaries norm, this norm is positive when all distances between turbines are larger than the minimum distance (in this work set to one rotor diameter). In this case, the norm returns the minimum distance between two turbines in the wind farm layout. In the case where two or more wind turbines are violating the constraint, the norm returns the sum of all the (negative) distance exceedances associated with pairs of turbines that fail to meet the requirement. The mathematical expression of the norm is given as follows

$$\text{Norm} = \begin{cases} \min_{i,j}(\overline{WT_i - WT_j}), \text{ when no turbine fail} \\ \sum(\overline{WT_i - WT_j} - MinD), \quad \forall(i,j) \in \text{Failing Turbines} \end{cases} \tag{20}$$

Similarly to the SLP domain boundary norm, this norm is "gradient friendly", as it shows in which direction the optimization algorithm needs to move the turbines to increase the norm.

As mentioned previously, the SGA algorithm is not behaving well with constraints. For this reason, a different approach is taken for the SGA algorithm. It is assumed, that if two wind turbines are located under the minimum distance allowed, one of the wind turbines is not operating. This reduces the power production of the wind farm and therefore the energy efficiency of the wind farm. As all the other costs are assumed unchanged, this approach has the same effect as a penalty function. However, this approach is not "gradient friendly" and is therefore inappropriate for the SLP algorithm.

6.4 Optimality and convergence

The likelihood of a successful optimization is highly dependent on a proper selection of the optimization algorithm and in turn a proper definition of the settings for the particular algorithm. It requires a good portion of user experience to obtain a properly converged solution.

For the SGA related mapping of the feasible domain, a grid size of approximately 1000 grid cells was used, so that each turbine could potentially be located at the corresponding 1000 different positions within the wind farm feasible domain. This gives a chromosome length of 10 bits per turbine.

For the SGA algorithm, the following parameters need to be defined:

1. The size of the population, being the number of individuals defined in each generation. Note that one objective function evaluation is needed for each individual in each iteration. A population size of 20 was used in this work;
2. The likelihood of crossover, being switching over of chromosomes when mating individuals during the selection for the next generation. A crossover likelihood of 70% was used in this work;
3. The likelihood of mutation, being when an arbitrary? single bit of a chromosome is switched to introduce randomness into the solution. A mutation likelihood of 2.5% was used in this work;
4. The number of individuals from each generation that is allowed to survive into the next generation. The best individuals are selected and passed to the next generation, to ensure that the best solution so far is kept in the population. In this work the two best individuals were kept;
5. Scaling of the fitness for each individual to prevent too much skewness in the selection of next generation, since this could favour premature convergence. Scaling was set to 2 on basis of recommendations in [22].

Note that the population size of 20 used in this work is very low compared to what others have used for genetic algorithms, for example in [3]. The risk of using a small population is premature convergence, and therefore likelihoods of crossover and mutation need to be set sufficiently high when using such a small population size.

Also, note that the mapping of the turbines is such that the number of turbines is fixed, and each turbine can end up at each grid point. This is in contrary to the approach of others, e.g. in [3], where each grid point can either be a turbine or an empty spot. Thereby the number of turbines becomes variable.

For the SLP algorithm, the following parameters need to be defined:

1. The size of the displacement? limits, which is used to limit the allowable change for each of the design variables at each iteration. The displacement? limits are defined as a percentage of the defined minimum and maximum values for each design variable, and displacement? limits were in this work initially set between 0.625% and 2.5% depending on the problem;
2. The minimum displacement? limits, which is needed when using adaptive displacement? limits, so that the size of the displacement? limits cannot become smaller than this value. The minimum displacement? limits was set to 0.01%. However, this is of little practical importance;
3. The number of function evaluations needed before displacement?limits are automatically adjusted. The algorithm calculates the moving average of the objective function over the defined number of function evaluations, to detect if convergence is not smooth, and if this is not the case, displacement? limits will be reduced.

Note that in the present work, with up to 40 design variables and several integral constraints, convergence was very critical, and the optimum size of displacement? limits varied between problems. The size of the displacement? limits requires some tuning. If displacement? limits are set too high, convergence will be destroyed, due to the error made from the linearization around the present wind farm layout. Some of the design variables can end up outside of the feasible region, and constraints can be violated. This will show up as kinks in the convergence revealing a non-optimum setup. If displacement? limits on the other hand are too small, convergence will be smooth, but too many iterations will be needed before the optimum solution is found. This will show up as a very smooth and likely linear convergence, indicating that move limits could be increased.

When using a two step strategy with an *initial optimization* using the SGA algorithm and then subsequently *warm starting* on the optimization result with the SLP algorithm, the number of iterations needed for the two algorithms will be very different. The SGA algorithm converges very slowly and typically requires several orders of magnitude more iterations compared with SLP algorithm. A typical setup for the present work was to run between 500 and 1000 iterations using SGA algorithm followed by only between 20 and 30 iterations with SLP algorithm.

7 Optimization test cases

It is the purpose of this chapter to perform a sanity check and to demonstrate the capabilities of the TOPFARM optimization tool. This is done by investigating the sensitivity of annual energy production (AEP) to the different elements of the objective function.

Two different wind farm layouts will be used as test cases:

- A 3×3 wind farm layout similar to the one described in section 4.3 with nine 5 MW wind turbines;
- A 2×3 wind farm layout similar to the one introduced above, but with the middle row removed and hence including only six 5 MW wind turbines.

Figure 29 shows the 3×3 wind farm layout together with the wind rose used in the optimization.

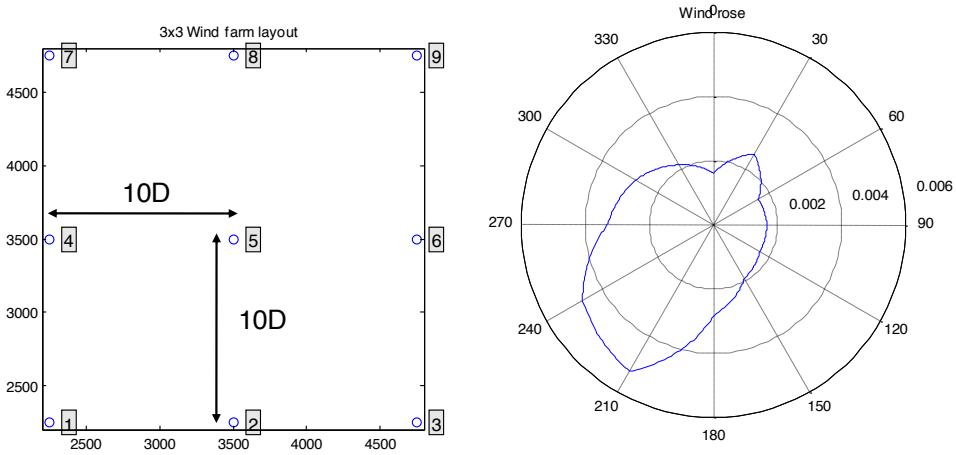

Figure 29 Initial wind farm configuration (left) and wind rose used as input for the optimization (right)

7.1 Maximum AEP for 3x3 wind farm test cases

All 9 turbine x and y coordinates were defined as design variables with maximum annual energy production as the optimization objective. Two optimizations were run:

1. The sequential linear programming algorithm (SLP) for 50 iterations using adaptive displacement? limits with an initial value of 2.5% of the feasible domain ??how to compare areal with distance??;
2. The genetic algorithm (SGA) for 50 iterations followed by an SLP optimization for refining the result by warm starting from the result of the SGA algorithm. A population of 20 was used with both crossover and mutation operators set active. Afterwards, 45 iterations were run using the SLP algorithm to refine the optimization result. Each design variable was represented by an 8 bit chromosome.

The results from the SLP optimization are shown in Figure 30, which shows the wind farm layout overlaid by AEP contour lines. It can be seen that the individual turbines were in general moved away from each other, and further that the turbines were moved away from the initial grid pattern, so that turbines are no longer standing strictly on lines. However, the initial configuration is still recognizable.

Figure 30 also shows the convergence of the objective function versus the number of iterations carried out. The convergence was stable, and the optimum value is found after approximately 25 iterations. Table 1shows the AEP in percentage of the solitary reference turbine. It can be seen that the overall wind farm performance was improved by 1.5%, mainly resulting from the new locations of turbines 5, 6, 8 and 9, since these were moved further away from the upstream turbines 1, 2, 3 and 4 in the dominating wind direction regime.

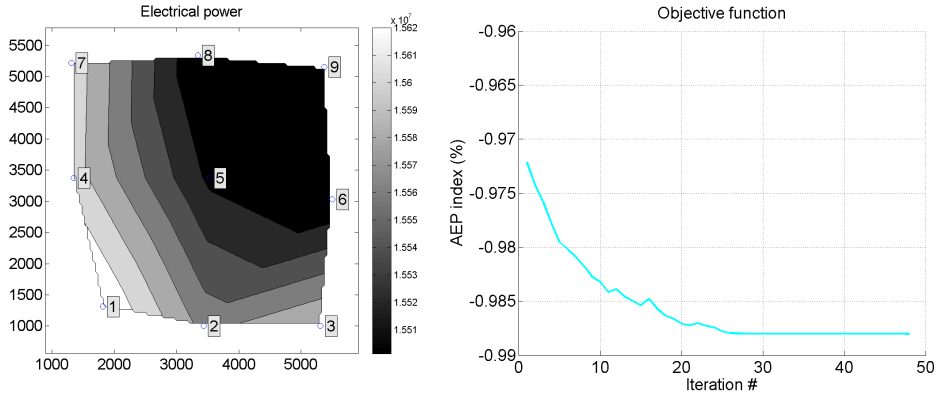

Figure 30 Optimum configuration and optimization convergence versus number of iterations (SLP optimization)

Figure 31 shows the results from the combined SGA/SLP optimization. It is evident that the global approach used by the SGA algorithm caused a significant change in the wind farm layout, so that the optimization result no longer resembles the initial configuration. The convergence of the objective function versus the number of iterations carried out shows that the SGA method converges slowly, and that improvements in the objective function appear as jumps rather than continuously due to the genetic principle used. It can also be seen, that the use of the SLP algorithm to refine the optimization result is successful. If the SGA optimization, however, had run for more iterations, it is likely that the change from the SLP optimization would have been less.

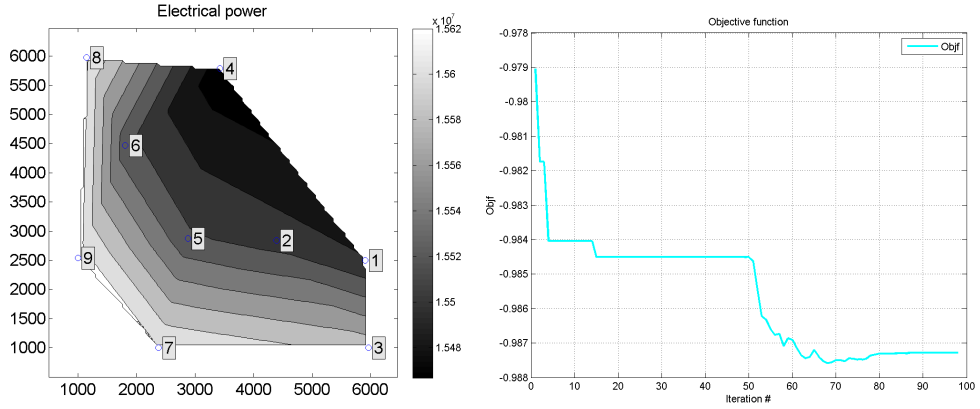

Figure 31 Optimum configuration and optimization convergence versus number of iterations(SGA optimization with SLP refinement)

Table 1shows a total AEP improvement of 1.5%. Note that it does not make sense to compare the change in AEP on the turbine level because of the significant difference from the initial configuration.

		SLP optimization		SGA optimization	
Turbine	**Initial AEP**	**Final AEP**	**Improvement**	**Final AEP**	**Improvement**
1	98,50%	99,25%	0,74%	98,36%	-0,14%
2	97,74%	98,82%	1,08%	98,41%	0,68%
3	97,69%	99,00%	1,32%	98,94%	1,25%
4	97,85%	99,05%	1,20%	98,14%	0,28%
5	96,54%	98,45%	1,91%	98,50%	1,97%
6	96,48%	98,36%	1,88%	98,52%	2,04%
7	97,81%	99,08%	1,27%	99,12%	1,31%
8	96,50%	98,36%	1,86%	99,13%	2,63%
9	96,08%	98,47%	2,39%	99,18%	3,10%
Average	**97,24%**	**98,76%**	**1,52%**	**98,70%**	**1,46%**

Table 1 Individual turbine annual energy production relative to the solitary reference turbine for SLP and SGA optimizations. ??refererer begge resultater i denne model til delelementerne i SGA/SLP approachen??

The above optimization results verify the integrity of the interfacing between HAWTOPT and the TOPFARM wind farm calculation modules as well as the HAWTOPT optimization tool usage of the SLP and SGA algorithms. Furthermore, the results show that the two different optimization algorithms may be combined for, on one side, to apply a global method, and, on the other side, to refine the solution to an optimum.

Both the above solutions show approximately the same improvement in AEP. The fact that there are more solutions raises a warning of risking to arrive in a local minimum. That fundamentally different solutions yield the same improvement in AEP furthermore means that the optimization problem is not closed very well, and it becomes clear/evident that maximizing AEP without looking at costs is not practical. The optimization problem will be better defined, when either constraints are applied to allowable loads, or costs or the financial balance are directly optimized, as it is demonstrated in the following sections.

7.2 AEP against electrical grid costs for 2x3 wind farm test case

This section investigates the relation between annual energy production and grid costs for the 2×3 wind farm test layout. Figure 32 shows the initial wind farm layout together with the initial electrical cabling. Note that the traveling salesman method was used to define the electrical cable path. The six turbine x and y coordinates were defined as design variables with maximum annual energy production as the optimization objective. The value of the grid costs (CG) was controlled by applying a ‘less than’ constraint to control the maximum allowable value. The SGA/SLP algorithm approach was used with settings equal to those specified in the previous section.

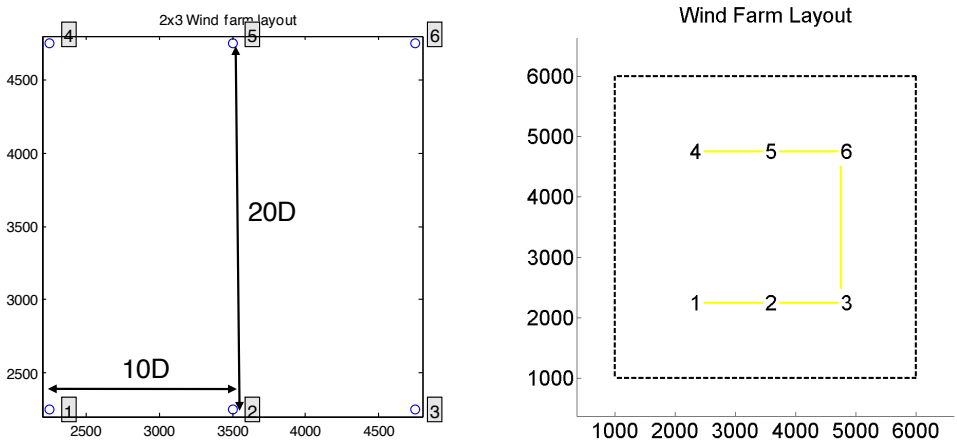

Figure 32 2×3 wind farm test case. Turbine numbers start with 1 at the lower left ending with 6 at the upper right. The initial cable path can be seen to the right

By running different optimizations with different constraint values for the grid costs, Pareto frontier could be obtained for the relation between grid costs (*CG*) and AEP and *CD*, respectively. Figure 33 shows the optimum AEP that can be achieved at different levels of *CG* (left) and the corresponding consequence on *CD* (right). It can be seen that constraining *CG* leads to a drop in AEP. This is not surprising, because reduced grid costs lead to shorter cable lengths and thereby an increase in wake operation due to the reduced distance between turbines. It can also be seen, that there is a non-linear relation between *CG* and AEP, so that in a certain regime a comparatively large reduction in *CG* can be obtained with only little reduction in AEP. However, when the grid costs are constrained to less than index 0.4, the drop in AEP appears to be significant.

The corresponding change in *CD,* when reducing *CG*, is that *CD* increases corresponding to the shorter distance between turbines, which leads to higher loads. However, for a *CG* index less than 0.4 a drop in *CD* appears. This can be due to the dynamic wake meandering flow model used in the load calculations. Having a very limited distance between turbines is not sufficient for the meandering to cause high fatigue loads for, e.g., the tower loads.

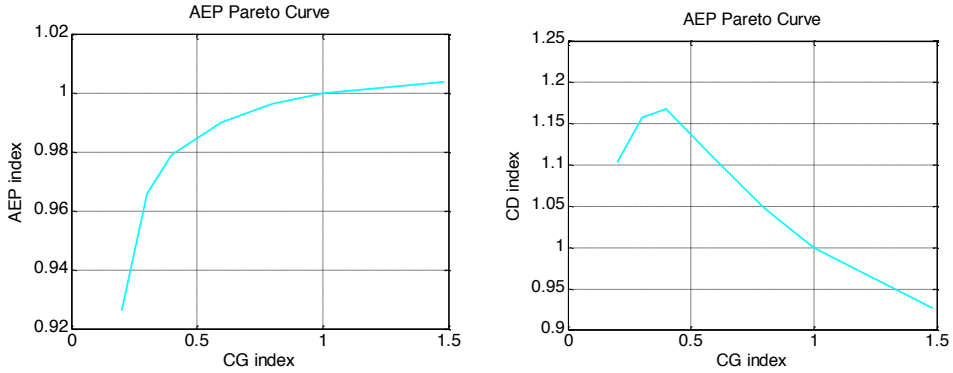

Figure 33 Pareto frontier for AEP versus grid connection costs (CG) normalized on basis of the initial configuration (left) shown with consequence on CD (right)

The optimum trade-off between *CG* and AEP has to be defined from the full financial balance, and it will depend on the actual case considered together with other significant costs that were not considered in this section. As a simple first order

approximation, it can be decided from Figure 33 that a *CG* index of 0.4 is a preferable choice. Picking this value, Figure 34 shows the corresponding optimized wind farm layout together with the energy production contour lines in the wind farm. The turbines are predominantly on a line facing the dominating wind direction from the wind rose, which seems sensible when seeking to minimize grid costs at minimum possible loss in AEP.

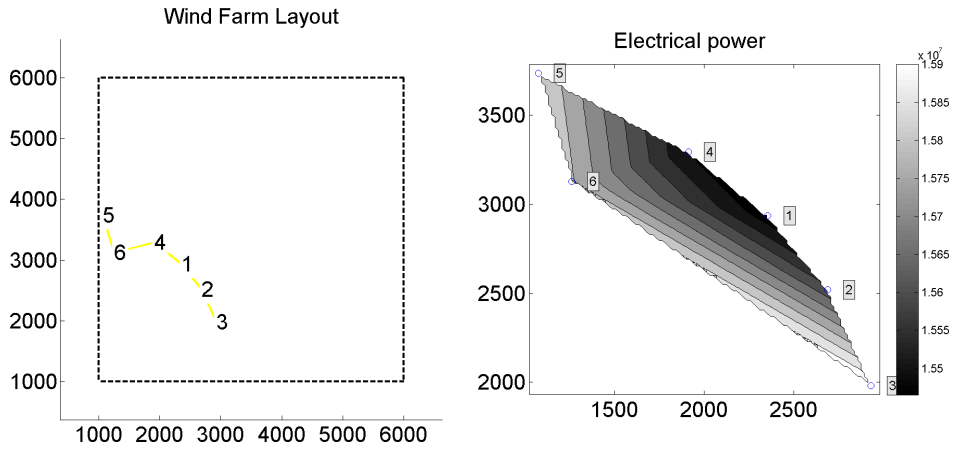

Figure 34 Optimum configurations at [CG = 0.4, AEP = 0.968].

The analysis in this section revealed the increase in AEP associated with reducing grid costs, and further that turbine degradation costs increase, when grid costs are decreased as a consequence of the reduced spacing between turbines.

7.3 AEP against foundation costs for 2x3 wind farm test case

This section investigates the relation between annual energy production and foundation costs for the 2×3 wind farm test layout. Figure 35 shows the initial wind farm layout together with a map of the water depth. The initial wind farm layout is placed in the center of the domain without special consideration on the water depth, which leads to higher foundation costs for the turbines 2 and 5 compared to the other turbines. Turbine x and y coordinates were design variables with maximum annual energy production as the optimization objective, and the value of the foundation costs (CF) was controlled by constraints. The SGA/SLP algorithm approach was used with settings equal to those specified in the previous sections.

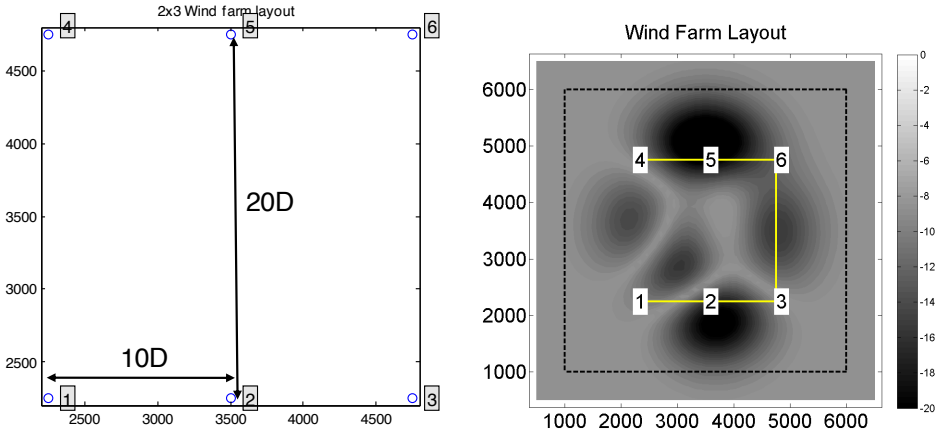

Figure 35 2×3 wind farm test case (left) shown together with sea depth levels (right).

Optimizations were run with different constraints on the foundation costs, and a Pareto frontier could thus be obtained for the relation between foundation costs (*CF*) and AEP. Figure 36 shows the optimum relation between AEP and *CF* (left) and the consequence on *CG* (right). It can be seen that AEP can be increased even though *CF* is reduced. When the *CF* index was reduced to below 0.65, a solution was no longer possible, which indicates that a certain minimum foundation cost was reached depending on the actual water depth contour map. As long as the domain allows the placing of turbines on shallower water, there is no consequence on AEP. This would of course be different, if only a smaller area of shallow water existed within the domain.

It can be seen in Figure 36 (right) that the reduction in *CF* is associated with a significant increase in *CG*. The need for putting the turbines at more shallow waters impose increased grid costs, due to the longer cables needed.

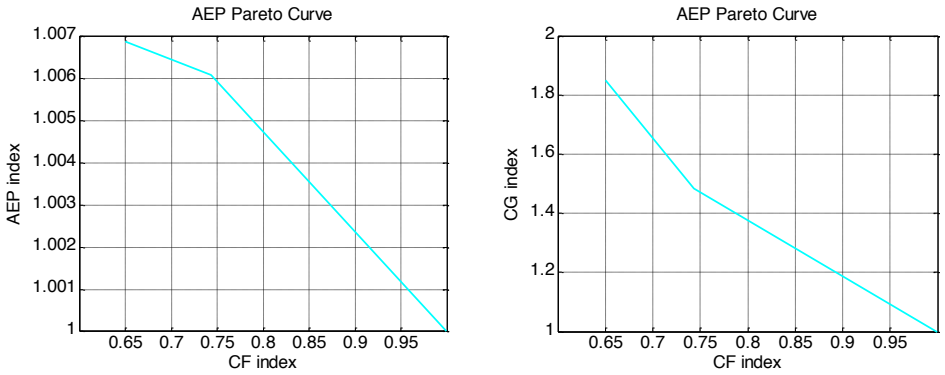

Figure 36 Pareto curve for AEP versus foundation costs (CF) normalized on basis of the initial configuration (left) shown with consequence on CG (right)

Figure 37 shows the solution at a *CF* index of 0.65. It can be seen that all turbines are placed away from large water depths, and that the entire domain is used to keep the turbines apart, since this increases AEP. The corresponding energy production contour map shows very little differences between the turbines, with turbines 1 and 3 having the lowest values. It can also be seen, that the cable length is significantly larger than the one for the initial design.

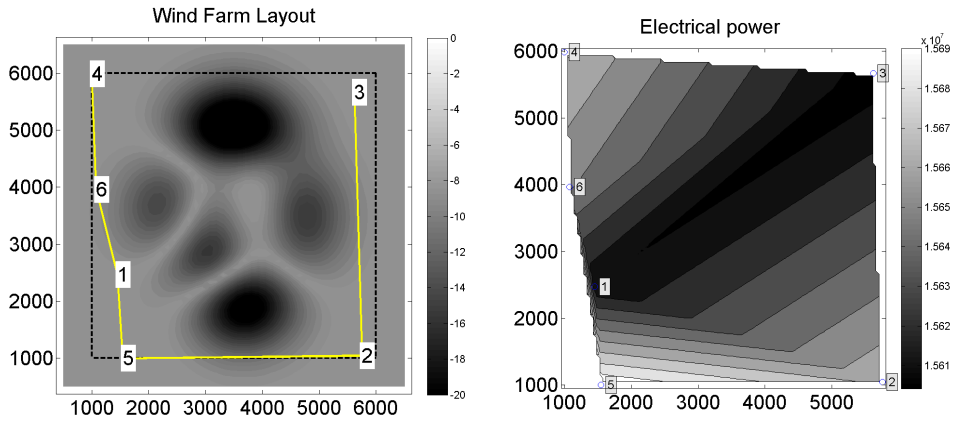

Figure 37 Optimum configurations at [CF = 0.65, AEP = 1.0069].

The results in this section revealed that foundation costs can be reduced with insignificant impact on annual energy production, as long as sufficient space is present in the domain. However, putting turbines on more shallow water is likely to increase grid costs.

7.4 AEP against turbine degradation for 2x3 wind farm test case

This section investigates the relation between annual energy production and turbine degradation costs for the 2×3 wind farm test layout (Figure 35). The optimization setup is equal to one in the previous sections.

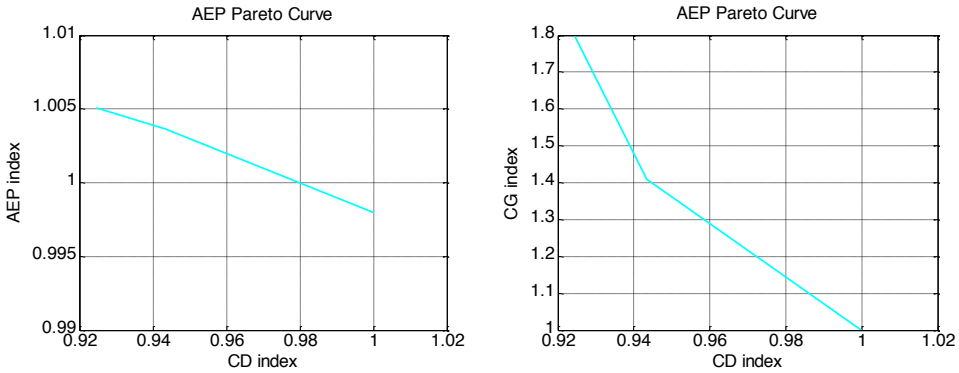

Figure 38 Pareto curve for AEP versus turbine cost degradation (CD) normalized on basis of the initial configuration (left) shown with consequence on CG (right)

Optimizations were run with different constraints on the turbine degradation costs, and consequently a Pareto frontier could be obtained for the relation between turbine degradation costs (*CD*) and AEP (Figure 38). However, a solution could not be obtained for a *CD* index value less than 0.925. This indicates that the turbine degradation is closely linked to AEP. Figure 38 also shows the relation between *CD* and *CG*, identifying a significant increase in *CG* when reducing *CD*.

Figure 39 shows the optimized wind farm layout corresponding to a *CD* index value of 0.925 together with the energy production contour plot. The results are somewhat similar to those of the previous section. The reduction in *CD* implies that the turbine spacing is increased, which in turn increases the grid costs.

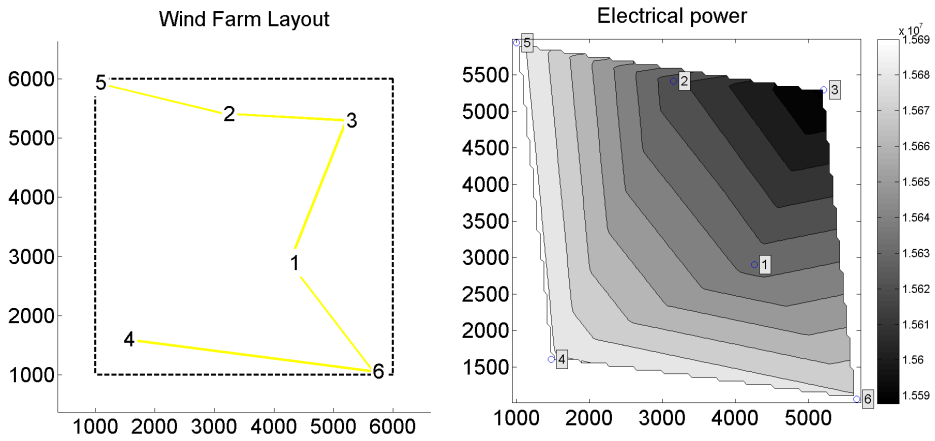

Figure 39 Optimum configurations at [CD =0.925, AEP = 1.005].

The results in this section demonstrated that turbine degradation is closely linked to annual energy production, and further that grid costs are significantly increased

when turbine degradation is reduced due to the higher spacing required between turbines.

7.5 Optimum financial balance for 2x3 onshore wind farm

It is the purpose of this section to find the optimum financial balance for the 2×3 wind farm test case at an onshore location. The onshore location implies that foundation costs are assumed to be independent on turbine location and therefore constant. These costs are therefore not a part of the financial balance, which consequently consists of costs of grid, turbine degradation and O&M balanced by energy production.

The initial 2×3 wind farm layout is shown in Figure 32. The six turbine x and y coordinates were defined as design variables with maximum financial balance as the optimization objective. Including all the costs directly in the financial balance eliminated the need for applying constraints. The SGA/SLP algorithm approach was used with settings equal to those specified in the previous sections. Alternative approaches using only SGA and only SLP were also tried out to challenge and find the most suitable optimization setup.

Figure 40 shows the optimized wind farm layout together with the energy production contour plot. It is evident that the turbines have departed completely from the 2×3 grid pattern, and they are instead forming a V-pattern facing the main wind direction from the wind rose (cf. Figure 29). The spacing between turbines has in general been reduced. It can also be seen, that the difference in energy production between the turbines is limited.

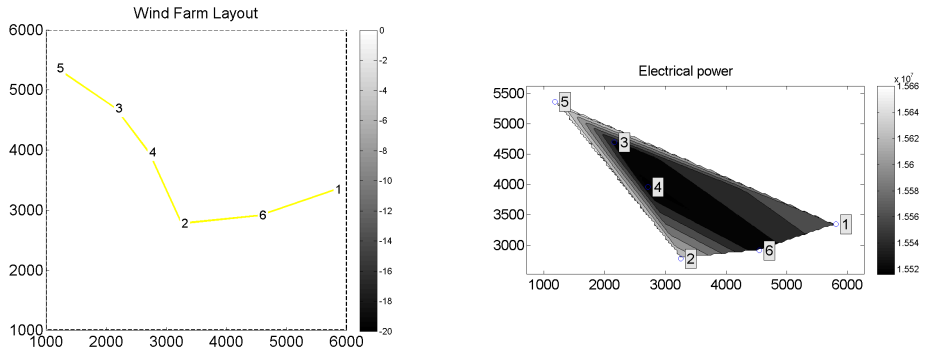

Figure 40 Optimization result (left) shown together with the energy production contour plot for the optimization result (right).

The overall improvement in the financial balance was 0.9 MEuro. Figure 41 shows the change in the different financial balance components, which caused the overall improvement. The change in the energy production value (WP) was slightly favorable, and grid costs were reduced at the expense of a slight increase in turbine degradation costs. The major cause of the overall improvement was the change in grid costs. It can be seen in Figure 41, that there were no significant differences in the included costs between the different turbines. The reason for turbine 1 and 5 having the lowest grid costs is, that they are at the end of the cable path.

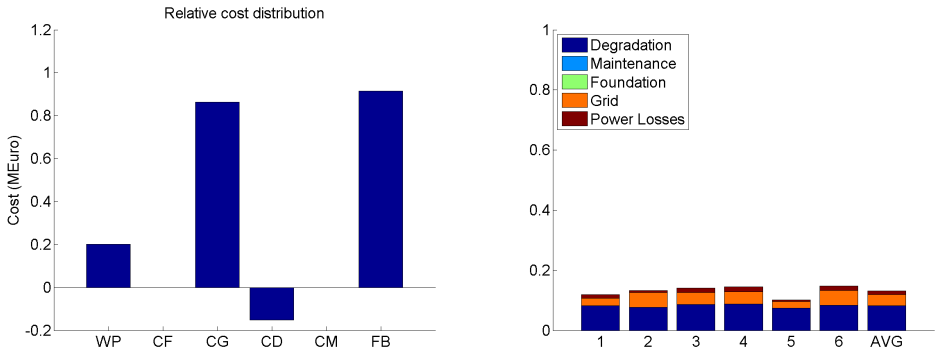

Figure 41 Change in relative costs for the optimization result (left) shown together with the financial balance breakdown for the individual turbines (right).

Figure 42 shows the optimized wind farm layout and the changes to the financial balance from using the SLP algorithm only. A total of 50 iterations were run. The resulting improvement of the financial balance is only a fraction of the result in Figure 41, and it is evident that this optimization results in a local optimum, where the initial configuration is still recognizable. This puts a question mark to the usage of stand-alone gradient based optimization approaches for wind farm layout, and emphasizes the need for involving a global method.

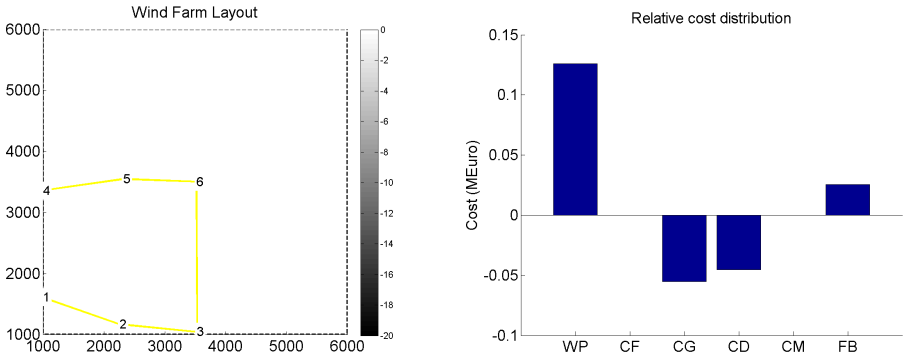

Figure 42 Optimization result (left) shown with changes in relative costs for the optimization result (right) from using the SLP algorithm.

Figure 43 shows the optimized wind farm layout from using the SGA algorithm only without subsequently refining the optimization result with the SLP algorithm. It can be seen that the result is quite similar to the results shown in Figure 41, but the resulting improvement of FB is approximately 0.1 MEuro less. This means that the combination of the SGA and the SLP algorithms was successful, and even though the major part of the optimization result is due to the SGA algorithm, the SLP refinement is still justified. In this section, 150 iterations were run using the SGA algorithm. Clearly, the need for the SLP refinement is depending on the number of iterations run with the SGA algorithm and the number of turbines in the wind farm.

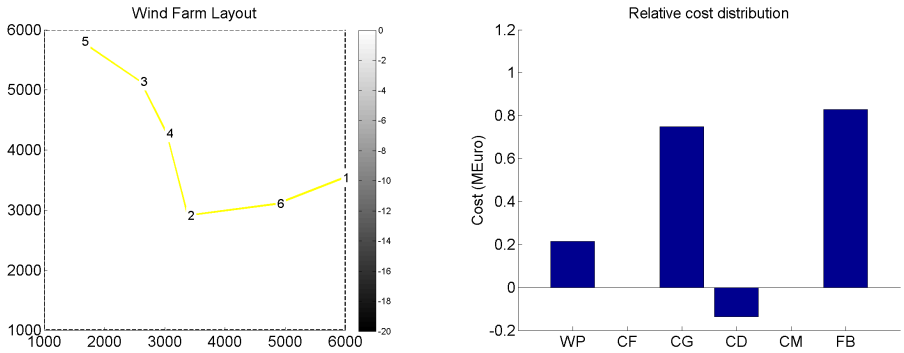

Figure 43 Optimization result (left) shown with changes in relative costs for the optimization result (right) from using the SGA algorithm.

The results from this section showed that the financial balance for the 2×3 onshore wind farm could be improved by 0.9 MEuro. The improvement was mainly due to the obtaining of a layout with reduced grid costs and only to a smaller degree changes in energy production and turbine degradation costs.

7.6 Optimum financial balance for 2x3 offshore wind farm

This section investigates the optimum financial balance for the 2×3 offshore wind farm test case shown in Figure 35. Compared to the previous section, foundation costs are now included in the financial balance. Except for the foundation costs, the optimization setup was similar to the one defined in the previous section using the SGA/SLP algorithm approach.

Figure 44 shows the optimized wind farm layout (left) together with the energy production contour plot (right). The resulting wind farm layout is very close to be a straight line oriented towards the dominant wind direction, where the individual turbines are nicely placed at the lowest possible water depths.

Figure 45 shows the change in the different financial balance components compared to the base line configuration as well as the financial balance contribution from each of the turbines. The overall improvement in the financial balance was 9.7 MEuro, which is substantially more than the result from the onshore optimization in the previous section. It can be seen that it is mainly cost reductions for foundation and grid that caused the improvement, whereas energy production and cost of turbine degradation are nearly unaffected.

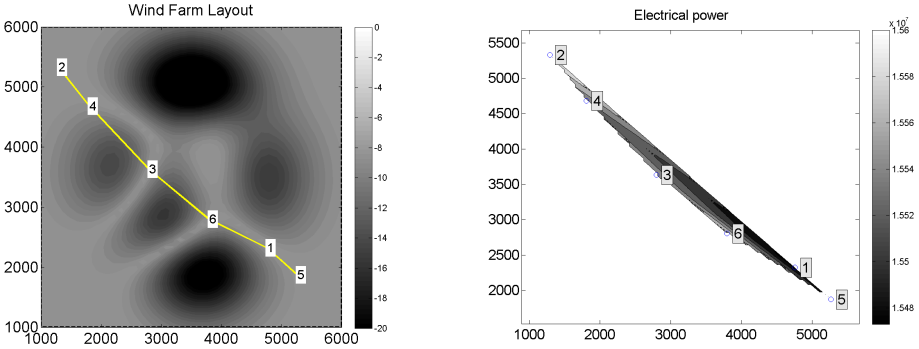

Figure 44 Optimization result (left) shown with the energy production contour plot for the optimization result (right) as based on the SGA/SLP algorithm approach.

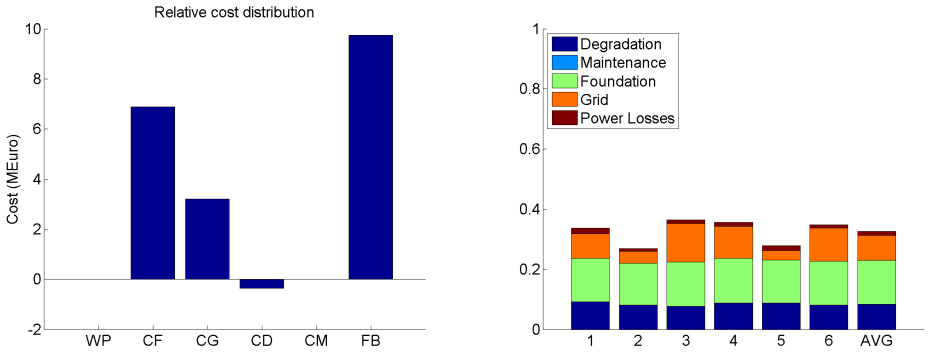

Figure 45 Change in relative cost for the optimization result (left) shown together with the financial balance breakdown for the individual turbines (right).

Figure 46 and Figure 47 show results from using the SLP and the SGA algorithms, respectively, as stand-alone algorithms. In both cases it is evident that foundation costs were reduced. Both optimization approaches resulted in significant improvements of the financial balance, but still less compared to the SGA/SLP approach, even though the SGA result shown in Figure 47 comes very close.

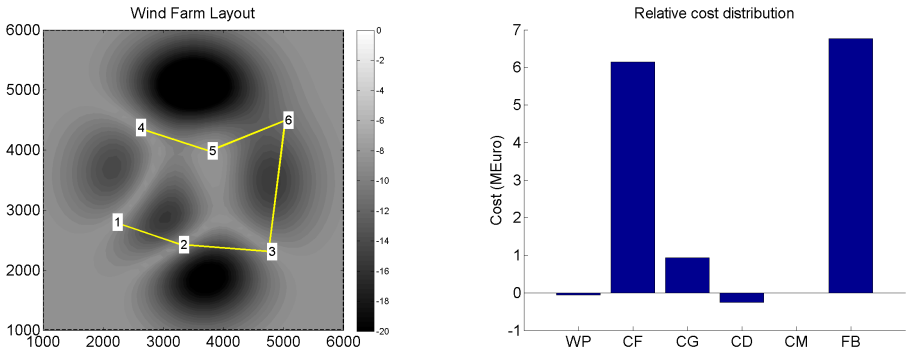

Figure 46 Optimization result (left) shown with changes in relative costs for the optimization result (right as based on the SLP algorithm approach.

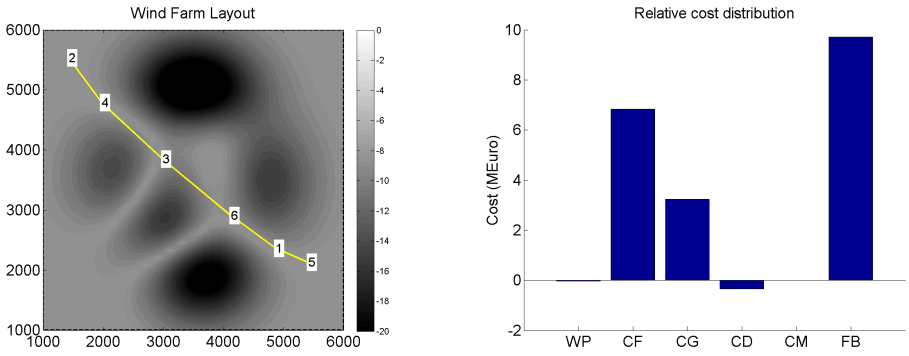

Figure 47 Optimization result (left) shown with changes in relative costs for the optimization result (right) as based on the SGA algorithm approach.

8 Middelgrunden

The purpose of this chapter is to demonstrate the capability of the TOPFARM optimization platform in relation to a re-design of the layout of the offshore Middelgrunden wind farm.

8.1 Test case description

Middelgrunden is a famous offshore wind farm in front of Copenhagen's coast. It is composed of 20 Bonus B80 2MW wind turbines with a rotor diameter of 76 m and a hub height of 64 m. The wind turbines are arranged in an arc with a turbine spacing of 2.3D (see Figure 48).

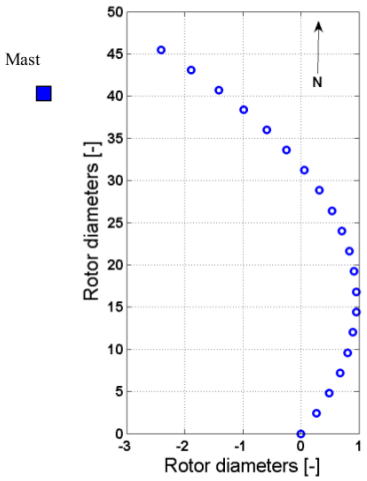

Figure 48 Middelgrunden layout [27]

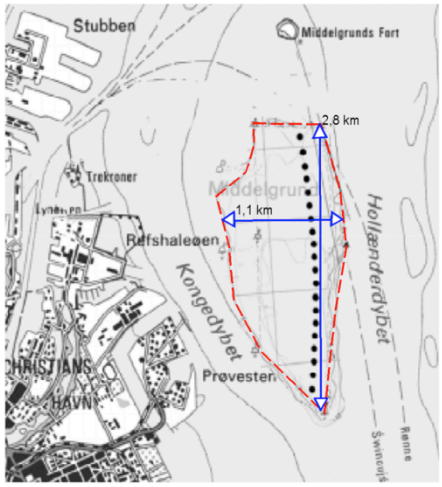

Figure 49 Allowed wind turbine position area [27]

The wind farm is located on an area relatively elevated compared to the averaged surrounding water depth of this location. The limits of the wind turbine allowed positions are following closely the limits of the elevated area of the wind turbine site (see Figure 49).

Detailed information about the wind climate of the Middelgrunden site is available in a technical report by Hansen [27]. The wind speed distributions for a number of wind sectors are used together with the analogous turbulence intensity distributions to form the inputs needed for setting up the computation. Figure 50 shows the overall wind speed distribution and Figure 51 shows the overall turbulence intensity distribution.

The input file, which was generated on basis of [27] and used for the optimization, is given in Appendix 2.

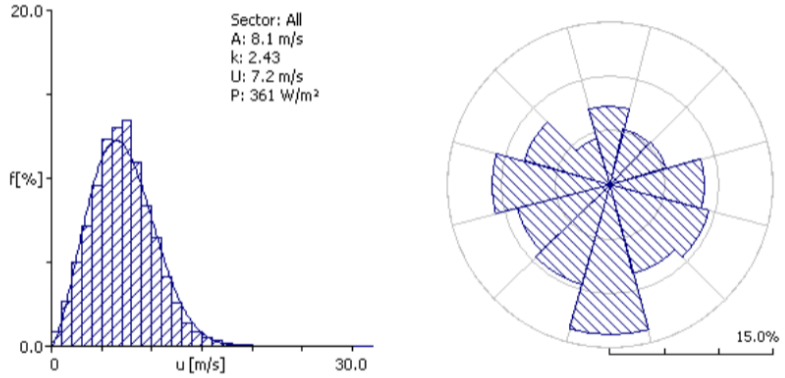

Figure 50 Middelgrunden wind speed distribution [27]

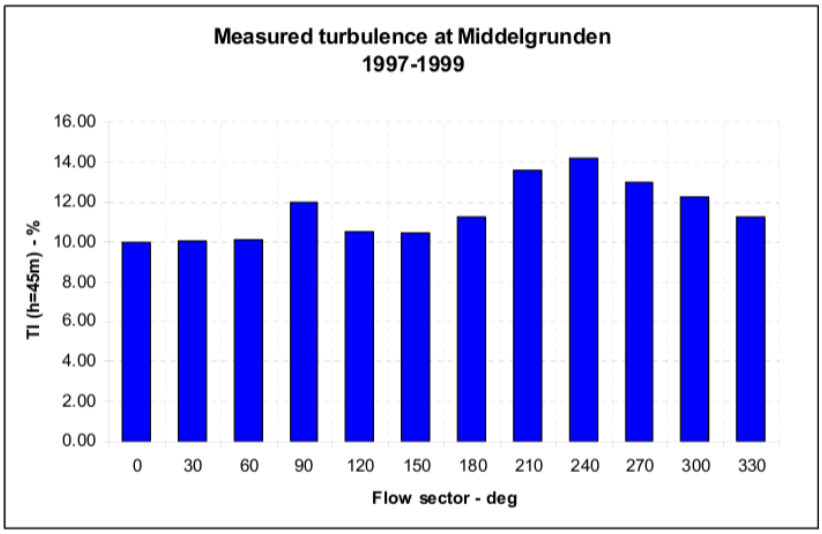

Figure 51 Middelgrunden turbulence intensity distribution [27]

Basis on the wind farm layout shown in Figure 48 and the wind climate illustrated in Figure 50 and Figure 51, the power production and turbine loads can be calculated for each of the turbines. Figure 52 shows the corresponding contour plots, which were generated based on the values for the individual turbines. Due to the location of the turbines on an arch with small curvature, it is difficult to obtain contour lines, and therefore difficult to really see the difference between the turbines. However, it is clear, that it is the turbines to the very south, which show the highest power production. The total energy efficiency is calculated to 83.9%, where this would be 100% for a stand-a-lone reference turbine. It is obvious, that the dense spacing between the turbines has a consequence on the energy efficiency. For the tower base moments, it is also the turbines to the south that have the lowest load values.

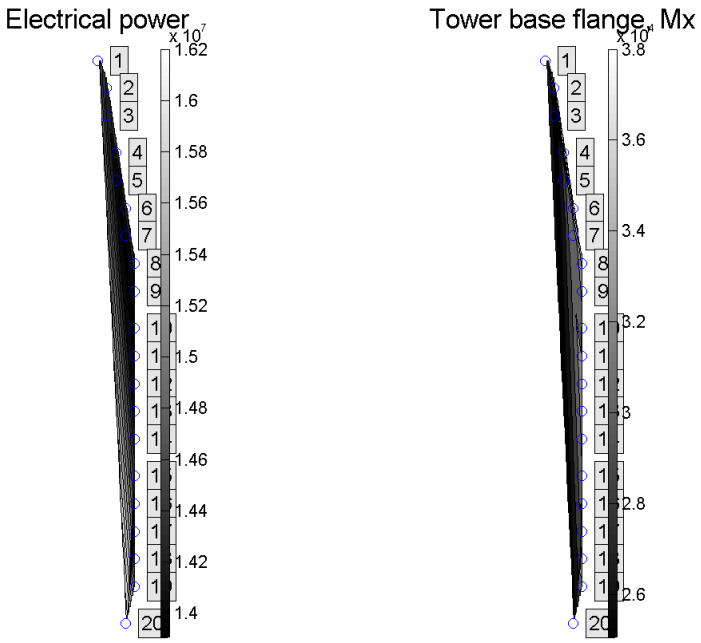

Figure 52 Energy production contour plots (left) and Tower base over turning bending moment (right) for the Middelgrunden base line layout

Figure 53 shows the financial balance components for each of the turbines in the base line layout as well as the average for all turbines. The values shown for each component are normalized to the value of the energy production for a stand-a-lone turbine. Furthermore, the energy production is expressed as a power loss by using the energy efficiency rather than the energy production. In this way, all the different components express a loss in the financial balance, and the total sum of all losses needs to be counterbalanced by the value of the energy production ??of an equal number of solitary turbines??.

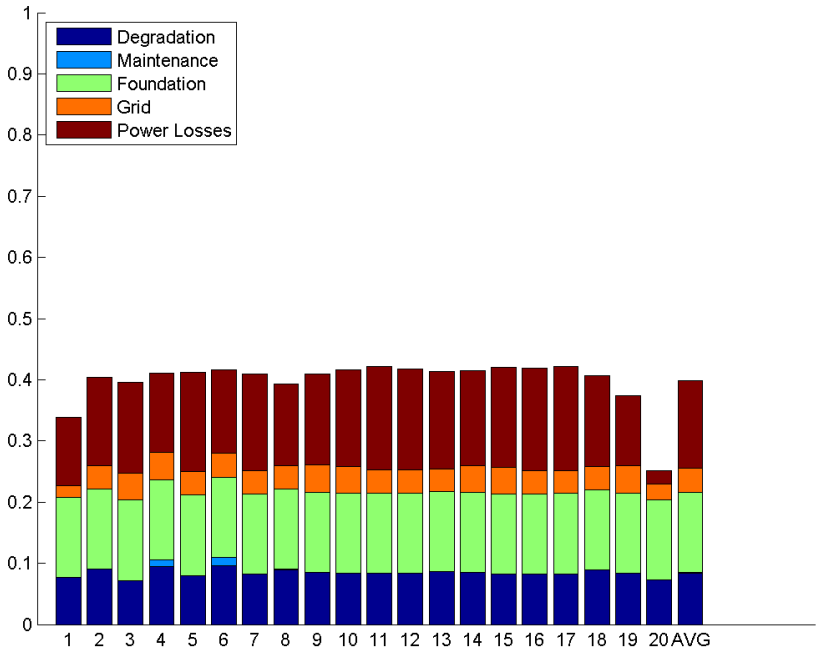

Figure 53 Financial balance components for each turbine for the Middelgrunden base line layout

8.2 Optimization result

The first level of the optimization ran the SGA algorithm for 1000 iterations, and subsequently the second level ran the SLP algorithm for 20 more iterations. Further iterations could not improve the financial balance. The initial SGA run resulted in an improvement of the financial balance of 0.6 M€, and the SLP warm start run resulted in a total improvement of the financial balance of 2.1 M€ compared with the base line.

Figure 54 shows the convergence of the objective function (i.e. the negative financial balance) for the two levels of multi-fidelity optimization considered. The SGA algorithm clearly converges. Due to the nature and principle of this algorithm, it converges in steps. Convergence is very stable but slow, and after approximately 525 iterations there appears to be only insignificant improvement of the objective function. However, despite the many iterations run it cannot be excluded, that further reductions of the objective function could have been possible.

The SLP algorithm ran for 20 iterations, after which no further improvement of the solution was possible. Convergence of the SLP run is not monotonic, as severe kinks are seen for the value of the objective function plotted against the number of iterations. The displacement? limits are intensively adjusted during the optimization, and despite the kinks a trend towards reducing the objective function is though seen.

The 20 turbines result in 40 design variables for the SLP approach, and with constraints on turbine spacing and domain boundaries the optimization problem is very complex. This explains the kinky appearance of the convergence, where the non-linearity of the optimization problem makes the size of the displacement?-limits a challenge for the SLP algorithm.

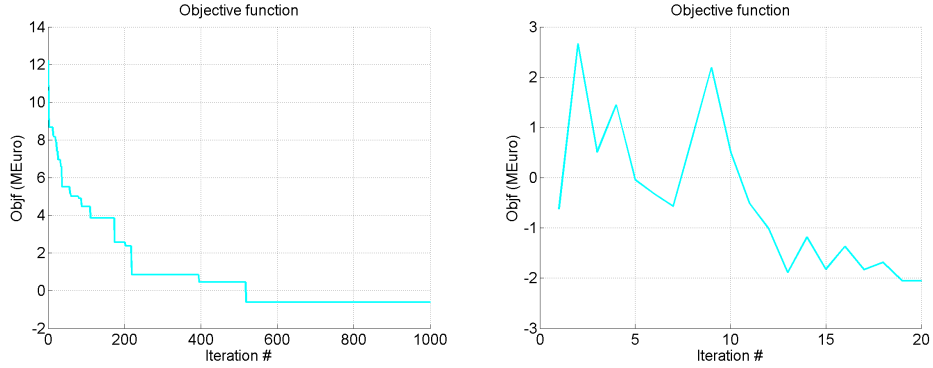

Figure 54 Optimization convergence of the SGA algorithm (left) and warm start of the SLP algorithm based on the SGA result (right)

The large difference between the financial balance after the SGA based optimization and the financial balance after the SLP based refinement can be explained by the crude penalty function applied on the minimum distance between turbines when using the SGA algorithm, which reduces the power production of the wind farm. Because of the local nature of the SLP algorithm, it is able to comply more efficiently with the constraint on the minimum distance, and thus simply increase the distance between turbines that ended up too close to one another using the SGA approach.

Figure 55 shows the resulting wind farm layout together with the changes in the financial balance caused by the optimization. When looking at the solution, it is fundamentally different from the base line layout, as the turbines are no longer arranged on line with a limited spacing between turbines. The resulting layout makes use of the entire feasible domain, and the turbines are no longer placed in a regular pattern. A closer look on the financial balance changes in Figure 55 shows, that the foundation costs have not been increased, because all the turbines are still placed at shallow water locations. The major changes involve energy production and electrical grid costs.

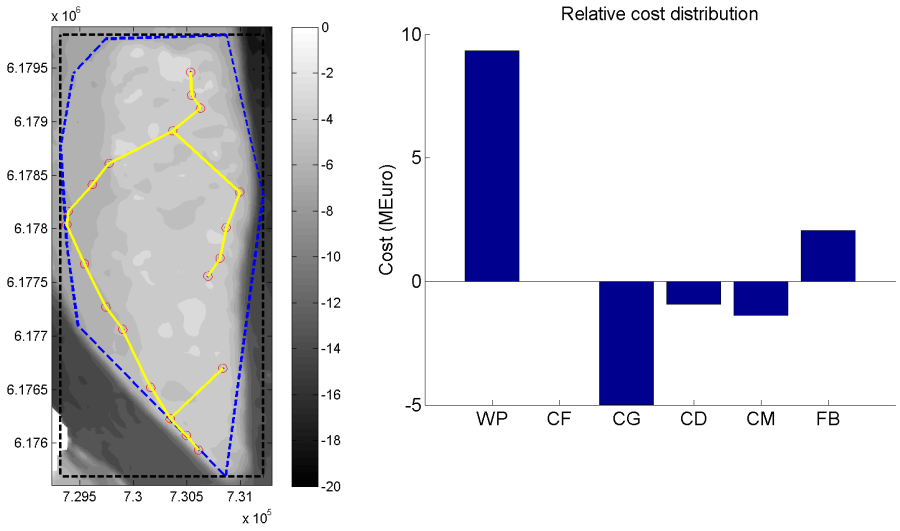

Figure 55 Optimum wind farm layout (left) and financial balance component changes relative to the base line design (right)

Figure 56 shows the details of changes in the financial balance components for each of the turbines relative to the base line layout, and Figure 57 shows how energy production and lifetime equivalent tower base over-turning moment changes between the turbines in the wind farm.

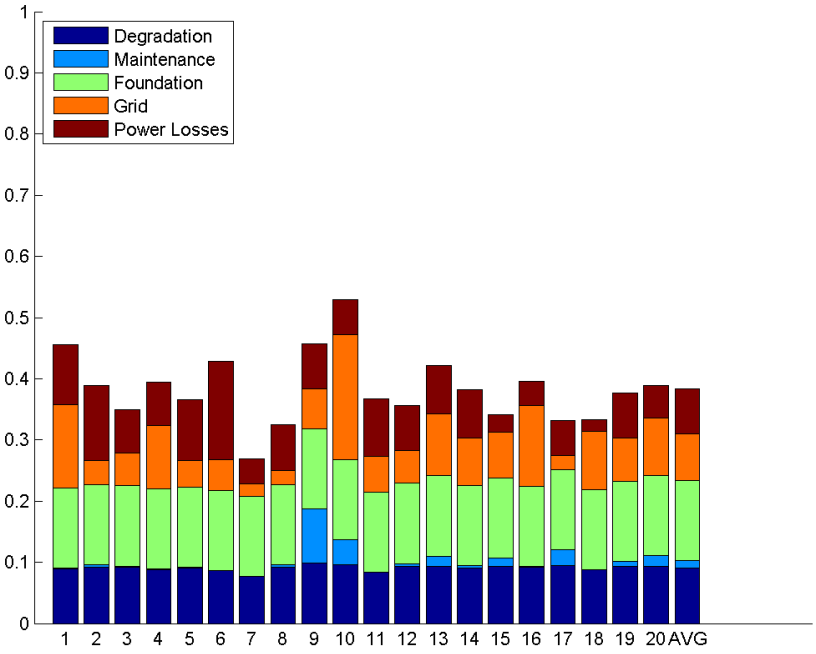

Figure 56 Changes in the optimized financial balance components for each turbine relative to the base line layout

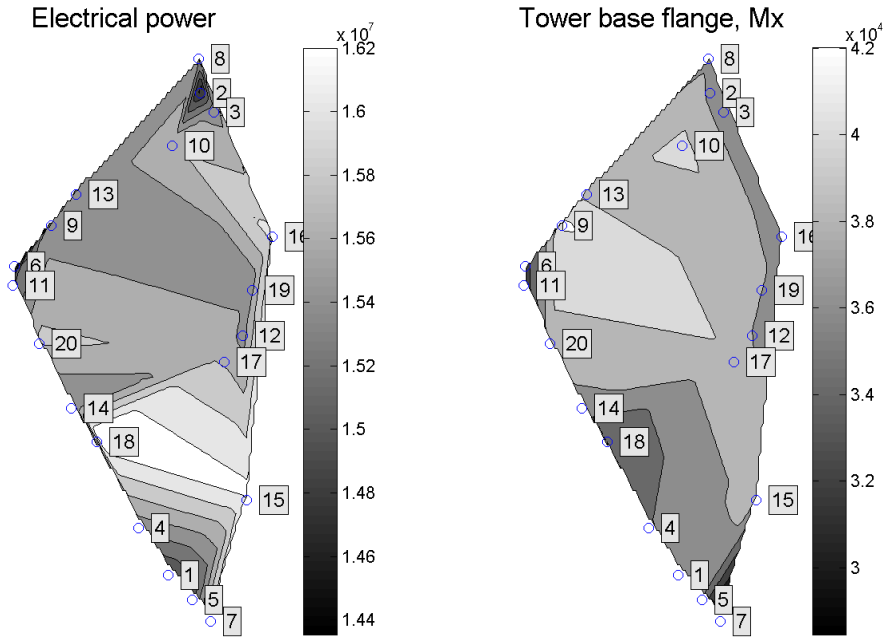

Figure 57 Contour plots of energy production (left) and of Tower base over turning bending moment (right)

It appears from Figure 56 that a few turbines, e.g., 9 and 10, have high O&M costs in contrast to the initial base line layout, whereas most turbines have high annual energy efficiency. Turbine 10 has a relatively high energy production and a

relatively high tower based flange moment, probably due to the wake meandering of turbines 13 and 9. This shows that the fatigue loads can have an important influence on the financial balance, which would not be captured by an optimization purely based on the power production.

The dark areas to the left in Figure 57 show turbines having comparatively lower energy production efficiency, and the light areas to the right in Figure 57 show turbines with comparatively higher tower base loads. The fact that there seems to be some of the turbines that experience comparatively high degradation and O&M costs is supported by the contour plot showing a few problem areas within the wind farm. Also a few problem areas appear for the energy production. The optimization result therefore leaves an open a question mark on whether the global optimum was found. It is likely, that adjustments in some of the areas in the wind farm can lead to further improvements of the financial balance, but it is not likely that a significant change in the value of the improvement is obtainable.

8.3 Alternative solutions

Looking at the results from the previous section, it cannot be excluded that the results can be improved by further iterations, or that a different optimization approach using the same financial balance would lead to another result. To investigate this, two alternative optimizations were carried out in the present section:

1) Running with the SGA algorithm for 160 iterations and then subsequently refining using the SLP algorithm warm started based on the SGA result;
2) SLP cold start based on the base line layout.

The results from 1) are shown in Figure 58, whereas results from 2) are shown in Figure 59.

The improvement in the financial balance from 1) is 1.6 M€, which is less than the improvement from the previous section. Figure 58 shows that the resulting wind farm layout is different, but also that the trends in the changes of the financial balance are the same as for the solution in the previous section.

The improvement in the financial balance associated with 2) is 1.2 M€, which is less than obtained from the other solutions. By doing a cold start of the SLP algorithm based on the initial design, it is not possible to obtain other than marginal adjustments to the individual turbine locations. It is therefore remarkable, that the relative significant improvement in the financial balance is possible, and further that it origins mainly from an improvement of the energy production. On one hand this case illustrates the weakness of the SLP algorithm in being captured in a local optimum. On the other hand this case also showed the effectiveness of the local refinements made possible by the SLP approach.

Both the alternatives in this section underlined that multiple solutions exist with slightly different values for the financial balance. When deciding on the final wind farm layout in an actual design case, it is therefore important to consider the local financial balance for each turbine, as well as other factors that may influence decision making but not being present in the cost function. This could, e.g., be power quality for the wind farm as a whole, where it might be desirably to have a minimum variation of the wind farm power output with wind direction.

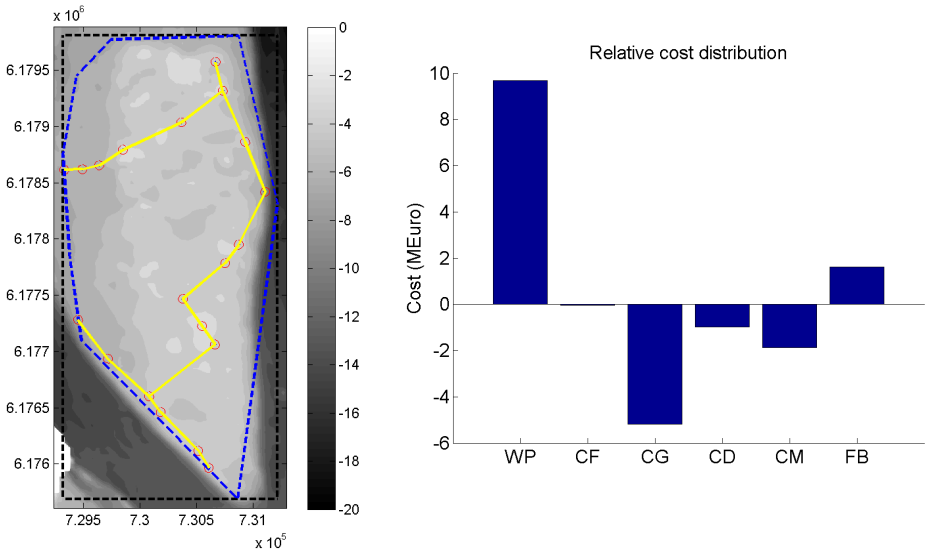

Figure 58 Optimum wind farm layout (left) and financial balance component changes relative to the base line design (right) associated with a SLP warm start after 160 SGA iterations

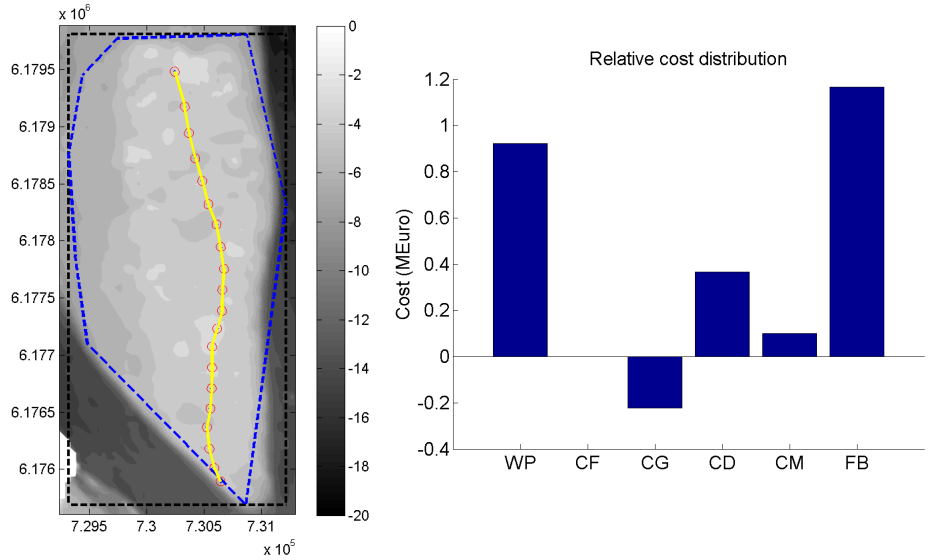

Figure 59 Optimum wind farm layout (left) and financial balance component changes relative to the base line design (right) for SLP cold start as based on the base line layout

8.4 Variation of electrical grid costs

The Middelgrunden optimization result (Figure 55) revealed that the trade-off between energy production and electrical grid costs, degradation costs and O&M costs is decisive for the optimization result. The resulting improvement of the financial balance of 2.1 M€ originated from a very large increase in the energy production value of 9.3 M€, counterbalanced by mainly increased electrical grid costs. The optimization result is therefore sensitive to the cost modeling, which in this case stresses the importance of an accurate modeling of the electrical grid costs. It is therefore a weak point in the current work, that only little sophistication has

gone into the modeling of electrical costs. It is e.g. not considered that cables between clusters of turbines may be more expensive than cables connecting connecting single turbines, and that costs for laying down cables should depend on the local water depth conditions.

To investigate the sensitivity of the optimization result to the modeling of electrical grid costs, two additional optimizations were run:

1) Applying a scale factor of 0.5 on electrical grid costs in the financial balance;
2) Applying a scale factor of 2 on the electrical grid costs in the financial balance.

The results from 1) are shown in Figure 60, whereas the results from 2) are shown in Figure 61. The resulting improvement of the financial balance in case 1) was 4.2 M€, and the improvement in case 2) was -5.5 M€. In both cases, the electrical grid costs for the base line were also scaled accordingly. ??How can the optimization end up with a negative improvement of the financial basis relative to the base line layout – in this case it could at least stick to the base line layout ??

When looking at the details in Figure 60 it can be seen that the reduced grid costs have caused longer distances between turbines, which in turn has resulted in a larger improvement of the energy production (*WP*) compared to the initial optimization test case shown in Figure 55. The grid connection costs (*CG*) have been decreased, which provides the basis for improving the financial balance by 4.2 M€.

Figure 61 shows significantly shorter cable length caused by increasing the grid costs with a factor of 2. The cable length is not very different from the initial optimization in Figure 55, but the electrical grid costs (*CG*) are inevitably higher, and this causes the improvement in the financial balance to become negative ?? difficult to understand when it is stated above that “the electrical grid costs for the base line were also scaled accordingly” ??. This means that the Middelgrunden base line layout is better than the optimization result, which is due to the dense turbine spacing used. It also means that the optimization algorithm is not able to retrieve the base line layout ??but it should??.

The differences introduced in electrical grid costs for the different optimization results have caused differences in turbine spacing, and demonstrated different possibilities for improving the financial balance, which has underlined the importance of accurate inclusion and modelling of the electrical grid costs. A more sophisticated model, such as the one advocated in [5], could be considered infuture work.

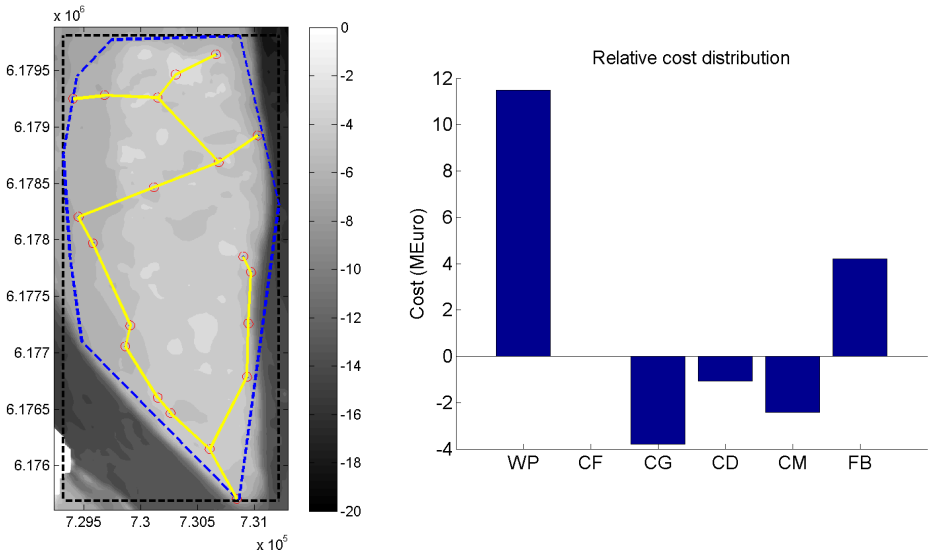

Figure 60 Optimum wind farm layout (left) and financial balance component changes relative to the base line design (right) for SGA/SLP warm start with electrical grid costs scaled with a factor of 0.5

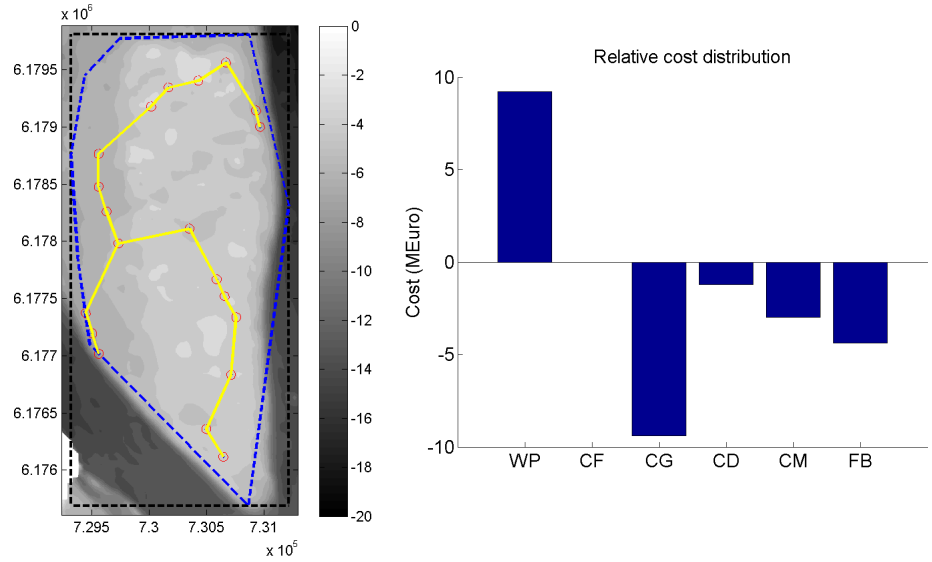

Figure 61 Optimum wind farm layout (left) and financial balance component changes relative to the base line design (right) for SGA/SLP warm start with electrical grid costs scaled with a factor of 2

9 Stags Holt/Coldham

The purpose of this chapter is to demonstrate the capability of the TOPFARM optimization platform in relation to a re-design of the layout of the on-shore Stags Holt/Coldham wind farm.

9.1 Description of the test case

The Stags Holt/Coldham site is in reality two wind farms composed of in total 17 Vestas V80 wind turbines with a 80 m rotor diameter and a hub height of 60 m. It is an on-shore wind farm located in between March and Wisbech in Cambridgeshire, UK. The layout and the boundary enclosing the area restriction of the optimisation are shown in Figure 62.

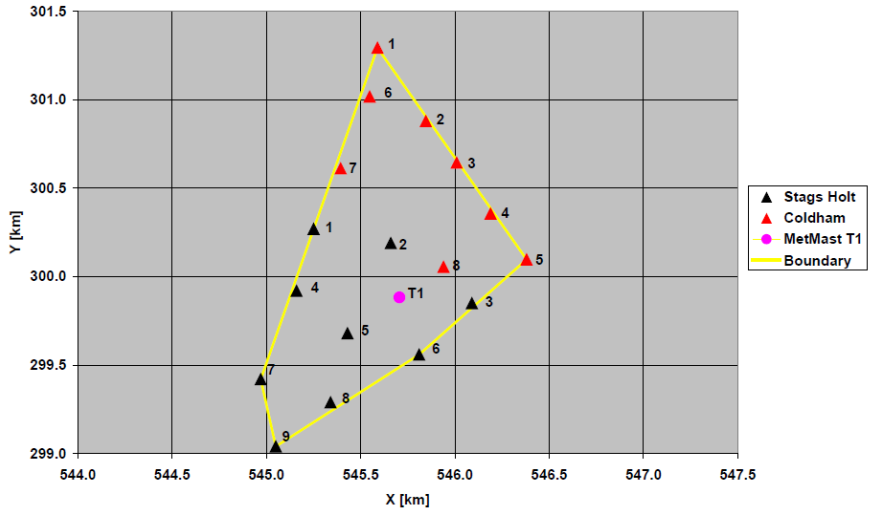

Figure 62 Stags Holt / Coldham layout and allowed area for wind turbine locations ***[Error! Reference source not found.]***

The wind farm is located on land at flat and homogeneous terrain. Foundation costs are therefore not relevant to the optimization and consequently omitted from the cost function financial balance.

Detailed information about the Stags Holt/Coldham site, including the full description of the wind climate, can be found in an external technical report [**Error! Reference source not found.**]. The wind rose and the turbulence intensity distribution are illustrated in Figure 63.

The input file used for this optimization is given in Appendix 3. Thse were generated based on [**Error! Reference source not found.**].

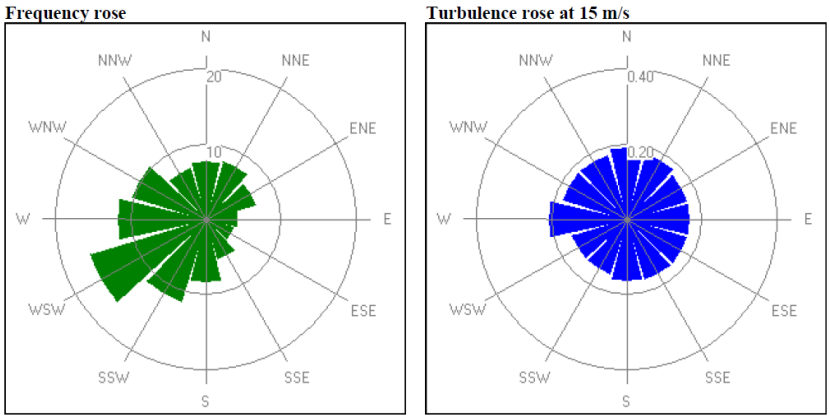

Figure 63 Stags Holt/Coldham wind rose and turbulence rose ***[Error! Reference source not found.]***

Figure 64 shows contour lines of power production and tower base overturning moments generated on basis of these values for the individual turbines. The wind rose in Figure 63 defines South-West as the dominating wind direction, which seems to be the direction with the smallest projected "width" of the wind farm due to the defined boundary. Consistent with this observation it can be seen, that energy production is highest towards the South-West corner of the wind farm and reduces toward North-East, with the turbines 13 and 17 having the lowest power production. The tower base moment ?? exhibits the highest loads for the turbines 2, 5, 11 and 12, which are located in the central part of the wind farm. The total energy efficiency is calculated to 89.4% relative to 100%, which corresponds to a stand-a-lone reference turbine at the same wind climate. The relatively dense spacing between the turbines is causing the energy efficiency to drop compared to the ideal value.

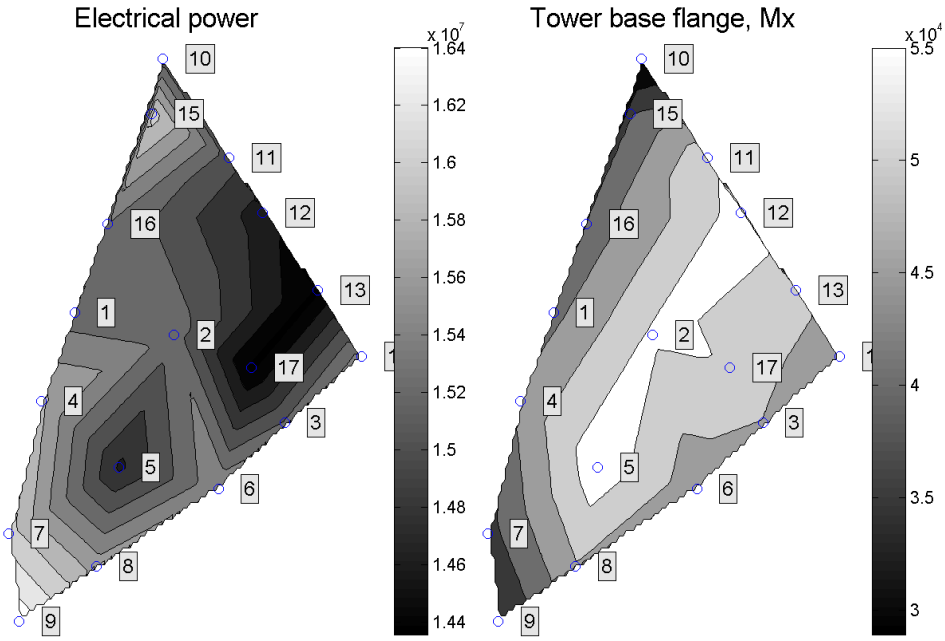

Figure 64 Contour plots of energy production (left) and Tower base over turning bending moment (right) for the Stags Holt/Coldham base line layout

Figure 65 shows the financial balance components for each of the turbines as well as the average for all turbines normalized with the value of the energy production for a stand-a-lone turbine. The energy production is expressed as a power loss by using the energy efficiency rather than the energy production. In this way, all the different components express a loss in the financial balance, and the total sum of all losses needs to be counterbalanced by the value of the energy production ??of an equal number of solitary turbines??. It can be seen, that there is a large variation in the power loss coefficient, as some turbines have a very little loss, whereas others have significant losses. The turbines 5, 12, 13 and 17 have the highest losses, which is caused by operation in wake conditions for predominantly more time than for example turbine 9. It can be seen that the electrical grid costs are in general small, and it is also noteworthy, that many turbines have a non-zero maintenance coefficient, indicating that turbine spacing is limited.

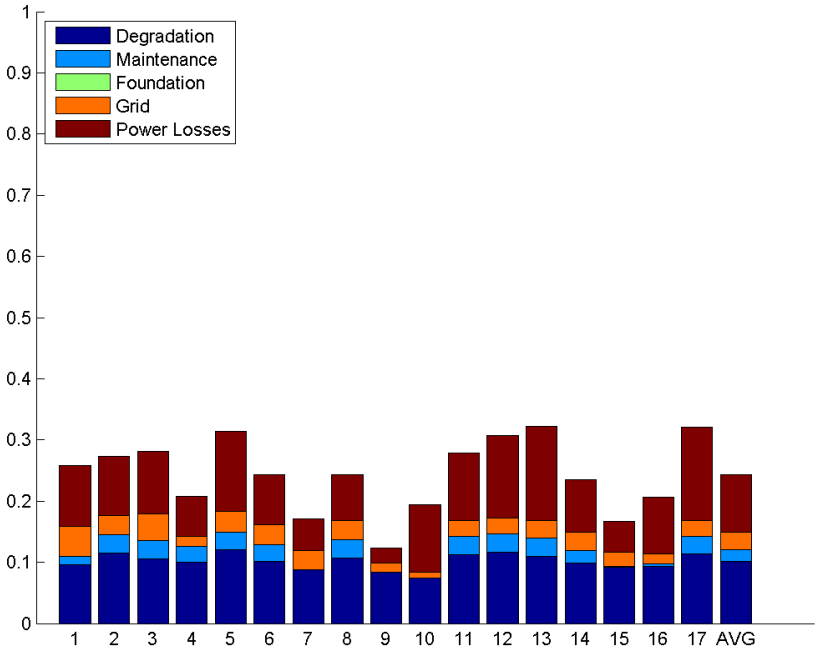

Figure 65 Financial balance components for each turbine for the Stags Holt/Coldham base line layout

9.2 Optimization results

The first level of optimization ran the SGA algorithm for 1000 iterations, and subsequently the second level ran the SLP algorithm for 30 more iterations. Further iterations could not improve the financial balance. The initial SGA run resulted in an improvement of the financial balance of 1.5 M€, and the SLP warm start resulted in a total improvement of the financial balance of 3.1 M€ compared with the base line.

Figure 66 shows the convergence of the objective function (i.e. the negative financial balance) for the two levels of multi-fidelity optimization considered. The SGA algorithm clearly converges. Due to the nature and principle of this algorithm, it converges in steps. Convergence is very stable but slow, and after approximately 750 iterations there appears to be only insignificant improvement of the objective function. However, despite the many iterations executed, it cannot be excluded that further reductions of the objective function could have been possible.

The SLP algorithm ran for 30 iterations, after which no further improvement of the solution was possible. Convergence for the SLP run is not monotonic, as kinks are seen for the value of the objective function plotted against the number of iterations. The displacement? limits are intensively adjusted during the optimization, and despite the kinks a trend towards reducing the objective function is though seen.

The 17 turbines result in 34 design variables, and even though this is less than in the previous chapter, it remains a challenge for the SLP algorithm to arrive at a converged solution. Displacement?-limits are adjusted, and both the boundary and the turbine spacing constraints are difficult to handle in the many dimensions spanning the design space of the optimization.

The difference in financial balance between the two optimization levels is basically caused by the SLP algorithm being able to improve energy production significantly by tuning of each turbines position and at the same time reduce grid costs.

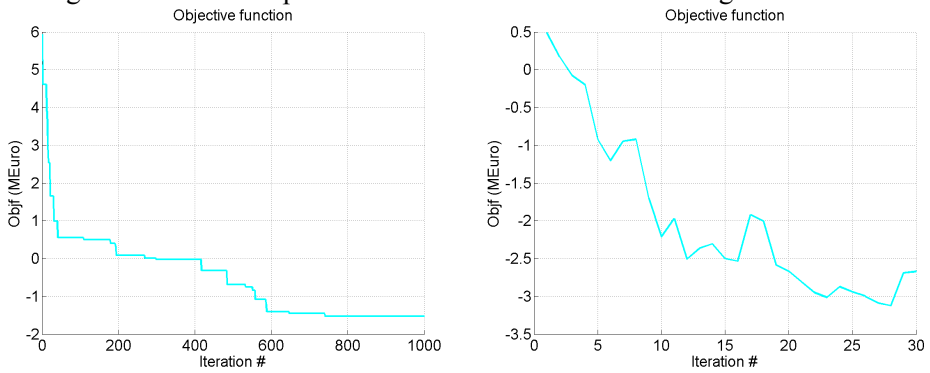

Figure 66 Optimization convergence from SGA (left) and warm start on basis of SGA result (right)

Figure 67 shows the resulting wind farm layout together with the changes to the financial balance components caused by the optimization. The solution is not fundamentally different from the base line layout. The turbines are not as regularly laid out but rather on different connecting strings, which reduces the electrical grid costs and even allow for improving energy production. The financial balance in Figure 67 shows, that the total improvement of the financial balance is contributed to by all components including turbine degradation and O&M.

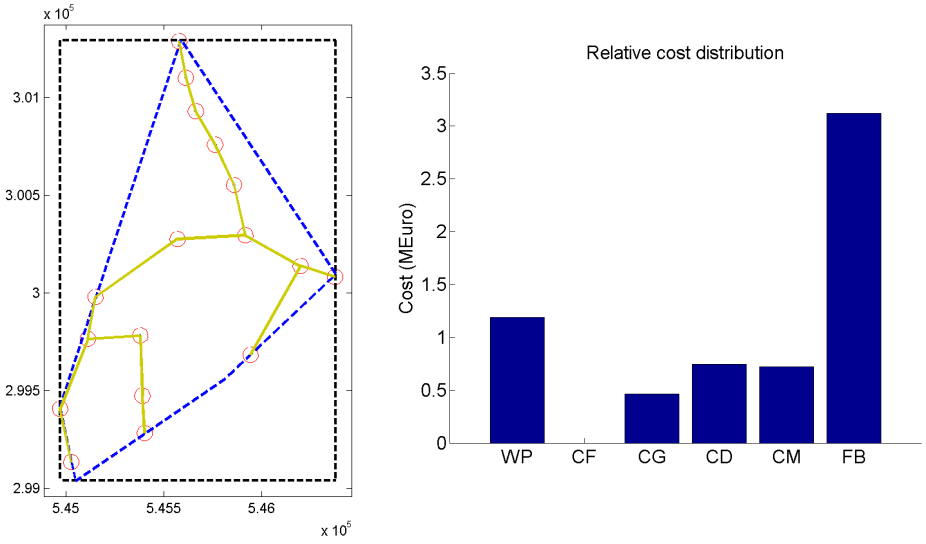

Figure 67 Optimum wind farm layout (left) and financial balance cost distribution relative to base line design (right)

Figure 68 shows the details of the financial balance components for each of the turbines as well as for the average of all turbines, and Figure 69 shows how energy production and lifetime equivalent tower base over-turning moment change between the turbines in the wind farm.

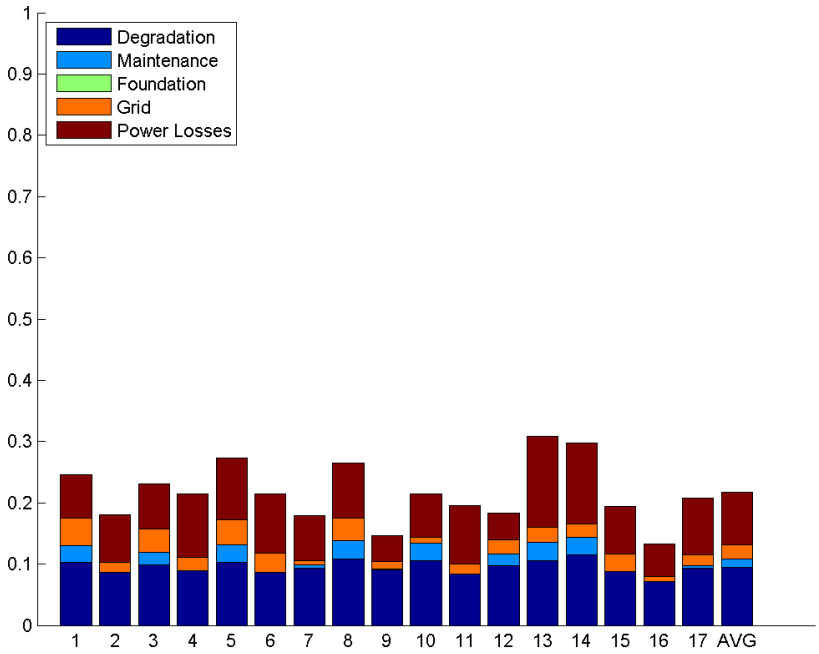

Figure 68 Financial balance components for each turbine

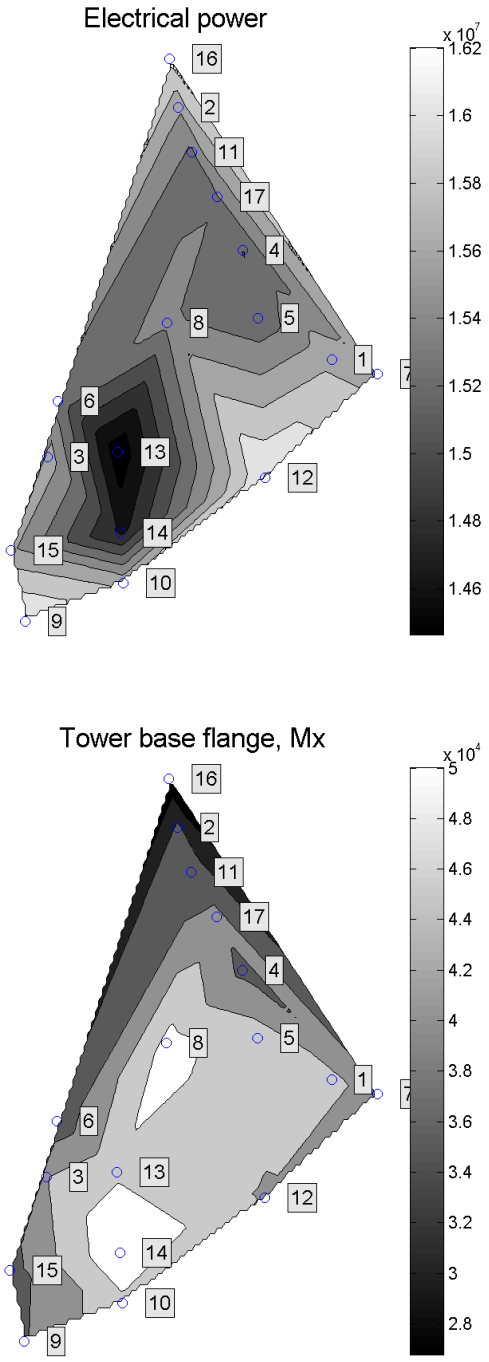

Figure 69 Contour plots of energy production (left) and Tower base over turning bending moment (right)

It can be seen in Figure 68that some turbines have significantly poorer financial balance than other. Turbine 1, 5, 8?, 13 and 14 all show unfavorable high values, whereas turbine 9 and 16 are the most efficient ones in the resulting wind farm layout. It is in general the turbines on the edge of the wind farm, which show the most efficient financial balance.

9.3 Alternative solutions

In this section, two alternative optimizations were carried out:

1) Running with the SGA algorithm for 160 iterations and subsequently refining with the SLP algorithm on basis of the SGA result;
2) SLP cold start on the base line layout.

The results from 1) are shown in Figure 70, whereas results from 2) are shown in Figure 71.

The improvement of the financial balance in case 1) is 2.1 M€, which is less than the improvement obtained in section 9.2. Figure 70 shows that the resulting wind farm layout is different, and also that the trends in the changes of the financial balance are different compared to the solution in section 9.2. The energy efficiency (*WP*) was reduced, whereas the other financial balance components were increased.

The improvement in the financial balance in case 2) is 2.2 M€. It is remarkable that the cold start of the SLP algorithm on the initial design makes it possible to change the individual turbine locations, so that a significant improvement in the financial balance is obtained. Most of this improvement originates from an increase in the energy efficiency (*WP*) with only marginal changes in electrical grid costs, turbine degradation and O&M.

Both alternatives shown in this section underlines that multiple solutions exist with slightly different values for the financial balance. When deciding on the final wind farm layout in an actual design case, it is therefore important to consider the local financial balance for each turbine and other factors, which eventually may influence decision making but not being present in the cost function. This could, e.g., be power quality for the wind farm as a whole, where it might be desired to have a minimum variation of the wind farm production with wind direction.

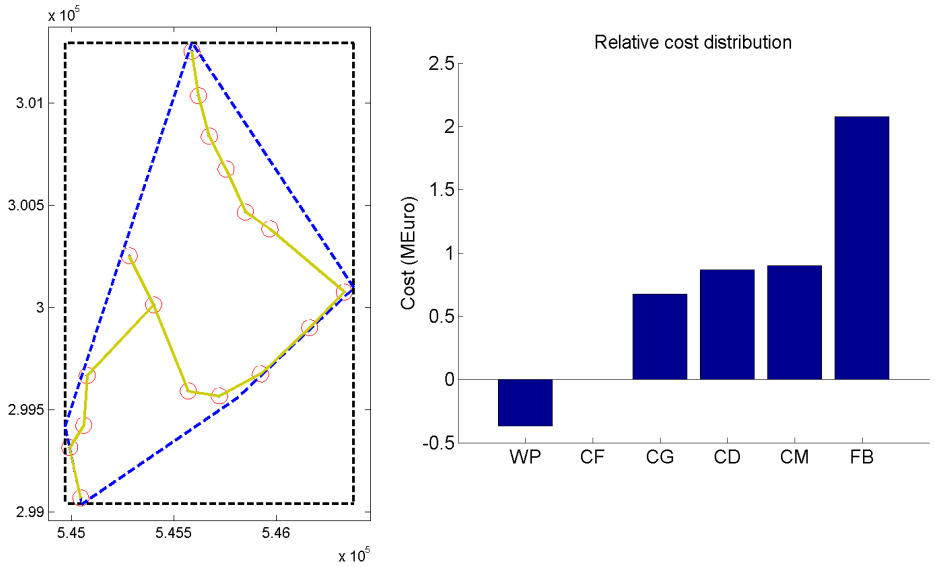

Figure 70 Optimum wind farm layout (left) and financial balance cost components relative to base line design (right) for SLP warm start after 160 SGA iterations

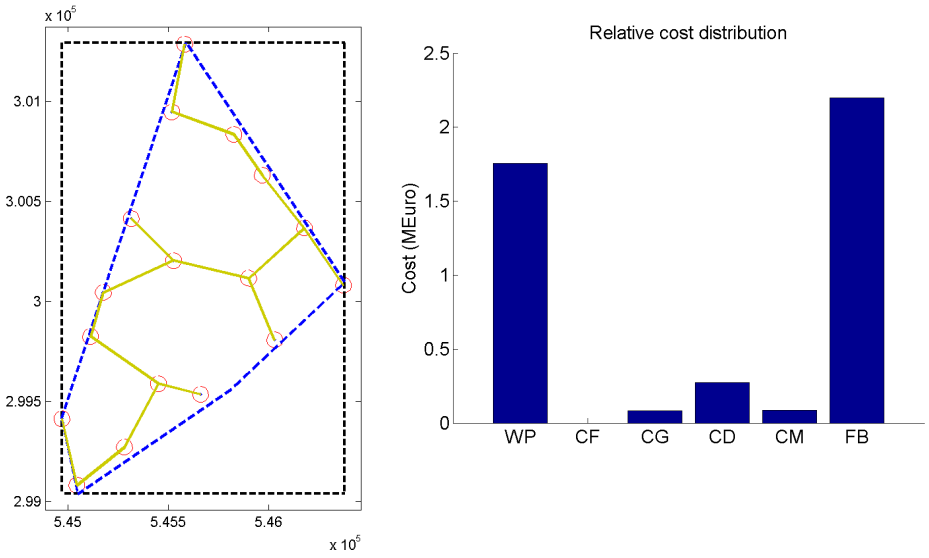

Figure 71 Optimum wind farm layout (left) and financial balance cost components relative to base line design (right) for SLP cold start on base line design

9.4 Variation of electrical grid costs

To investigate the sensitivity of the optimization result to the modeling of electrical grid costs, two additional optimizations were run:

1) Applying a scale factor of 0.5 on electrical grid costs in the financial balance;
2) Applying a scale factor of 2 on the electrical grid costs in the financial balance.

The result from case 1) are shown in Figure 72, whereas the results from case 2) are shown in Figure 73. The resulting improvement in the financial balance in case 1) was 1.5 M€, whereas the improvement from case 2) was 2.3 M€. In both cases, the electrical grid costs for the base line were also scaled accordingly.

When comparing the resulting wind farm layouts, there is not a significant difference in the total cable length, even though cables are longer for case 1) compared with case 2). When the electrical grid costs are scaled with a factor of 2, the optimum solution has significantly higher electrical grid costs, and the energy efficiency has been reduced. Therefore, the magnitude of the electrical grid costs clearly influences the resulting wind farm layout, and when the electrical grid costs increase, the energy efficiency is put under pressure, since it pays off to relax on this financial balance component to achieve lower electrical grid costs.

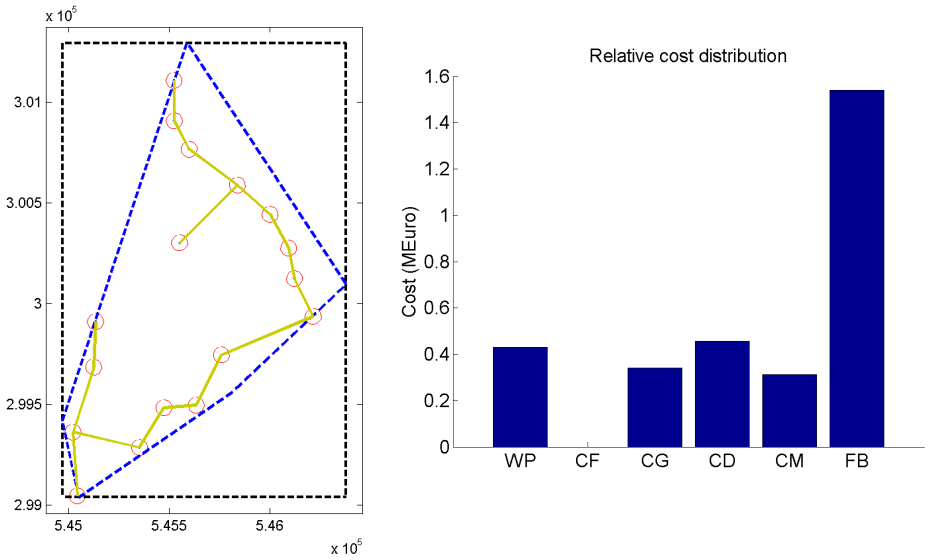

Figure 72 Optimum wind farm layout (left) and financial balance cost components relative to base line design (right) for SGA/SLP warm start with electrical grid costs scaled by 0.5

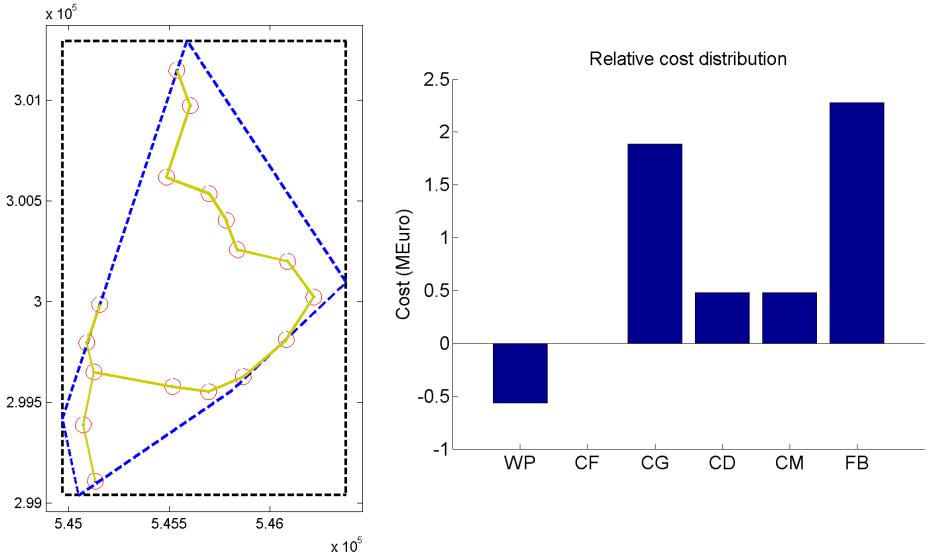

Figure 73 Optimum wind farm layout (left) and financial balance cost components relative to base line design (right) for SGA/SLP warm start with electrical grid costs scaled by 2.0

10 Conclusions

A wind farm optimization platform was presented in details and demonstrated on two test cases: 1) Middelgrunden and 2) Stags Holt/Coldham.

A multi-fidelity approach was found necessary and attractive to limit the computational costs of the optimization. A detailed flow model for the mean flow in a wind farm was used together with a fatigue load calculation approach taking into account dynamic wake meandering and using pre-calculated short term fatigue loads in a database for rapid calculation of lifetime equivalent loads and energy production. A cost function was defined for the financial balance composed by energy production, turbine degradation, O&M, electrical grid costs and foundation costs. The cost function was coupled to an optimizer for optimization of the financial balance, by adjusting the locations of individual turbines in a wind farm. The results are over all satisfying and are giving some interesting insights on the pros and cons of the design choices. They show in particular, that the inclusion of the fatigue loads costs gives some additional details in comparison with pure power based optimization.

The results from the 2×3 test case, together with Middelgrunden and Stags Holt/Coldham, have shown that both optimization concepts used in this study arrive at an optimum solution, and that the financial balance can be improved over the base line layouts. The global optimization approach that was used (SGA) yielded solutions with no resemblance with the initial base line layout, whereas it was clear, that the local gradient based method (SLP) may arrive at a local minimum, and that it is therefore most suited for refining optimization results. It appears that the combination of a global SGA approach with a local SLP refinement works well when taking the advantages from both: The SGA global method is not sensitive to local minima and can make use of a more clever and coarse design variable mapping, and the SLP method is efficient in refining the result and handling of constraints.

It is important to note that the total computational cost for the SGA cases is typically an order of magnitude higher than for the SLP case. The slow convergence of the global method is an issue when going to larger wind farms, where calculation costs can become excessive. Tuning of the calculation software and switching to a faster platform than Matlab can increase efficiency and the use of parallel computing can further bring down the total simulation time. This is needed to implement the last level of the multi-fidelity approach.

Another issue is the use of the entire wind farm financial balance as optimization objective, because this allows a few turbines in the selected layout to have a comparatively poor turbine financial balance compared to the average of the wind farm. This can cause a need for manual tuning of the result, and leaves open the question whether the solution is in fact global. Therefore, it should be looked into how the individual turbine financial balance can enter into the optimization objective function, possibly by optimizing on a subset of the wind farm or by composing the objective function differently.

The optimization results have also shown how the different components of the financial balance interact. It is clear that the foundation costs play a major role for offshore sites, in that the individual turbines are located in areas of shallow water. The outcome of the optimization will therefore be strongly governed by the possibilities for placing turbines on shallow water independently of the other

financial balance components. The optimizer is typically using the room for reducing the electrical grid costs without a significant drop in the energy efficiency. It is clear that there is a trade-off between electrical grid costs and energy production, in that shorter cables imply that turbines are located closer to each other, which results in wake losses and increased loads from wake operation. Both the degradation costs and the operation and maintenance costs will increase when the distance between turbines reduces and therefore contribute to the trade off going against shorter electrical cables.

When looking at most of the results, it cannot be excluded that the results can be improved with further iterations. It will always be the case that when deciding on the final wind farm layout, it is important to consider the local financial balance for each turbine and other factors that may influence decision making but not being present in the cost function. This could, e.g., be power quality for the wind farm as a whole, where it might be desired to have a minimum variation of wind farm power production with wind direction.

The Middelgrunden test case resulted in an improvement of the financial balance of 2.1 M€, originating from a very large increase in the energy production value of 9.3 M€ counterbalanced by mainly increased electrical grid costs. This test case emphasizes that the trade-off between on the one hand energy production and an the second hand electrical grid costs degradation costs and O&M costs is decisive for the optimization result. The optimization result is therefore sensitive to the cost modeling, and this stresses the importance for an accurate modeling of the electrical grid costs. It is therefore a weak point in the current work that only little sophistication has gone into the modeling of electrical costs, where it is not considered that cables between clusters of turbines may be more expensive than cables connection solitary turbines, and that costs for laying down cables should e.g. depend on the local water depth conditions.

The Stags Holt/Coldham test case resulted in an improvement of the financial balance of 3.1 M€. The improvement resulted from an increase in the energy efficiency together with cost reductions for electrical grid, turbine degradation and O&M. This test case showed that the micro tailoring of the individual turbine positions may lead to a significant improvement of the financial balance,?? and that the detailed wind climate information available is turned into an optimum position for each of the turbines what is the info here??.

References

1. Larsen, G., 2010, 'TOPFARM – next generation design tool for optimization of wind farm topology and operation … background, vision and challenges' Proc. TORQUE 2010: The Science of Making Torque from Wind, June 28-30, Crete, Greece, pp. 437-448.
2. Costa, P., Martins, A., & Carvalho, A. (2004). Optimization of energy generation in wind farm through fuzzy control. Retrieved October 20, 2010, from http://repositorio-aberto.up.pt/handle/10216/308.
3. Samorani, M. (2010). The Wind Farm Layout Optimization Problem. *PowerLeeds School of Business*. Retrieved October 20, 2010, from http://leeds.colorado.edu/uploadedFiles/_Documents/Faculty_and_Research/Working_Papers_Series/Operations_and_Information_Management/The Wind Farm Layout Optimization Problem (2).pdf.
4. Réthoré, P.E., (2010). "State of the Art in Wind Farm Layout Optimization". Wind Energy Research. http://windenergyresearch.org/?p=979.
5. Elkinton, C. N. (2007). Offshore wind farm layout optimization. RetrievedNovember 10, 2010, from http://adsabs.harvard.edu/abs/2007PhDT.....48E.
6. Larsen, G.C. (2009). "A simple stationary semi-analytical wake model". Risø-R-1713(EN).
7. Ott, S., (2009), "Fast linearized models for wind turbine wakes". Euromech Colloquium 508 on Wind Turbine Wakes, Madrid, 20-22 October. Extended abstract published in ISBN 9788474842203, pp. 11-13. …. Søren's R-1772 (EN) rapport burden ok erstatte denne reference
8. Larsen T.J., Hansen A.M., 2006, "Influence of Blade Pitch Loads by Large Blade Deflections and Pitch Actuator Dynamics Using the New Aeroelastic Code HAWC2," Proc. EWEC 2006, Athens.
9. Madsen, H.Aa., Larsen, G.C., Larsen, T.J., Troldborg, N., Mikkelsen, R. 2010 "Calibration and Validation of the Dynamic Wake Meandering Model for Implementation in an Aeroelastic Code." J. Solar Energy Eng. Nov. 2010, Vol. 132.
10. Larsen, G. C., Madsen, H. Aa., Thomsen, K., and Larsen, T. J., 2008, "Wake Meandering — A Pragmatic Approach," Wind Energy, 11, pp. 377–395.
11. Snel, H., Houwink, R., and Bosschers, J., 1994, "Sectional prediction of lift coefficients on rotating wind turbine blades in stall". ECN-C—93-052, Petten, December 1994.
12. Jonkman, J. "NREL 5MW Offshore Wind Turbine Specifications" http://wind.nrel.gov/public/jjonkman/NRELOffshrBsline5MW/NRELOffshrBsline5MW.pdf
13. Nieslony, A., (2010), "Rainflow counting function for Matlab". Matlab file exchange website.
14. Larsen, G., 2009, 'A simple generic wind farm cost model tailored for wind farm optimization', Risø-R-1709, Risø-DTU, June 2009.
15. Fingersh, L., Hand, M, Laxson, A, 2006. Wind Turbine Design Cost and Scaling Model. NREL report NREL/TP-500-40566.
16. Wind directions, Vol. 26 (2), 2007.
17. Fuglsang, P., and Madsen, H. A., 1995, ''Optimization of Stall Regulated Rotors,'' Proc. ASME Wind Energy – 1995, Houston, Texas, SED-Vol 16, pp. 151-158.
18. Fuglsang P. and Madsen H.A., 1999, ''Optimization method for wind turbine rotors,'' J. Wind Engineering and Industrial Aerodynamics Vol. 80 No 1-2, pp. 191-206.

19. Fuglsang P. and Thomsen, K., 2001, ‘‘Site Specific Design Optimization Of Wind Turbines, ‘‘ ASME J. Solar Engineering, Vol. 123, pp 296-303.
20. Vanderplaats, G. N., 1984, ‘‘Numerical Optimization Techniques for Engineering Design with applications,’’ McGraw-Hill Book Company, New York.
21. Arora, J.S. 2004, “Introduction to Optimum Design,” Elsevier-direct, ISBN 9788131201275.
22. Goldberg, D. E. 1989, *Genetic Algorithms in Search, Optimization & Machine Learning*, New York: Addison-Wesley, ISBN 0201157675.
23. Goffe, Ferrier and Rogers, 1994, ‘’Global Optimization of Statistical Functions with Simulated Annealing,’’ J. of Econometrics, vol. 60, no. 1/2, Jan./Feb. 1994, pp. 65-99.
24. Buhl, T., Larsen, G.C.(2010, ‘Wind farm topology optimization including costs associated with structural loading’ Proc. TORQUE 2010: The Science of Making Torque from Wind, June 28-30, Crete, Greece, pp. 449-460.
25. Applegate, D. L.; Bixby, R. M.; Chvátal, V.; Cook, W. J. (2006), The Traveling Salesman Problem, ISBN 0691129932.
26. Per Vølund, private communication.
27. Hansen, K.S. (2010) “Definition of local wind climate for Middelgrunden, DK Deliverable D17: EU – TOPFARM”. Technical report.
28. Veldkamp, D. (2010) “Data for Stags Holt/Coldham wind farm”. TOPFARM Project. Technical Report.

Appendix 1 Detailed fatigue load results

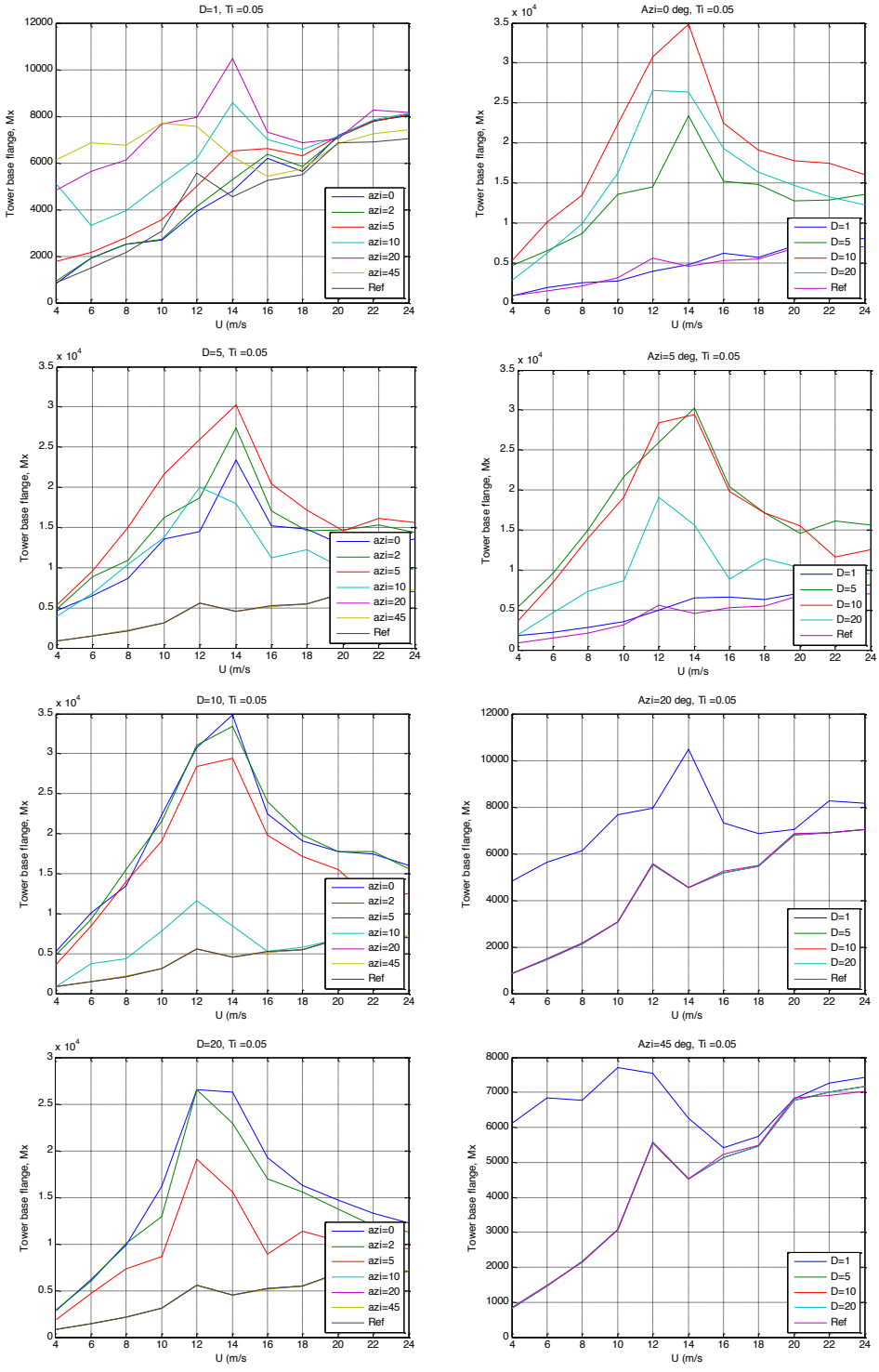

Figure 74 Tower base flange Mx (Sensor 17) equivalent load (m=4) versus wind speed for different wake distance (D) and wake azimuth (azi).

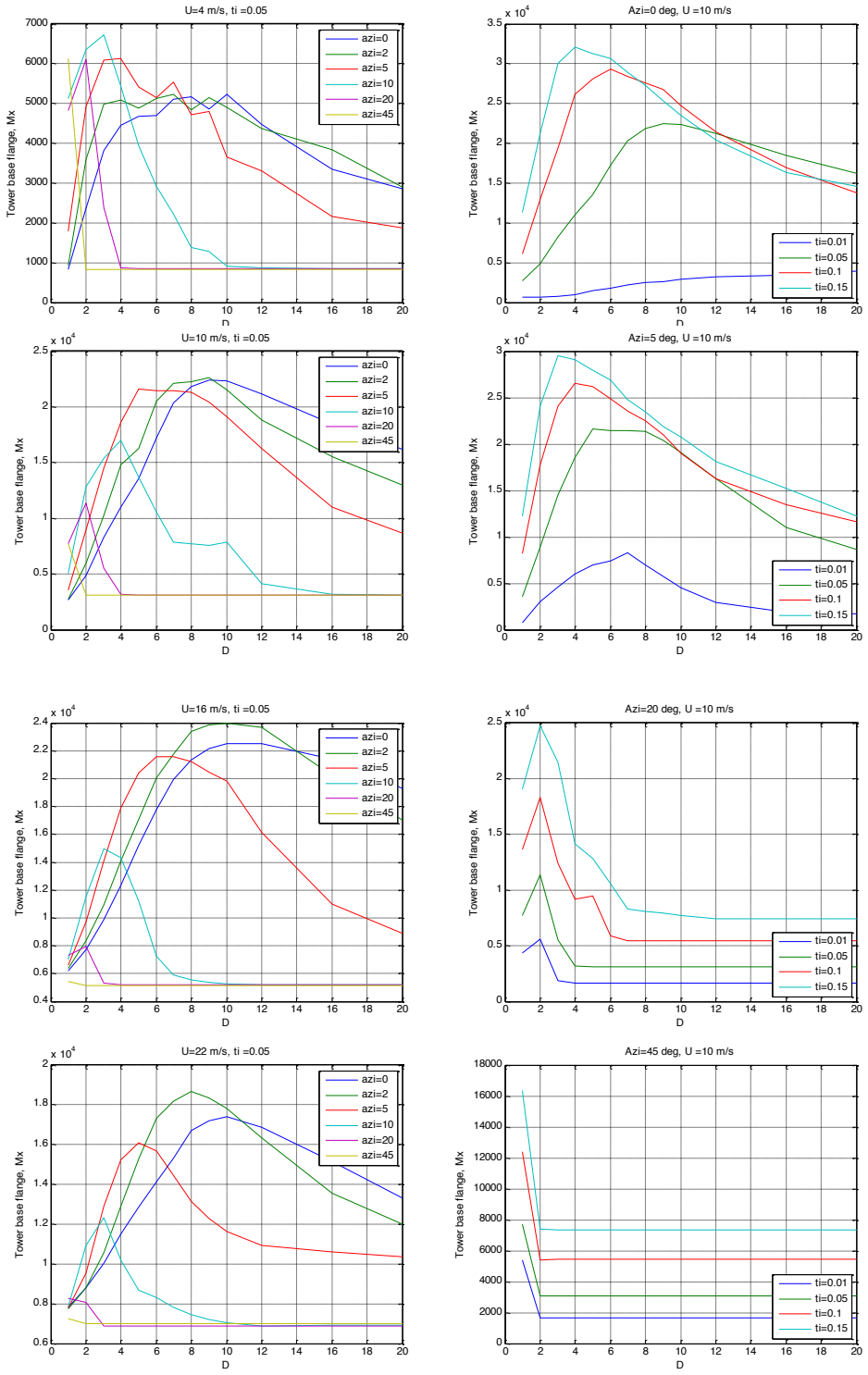

Figure 75 Tower base flange Mx (Sensor 17) equivalent load (m=4) versus wake distance (D) for different wake azimuth (azi) and turbulence

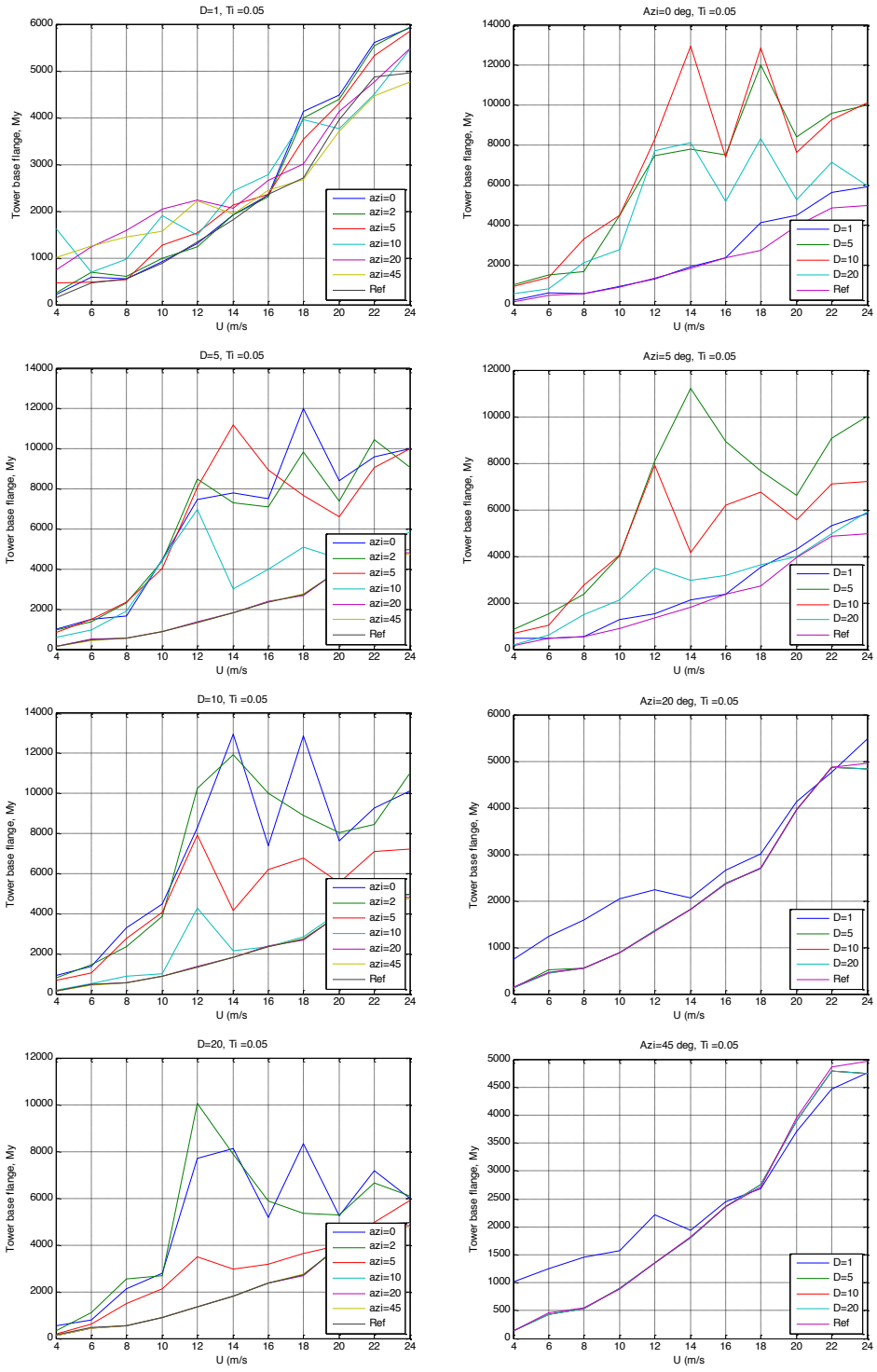

Figure 76 Tower base flange My (Sensor 18) equivalent load (m=4) versus wind speed for different wake distance (D) and wake azimuth (azi).

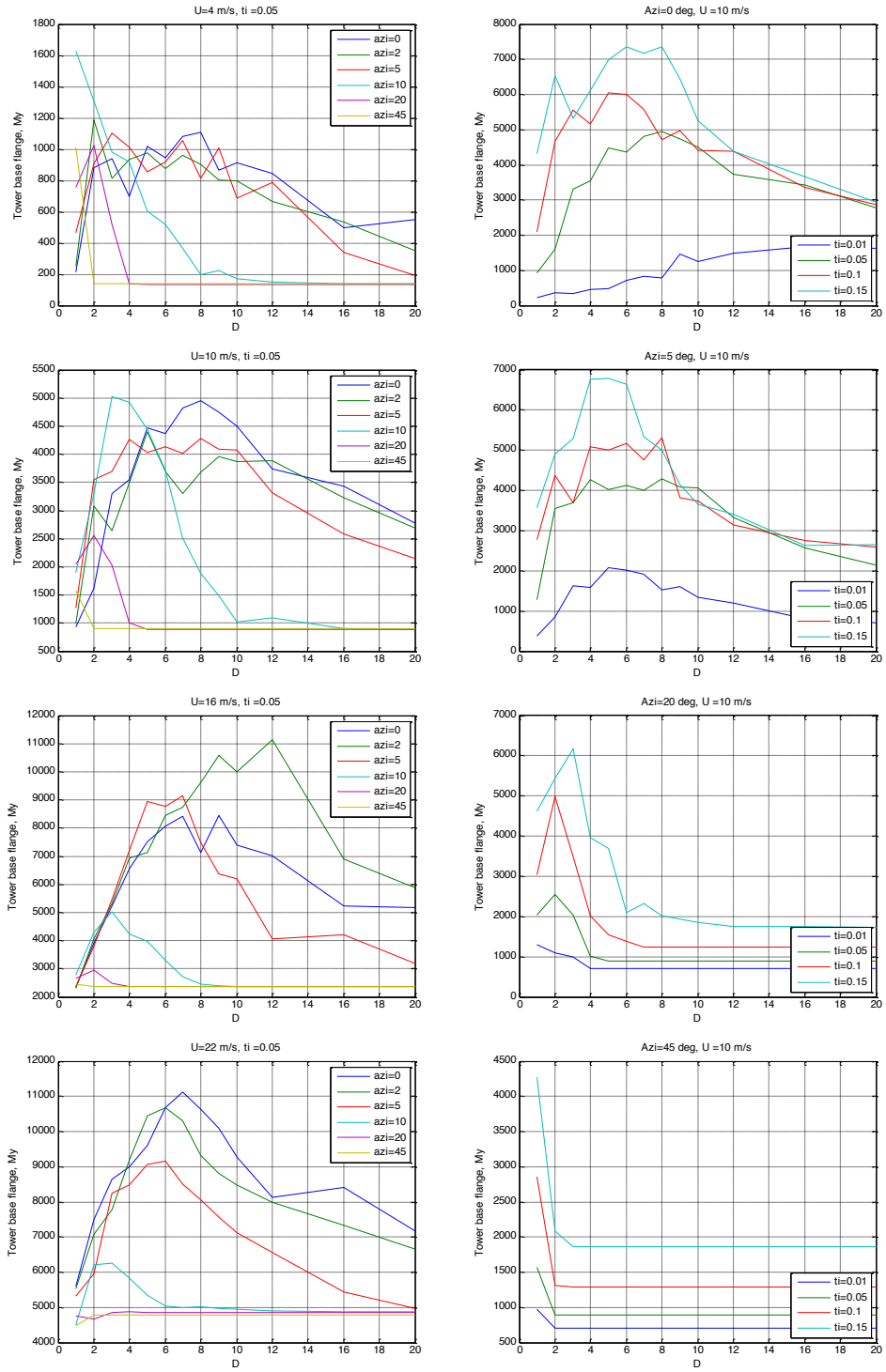

Figure 77 Tower base flange My (Sensor 18) equivalent load (m=4) versus wake distance (D) for different wake azimuth (azi) and turbulence

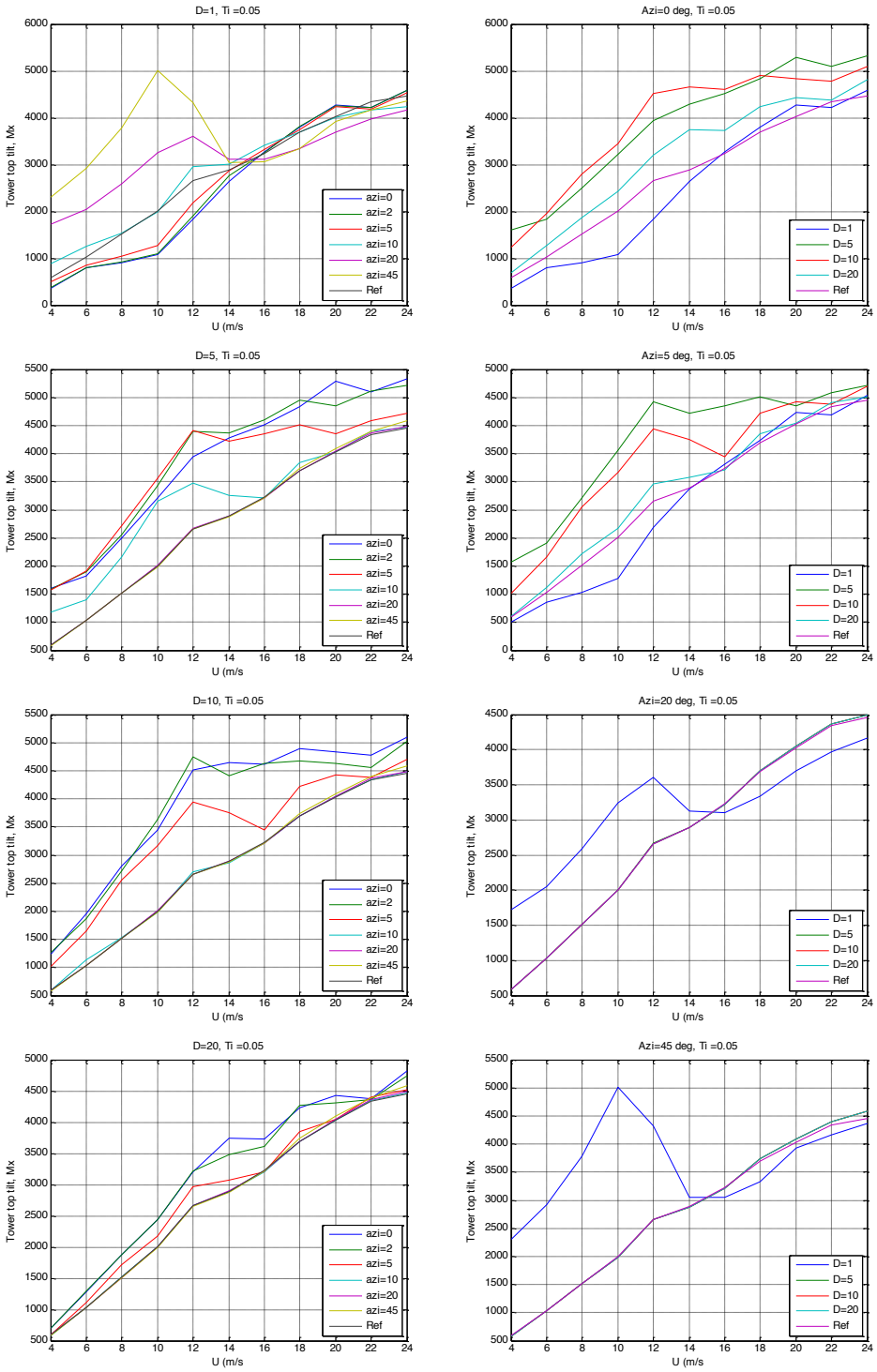

Figure 78 Tower top tilt, Mx (Sensor 20) equivalent load (m=8) versus wind speed for different wake distance (D) and wake azimuth (azi).

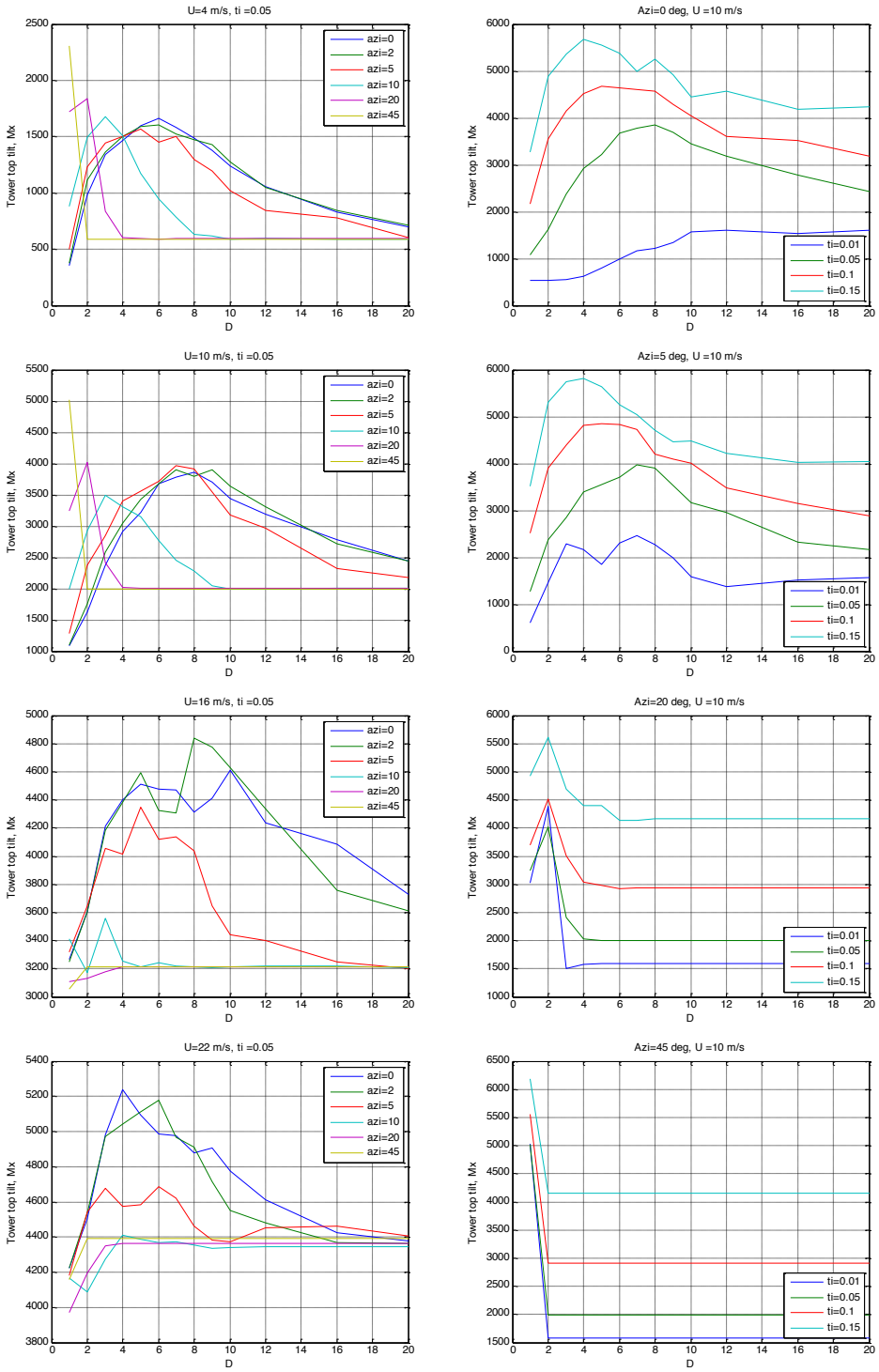

Figure 79 Tower top tilt, Mx (Sensor 20) equivalent load (m=8) versus wake distance (D) for different wake azimuth (azi) and turbulence

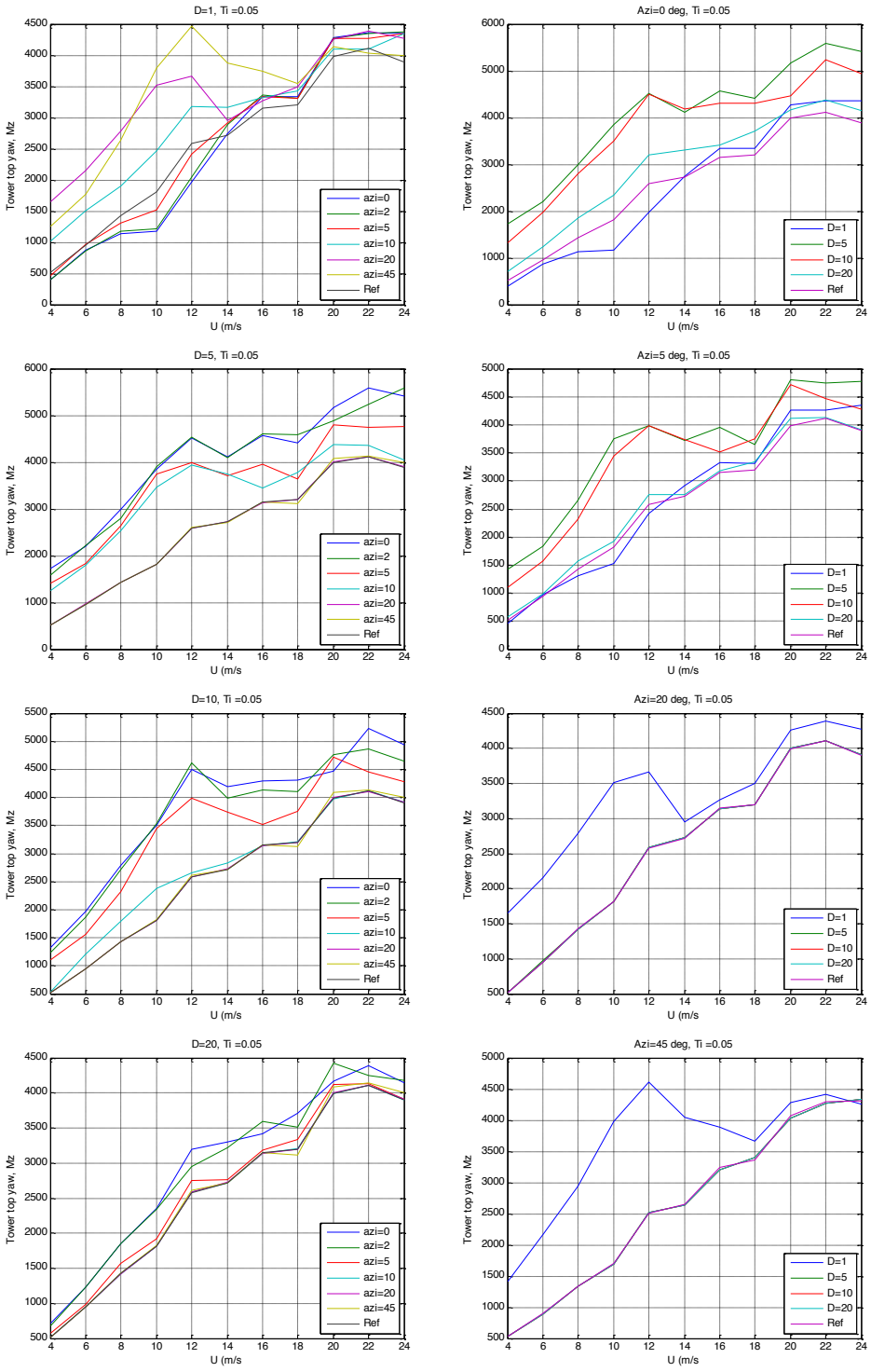

Figure 80 Tower top yaw, Mz (Sensor 22) equivalent load (m=8) versus wind speed for different wake distance (D) and wake azimuth (azi).

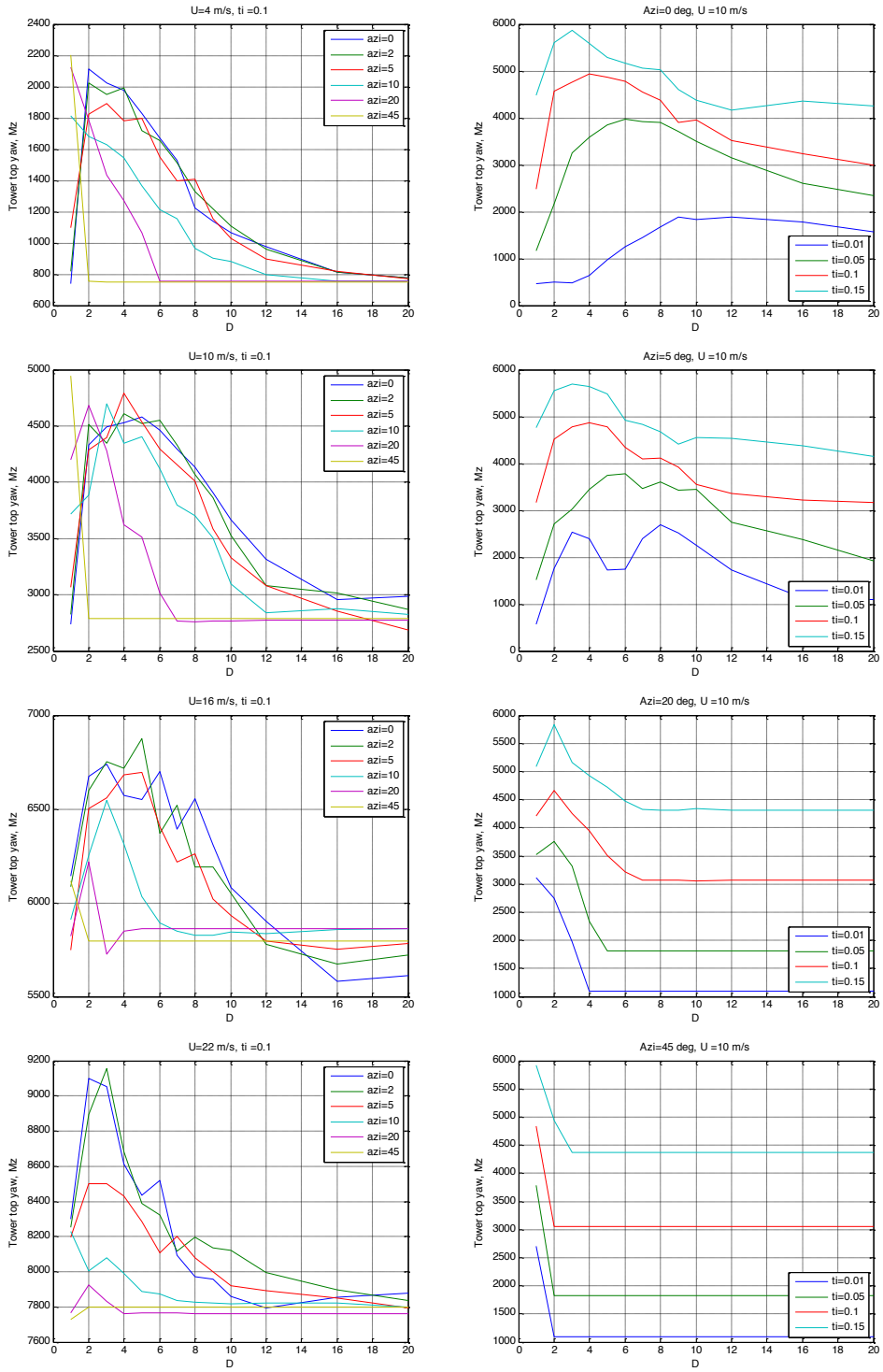

Figure 81 Tower top yaw, Mz (Sensor 22) equivalent load (m=8) versus wake distance (D) for different wake azimuth (azi) and turbulence ??this figure should be reorganized so that figure text is on the same side as the figure??

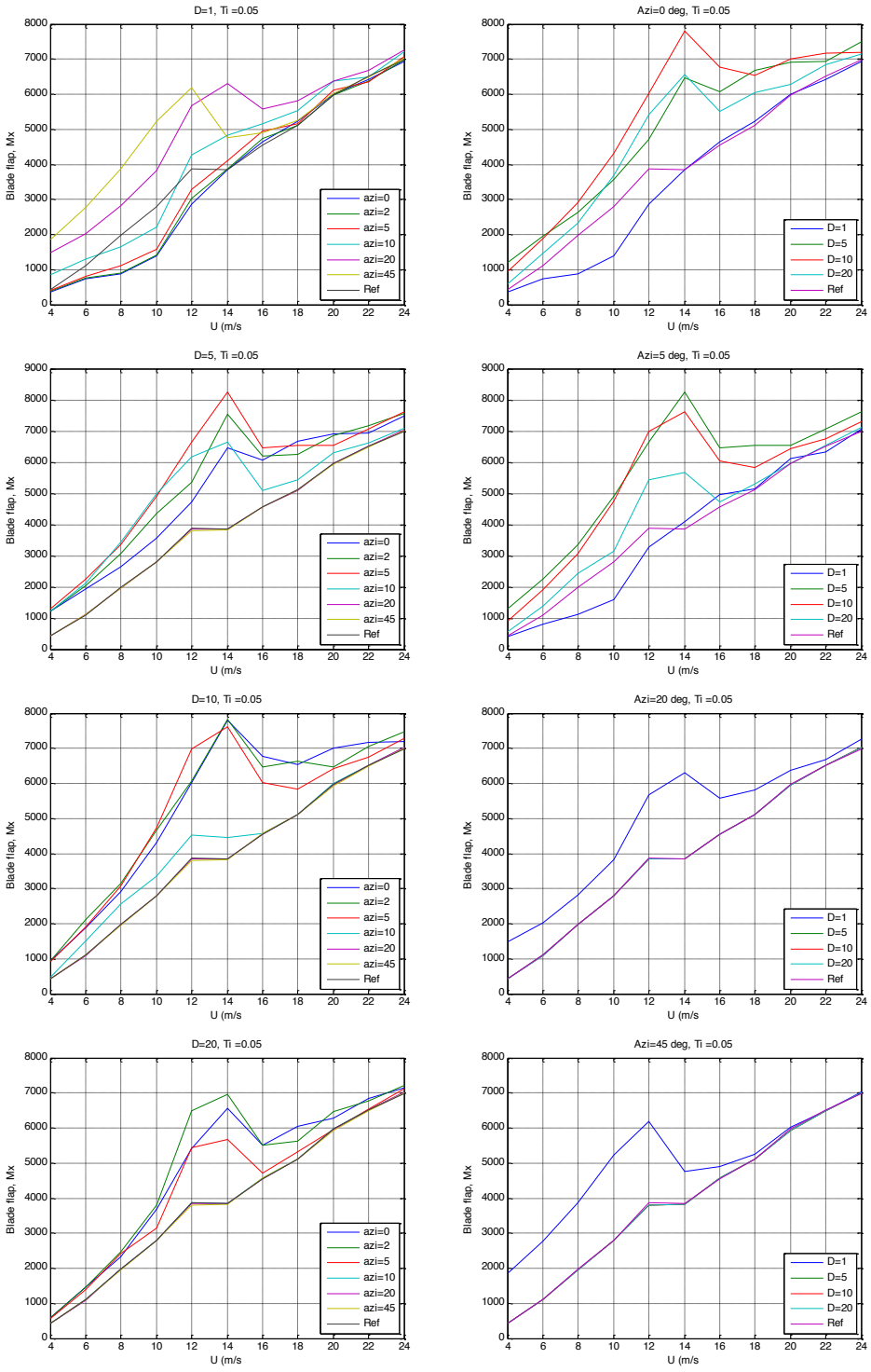

Figure 82 Blade flap moment, Mx (Sensor 29) equivalent load (m=12) versus wind speed for different wake distance (D) and wake azimuth (azi).

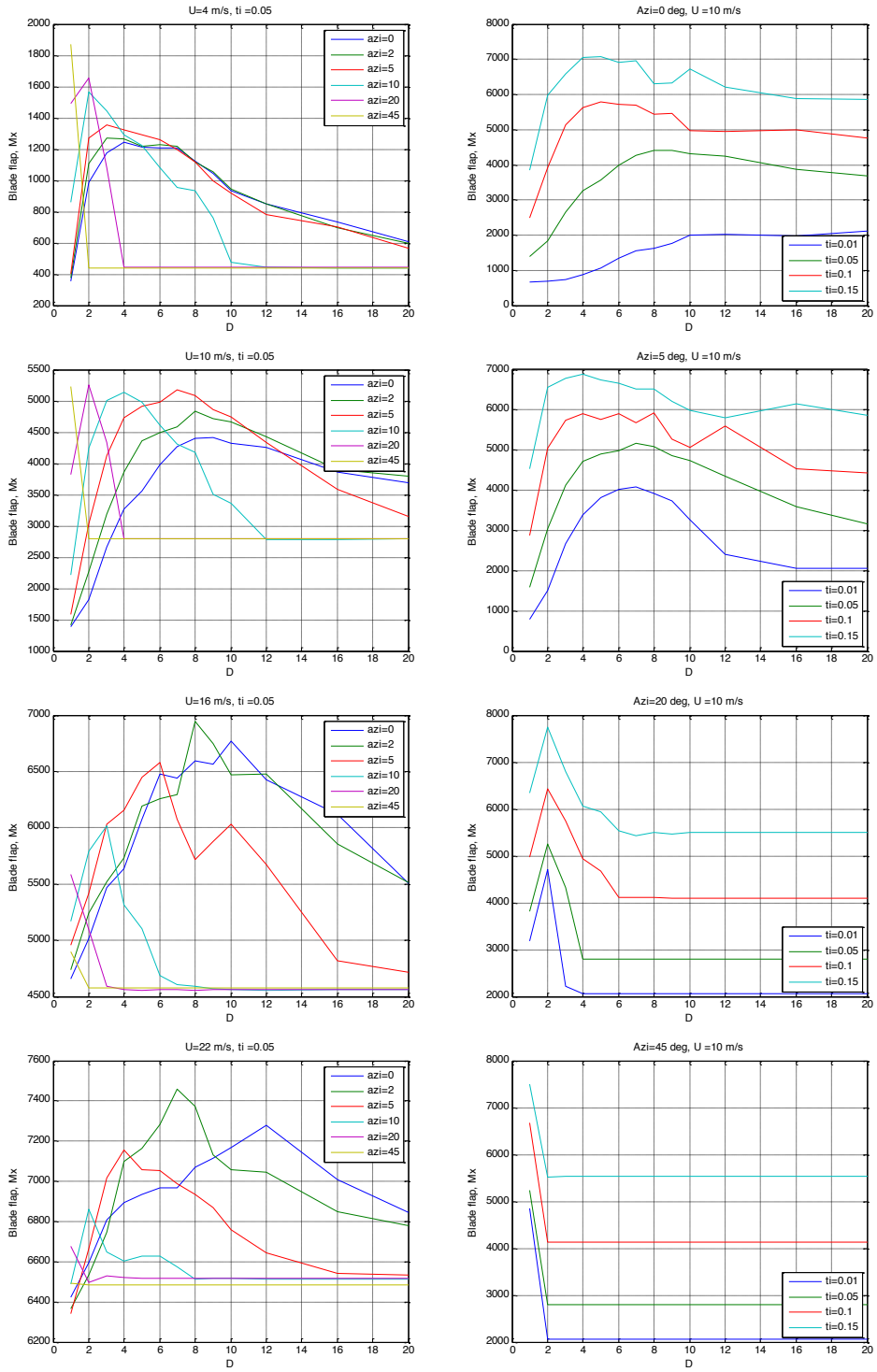

Figure 83 Blade flap moment, Mx (Sensor 29) equivalent load (m=12) versus wake distance (D) for different wake azimuth (azi) and turbulence

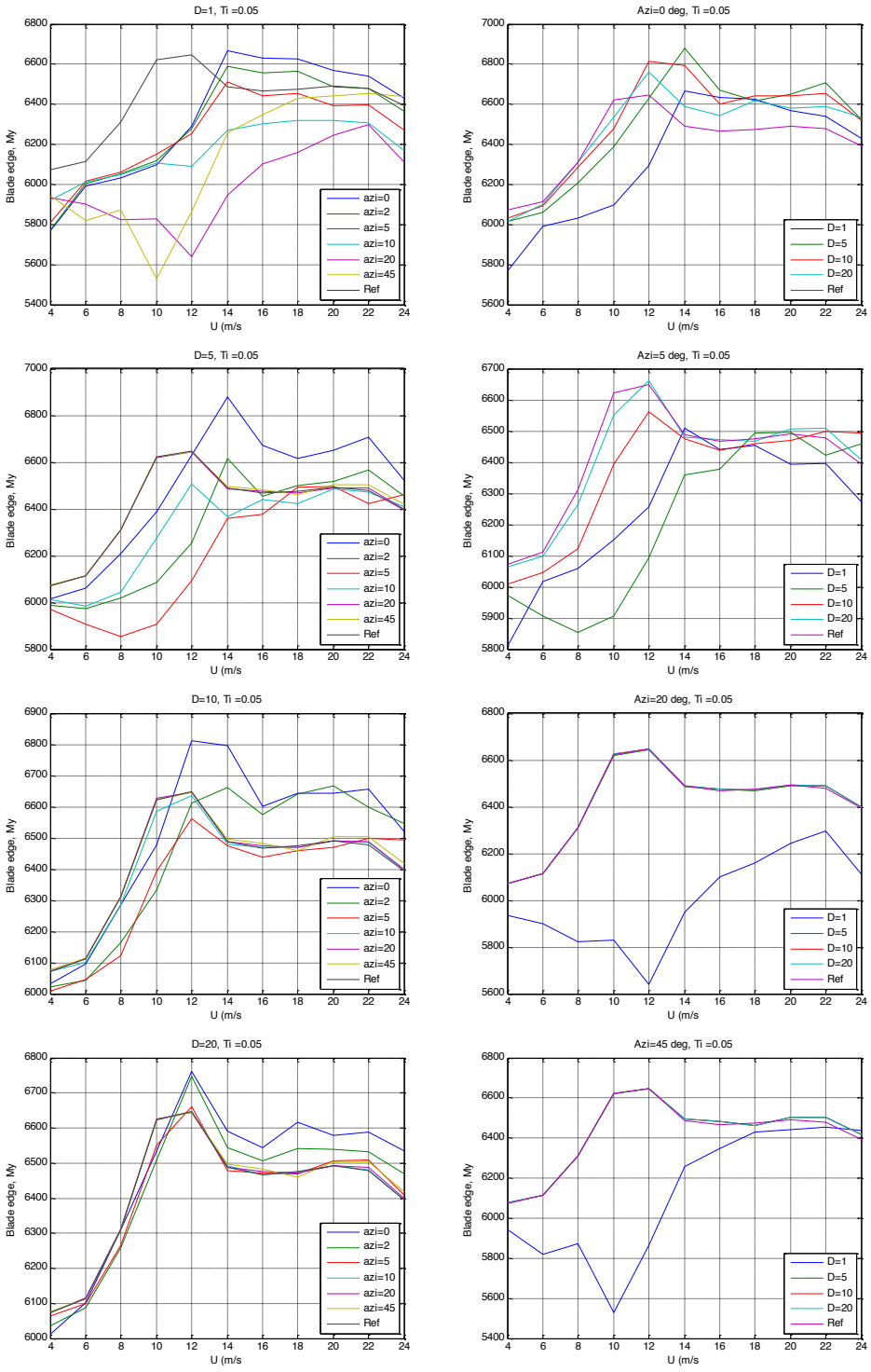

Figure 84 Blade edge moment, Mx (Sensor 30) equivalent load (m=12) versus wind speed for different wake distance (D) and wake azimuth (azi).

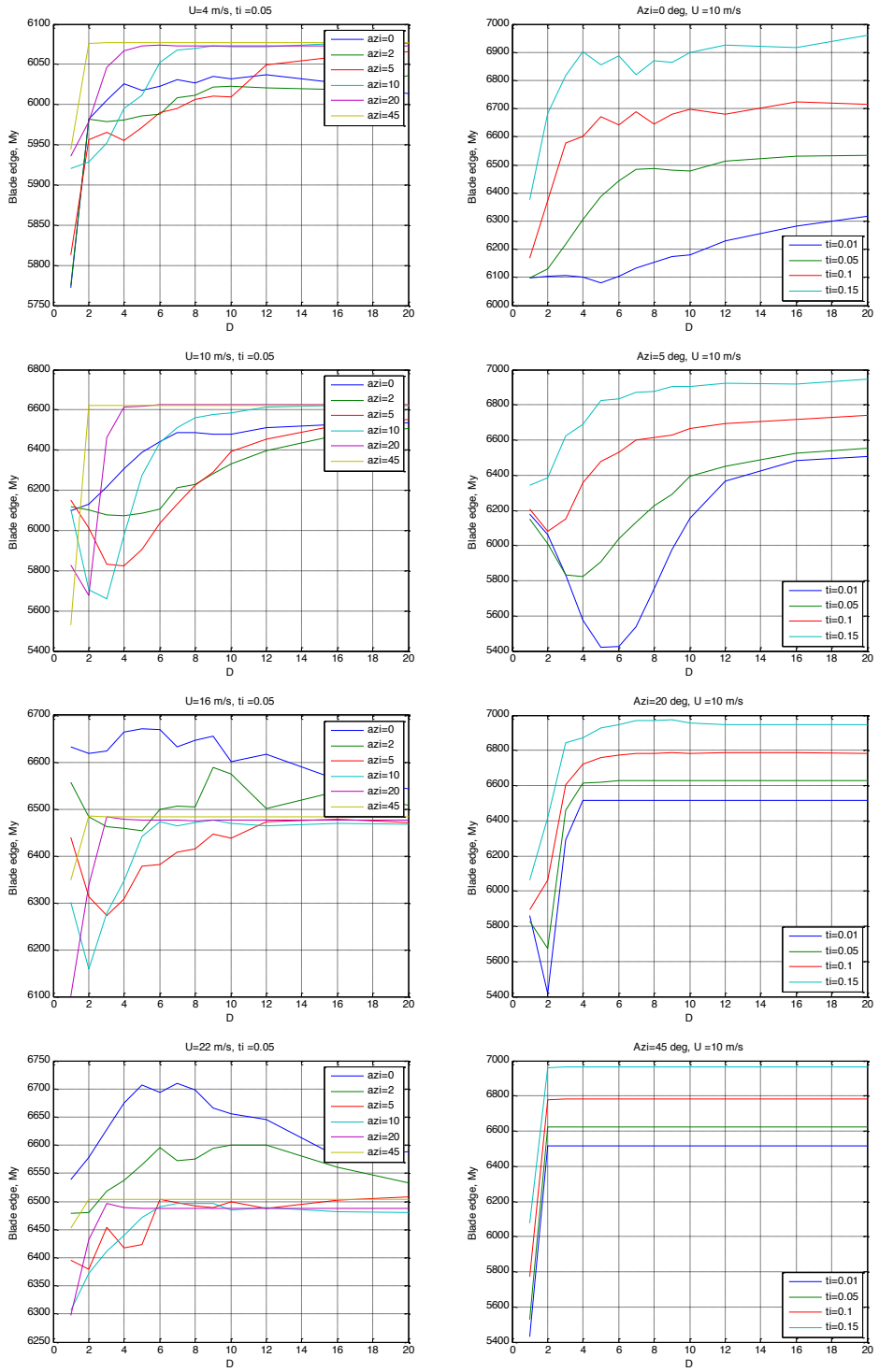

Figure 85 Blade edge moment, Mx (Sensor 30) equivalent load (m=12) versus wake distance (D) for different wake azimuth (azi) and turbulence

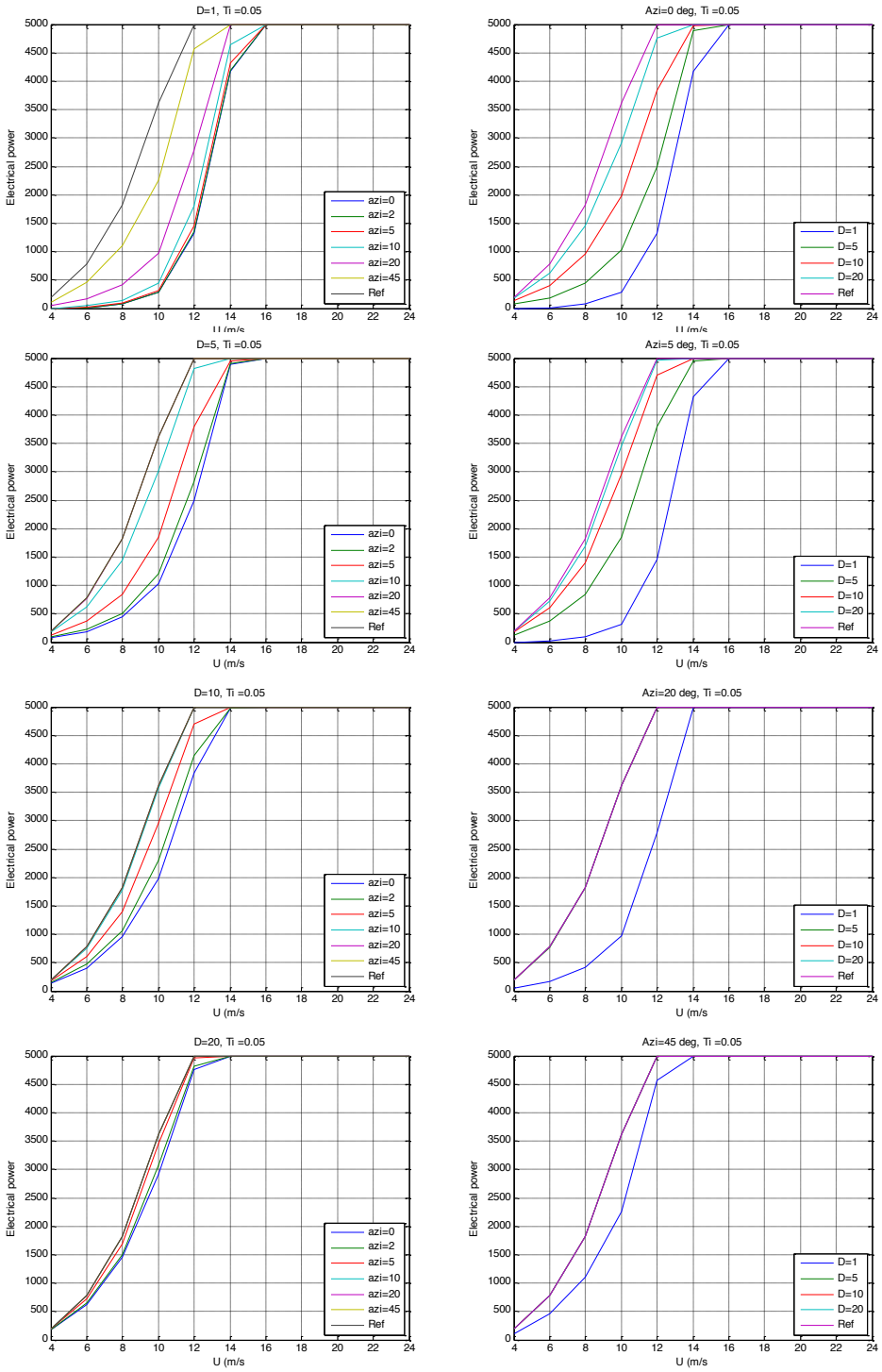

Figure 86 Electrical power (Sensor 88) versus wind speed for different wake distance (D) and wake azimuth (azi).

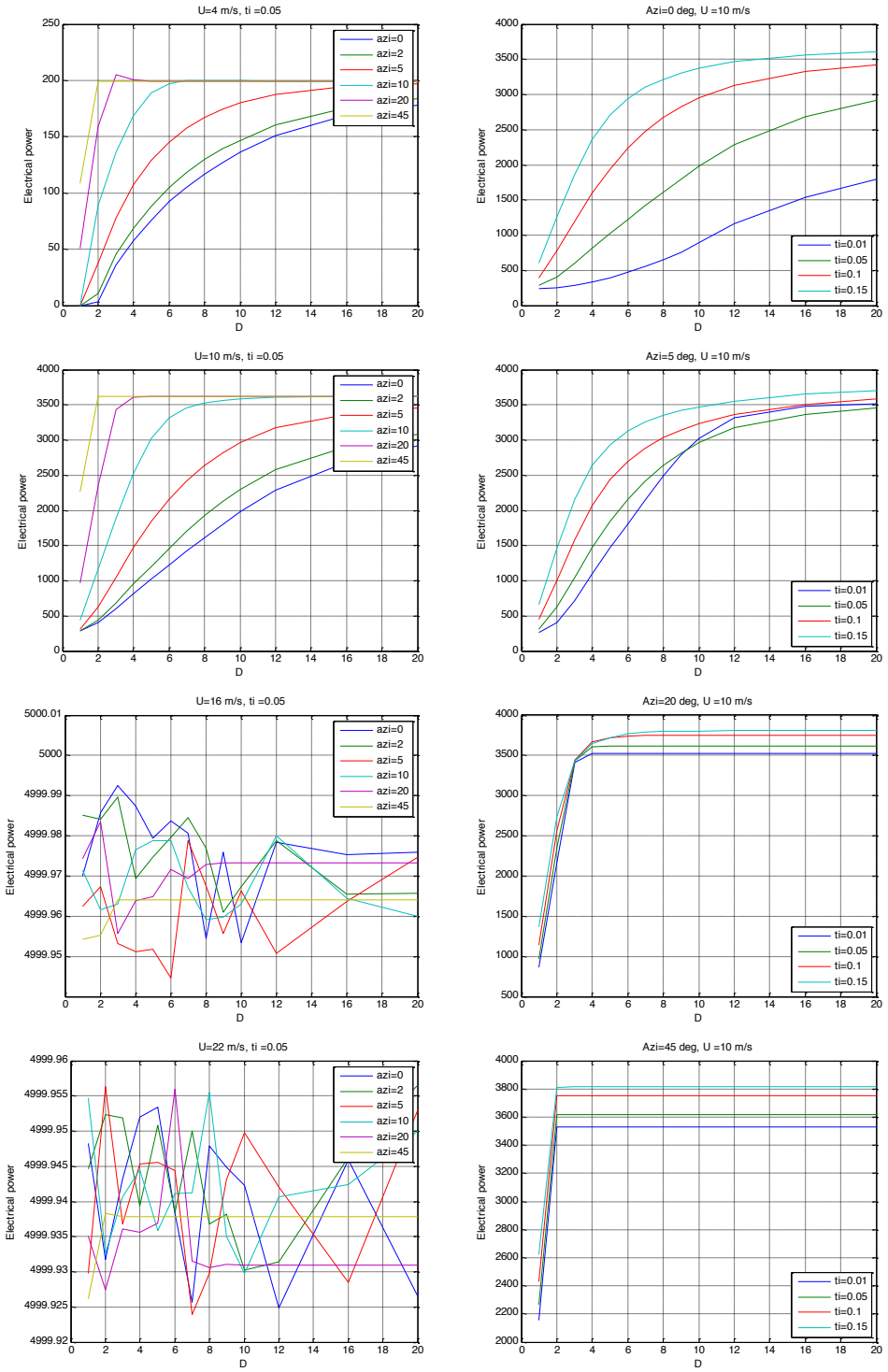

Figure 87 Electrical power (Sensor 88) versus wake distance (D) for different wake azimuth (azi) and turbulence

Appendix 2 Input file for middelgrunden

```
SiteType                Offshore
TurbineR                40  %Turbine radius
TurbineH                64  %Hub height
z0                      0.001
TurbinePower            2.00; %MW rated power
CutinWS                 5.0; % wind speed for which turbine starts
RatedWS                10.0; %Wind speed for which turbine reaches rated power
CutoutWS               25.0; %wind speed where turbine stops
MinTurbineDist         2 % Minimum number of turbine radia between turbines
NTurbineX               1
NTurbineY               20
xminbound               729314 % x boundary conditions in meters
xmaxbound               731220 % x boundary conditions in meters
yminbound              6175689  % y boundary conditions in meters
ymaxbound              6179809  % y boundary conditions in meters
polyBoundX   [729437 729314 729372 729478 730867 731220 730875 729741]
polyBoundY   [6179456 6178751 6177869 6177100 6175689 6178318 6179809 6179777]
WaterDepthFile          Middelgrunden.mat
CTCurve                 S2MW_ctcurve.csv
PowerCurve              S2MW_powercurve.csv
epsilon                 0.00001   % converging criteria
MaxIteNr                250        % nb opti iterations
% "Wind rose"
WindDirDegree    [0     30     60     90     120    150    180    210    240
270   300    330]
WindDirWindSpeed [7.54  6.77   6.86   7.27   8.02   7.44   7.34   6.74   6.87
7.07  6.76   5.92]
WindDirProp      [0.07  0.05   0.05   0.09   0.09   0.08   0.14   0.10   0.09
0.11  0.08   0.04]
WindDirK         [2.01  2.32   3.09   2.19   3.0    2.73   2.21   2.32   2.76
2.72  2.42   2.05]
WindDirIa        [0.094 0.082  0.085  0.098  0.085  0.099  0.114  0.115  0.109
0.127 0.128  0.121]
```

Appendix 3 Input file for Stags Holt / Coldham

```
SiteType                onshore
TurbineR                40  %Turbine radius
TurbineH                60  %Hub height
z0                      0.001
TurbinePower            2.00; %MW rated power
CutinWS                 5.0; % wind speed for which turbine starts
RatedWS                10.0; %Wind speed for which turbine reaches rated power
CutoutWS                25.0; %wind speed where turbine stops
MinTurbineDist          2 % Minimum number of turbine radia between turbines
NTurbineX               17
NTurbineY               1
xminbound               544970  % x boundary conditions in meters
xmaxbound               546380  % x boundary conditions in meters
yminbound               299040  % y boundary conditions in meters
ymaxbound               301295  % y boundary conditions in meters
polyBoundX              [545050 544970 545250 545589 546380 545810]
polyBoundY              [299040 299420 300270 301295 300097 299560]
CTCurve                 S2MW_ctcurve.csv
PowerCurve              S2MW_powercurve.csv
epsilon                 0.00001   % converging criteria
MaxIteNr                250        % nb opti iterations
% "Wind rose"
WindDirDegree    [0      30     60     90     120    150    180    210     240
270   300    330]
WindDirWindSpeed [7.05   6.47   6.01   6.18   6.64   7.21   7.63   7.98   7.86
7.60  7.26   6.99]
WindDirProp      [0.0483 0.0765 0.0483 0.0498 0.0499 0.0577 0.0847 0.1577
0.1411  0.099 0.0839 0.0645]
WindDirK         [2.19   2.08   2.12   2.28   2.38   2.46   2.25   2.43   2.47
2.32  2.26   2.32]
WindDirIa        [0.13   0.11   0.10   0.10   0.10   0.10   0.09   0.10   0.12
0.12  0.12   0.11]
```

Risø DTU is the National Laboratory for Sustainable Energy. Our research focuses on development of energy technologies and systems with minimal effect on climate, and contributes to innovation, education and policy. Risø has large experimental facilities and interdisciplinary research environments, and includes the national centre for nuclear technologies.

Risø DTU
National Laboratory for Sustainable Energy
Technical University of Denmark

Frederiksborgvej 399
PO Box 49
DK-4000 Roskilde
Denmark
Phone +45 4677 4677
Fax +45 4677 5688

www.risoe.dtu.dk